PROCESS TENSOR NETWORKS FOR NON-MARKOVIAN OPEN QUANTUM SYSTEMS

Gerald E. Fux

A Thesis Submitted for the Degree of PhD
at the
University of St Andrews

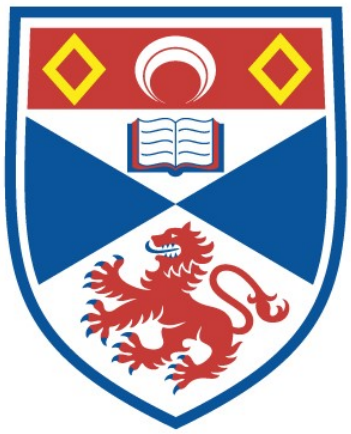

2022

Process Tensor Networks for non-Markovian Open Quantum Systems

Gerald E. Fux

University of
St Andrews

This thesis is submitted in partial fulfilment for the degree of
Doctor of Philosophy (PhD)
at the University of St Andrews

August 2022

Candidate's declaration

I, Gerald E. Fux, do hereby certify that this thesis, submitted for the degree of PhD, which is approximately 31,000 words in length, has been written by me, and that it is the record of work carried out by me, or principally by myself in collaboration with others as acknowledged, and that it has not been submitted in any previous application for any degree. I confirm that any appendices included in my thesis contain only material permitted by the 'Assessment of Postgraduate Research Students' policy.

I was admitted as a research student at the University of St Andrews in August 2018.

I received funding from an organisation or institution and have acknowledged the funder(s) in the full text of my thesis.

Date Signature of candidate

Supervisor's declaration

I hereby certify that the candidate has fulfilled the conditions of the Resolution and Regulations appropriate for the degree of PhD in the University of St Andrews and that the candidate is qualified to submit this thesis in application for that degree. I confirm that any appendices included in the thesis contain only material permitted by the 'Assessment of Postgraduate Research Students' policy.

Date Signature of supervisor

Permission for publication

In submitting this thesis to the University of St Andrews we understand that we are giving permission for it to be made available for use in accordance with the regulations of the University Library for the time being in force, subject to any copyright vested in the work not being affected thereby. We also understand, unless exempt by an award of an embargo as requested below, that the title and the abstract will be published, and that a copy of the work may be made and supplied to any bona fide library or research worker, that this thesis will be electronically accessible for personal or research use and that the library has the right to migrate this thesis into new electronic forms as required to ensure continued access to the thesis.

I, Gerald E. Fux, confirm that my thesis does not contain any third-party material that requires copyright clearance.

The following is an agreed request by candidate and supervisor regarding the publication of this thesis:

Printed copy

No embargo on print copy.

Electronic copy

No embargo on electronic copy.

Date Signature of candidate

Date Signature of supervisor

Underpinning Research Data or Digital Outputs

Candidate's declaration

I, Gerald E. Fux, understand that by declaring that I have original research data or digital outputs, I should make every effort in meeting the University's and research funders' requirements on the deposit and sharing of research data or research digital outputs.

Date Signature of candidate

Permission for publication of underpinning research data or digital outputs

We understand that for any original research data or digital outputs which are deposited, we are giving permission for them to be made available for use in accordance with the requirements of the University and research funders, for the time being in force.

We also understand that the title and the description will be published, and that the underpinning research data or digital outputs will be electronically accessible for use in accordance with the license specified at the point of deposit, unless exempt by award of an embargo as requested below.

The following is an agreed request by candidate and supervisor regarding the publication of underpinning research data or digital outputs:

No embargo on underpinning research data or digital outputs.

Date Signature of candidate

Date Signature of supervisor

Meinen Eltern und
meiner Schwester gewidmet.

Abstract

The advance of quantum technology relies heavily on an accurate understanding of the unavoidable interactions between quantum systems and their environment. While it is often adequate to account for the environment using approximate time-local (i.e. Markovian) equations of motion, in many scenarios such a description fails, and a more general non-Markovian theory becomes necessary. The failure of Markovian descriptions concerns not only quantitative aspects of the reduced dynamics of a quantum system, but also qualitative and conceptual aspects, such as the failure of the quantum regression formula relating the system's dynamics to its multi-time correlations. Despite considerable progress in recent years, the description and simulation of non-Markovian open quantum systems remains a conceptual and computational challenge. In this thesis we develop a versatile set of numerical methods for non-Markovian open quantum systems by combining the so-called process tensor framework with the numerical power of tensor network methods. The recently introduced process tensor is an alternative approach to open quantum systems and is—unlike the canonical approach based on dynamical maps—well suited for a rigorous characterisation of non-Markovian open quantum systems. We construct and apply process tensors in a matrix product operator form (PT-MPO) to yield a numerically exact, yet efficient representation of non-Markovian open quantum systems, which allows for a variety of practical applications. Building on the PT-MPO we introduce general methods to (1) efficiently find optimal control procedures for non-Markovian open quantum systems, (2) compute the dynamics and multi-time correlations of chains of non-Markovian open quantum systems, and (3) construct a time-translational invariant PT-MPO, which allows efficient computation of steady states even in non-equilibrium non-Markovian scenarios.

General acknowledgements

I sincerely thank my supervisors Jonathan Keeling and Brendon W. Lovett for their incredibly dedicated and competent support during the entirety of my PhD. I don't expect to anytime soon meet anyone who is as good a mentor, and professionally ethical and competent as Jonathan; or anyone who is as welcoming, encouraging, and well connected as Brendon. Cheers to the dream team!

I also thank the Condensed Matter Center for Doctoral Training (in particular Chris Hooley, Debra Thompson, and Julie Massey), the University of St Andrews, and ultimately the UK tax-payer for making my PhD a well supported, well organised and close to worry-free experience.

Funding

This work was supported by the Engineering and Physical Sciences Research Council (EPSRC) under grant number (EP/L015110/1).

Digital Outputs access statement

Digital outputs underpinning this thesis are available at DOI:10.5281/zenodo.4428316.

Contents

Chapter 1

Introduction

The theory of open quantum systems is one of the key ingredients for making quantum mechanics more applicable for experimental applications. It describes the dynamics of microscopic systems governed by the rules of quantum mechanics, but unlike the theory of closed systems, open systems additionally incorporate the unavoidable interactions with the environment. As such it is essential for the development of quantum computation and quantum communication devices [1, 2], but also key in understanding the role of quantum mechanics in biological systems [3–5] and the development of better photo-voltaic devices [6]. Because a full quantum mechanical treatment of the total system (i.e the open system together with its environment) is in almost all practical cases unfeasible, the main effort of the field is to find appropriate effective equations of motion for the open system alone, while accounting for the complex influence of the environment. The form of these equations depends heavily on the specific problem at hand.

Some physical scenarios allow for simple time-local effective equations of motion [7, 8]. Such a description is called *Markovian*, which means that the future evolution of the system only depends on its present state, but not explicitly on its history. Such a description is often adequate for scenarios with unstructured environments that couple weakly to the system of interest as, for example, often encountered in the field of quantum optics. There, one typically considers single atoms or high quality cavity modes that interact weakly with the surrounding electromagnetic field [9, 10]. The influence of the field onto the atoms or cavity modes can then often be described by some effective decay rate or driving term that does not depend on the history of the evolution.

Many interesting physical scenarios, however, do not admit such a simple time-local description and thus make a non-Markovian theory necessary [11–13]. These include scenarios where the environment is structured or the interaction with the open system is strong. In these cases the environment may retain information about past interactions with the system and then, with some time delay, act back on it, leading to time non-local effective equations of motion for the system. Compared to the predictions of a Markovian theory, non-Markovian equations of motion have the potential to capture physical effects that are obscured otherwise, which can lead to qualitatively different behaviour of the system, as seen for example in the spin-boson model phase transition [14]. In general, the complexity of such problems scales exponentially with the memory time of the environment, which makes both deriving and solving the effective equations of

motion a challenging task.

Non-Markovian open quantum systems appear in a number of relevant applications. Solid state based quantum devices, for example, such as quantum dots and nitrogen-vacancy colour centres in diamonds are promising platforms for quantum communication, quantum computation, and quantum sensing applications [2]. As these systems are part of a solid object they often interact strongly with the lattice vibrational modes, surrounding charges, or magnetic spins [15]. For an accurate computation of the evolution, the strength of the interactions with the environment demands a non-Markovian treatment in many cases [16–19]. The study of the evolution of a single excitation inside a larger object is also an important ingredient for the development of better light-harvesting devices [6] and understanding the role of quantum mechanics in biological systems [5]. In both light-harvesting devices and biological systems (such as the Fenna-Matthews-Olson complex [3]) considerable effort goes into understanding how the environment impedes or enhances the transport of energy [20]. Apart from these particular applications, the general theory of non-Markovian quantum systems is also of importance for fundamental research, such as the study of strong coupling quantum thermodynamics [21–27] and the development of theoretical tools for the characterisation of quantum devices [28].

While the theory of Markovian open quantum systems has resulted in a rich and well developed set of analytical and numerical tools within a well established mathematical framework, the treatment of non-Markovian scenarios is more challenging. There exist various approaches to general (non-Markovian) open quantum systems developed over the last several decades that can be roughly put into four categories: (1) perturbative approaches [29–34], (2) stochastic trajectory approaches [35–37], (3) methods that construct a larger Markovian system extended with the most relevant environment degrees of freedom [38–41], and (4) methods that keep track of the environment's time non-local influence onto the system [42–49]. The latter two approaches which explicitly or implicitly keep track of the environment have benefited enormously from the development of tensor network methods in recent years. Tensor network methods were originally designed for many-body quantum systems, where the key idea is to restrict the huge state space of many-body systems to a low-dimensional manifold that captures the physically most relevant correlations [50, 51]. For a wide class of many-body quantum systems this makes an effective numerical simulation feasible even for a large number of interacting quantum systems, for which a direct approach would be intractable. It is thus unsurprising that tensor network methods may benefit approaches that transform a non-Markovian open system into a Markovian many-body problem [38–41]. The same is in fact true, albeit maybe less obvious, for approaches which do not directly keep track of the environment but only of the influence of the environment onto the system [45, 49, 52–58].

Despite the large number of available approaches and numerical methods for general open quantum systems, there are still a lot of open challenges that are of importance to the applications mentioned above. While the perturbative and semi-analytical approaches often need to make crude approximations or are applicable only to a quite restricted set of problems, the numerical approaches often involve challenging computations. This makes, for example, optimisation of control protocols for non-Markovian quantum systems often an numerically unfeasible task, which would be particularly desirable for a design of quantum information devices [59, 60]. Also, there are physical

scenarios that include both many-body quantum systems *and* strongly coupled structured environments [61–65]. However, almost all methods for the study of many-body systems only consider closed or Markovian dynamics, while methods for the study of general open quantum systems are generically restricted to small system sizes. Furthermore, there appears to be some disagreement and possibly even confusion on a conceptual level in the community about how to describe the properties of an open quantum system. This conceptual disagreement is apparent, for example, in the zoo of inequivalent definitions and measures of quantum (non-)Markovianity proposed by different authors [66]. Although this might seem like an irrelevant dispute over the meaning of the word "Markovian", it often makes the literature cumbersome to follow or even prone to misinterpretation and incorrect conclusions, especially when a specific definition is assumed but not explicitly stated. Related to this are also other conceptual challenges, such as the questions on how to obtain correct multi-time correlations of the system and how to accommodate initial states that are not separable between the system and the environment.

In this thesis we will address several of these challenges by combining the so called *process tensor* framework [67] for general open quantum systems with the numerical power of tensor network methods. In chapter 2 we first give a brief introduction to the general theory of open quantum systems, the process tensor framework, and the theory of tensor networks. We then combine the process tensor framework with tensor network algorithms to yield the so called *process tensor* in *matrix product operator* form (PT-MPO). In chapter 3 we show how the PT-MPO may be employed to find optimal control procedures for general open quantum systems, and illustrate the procedure by optimising the shape of a laser pulse to prepare a quantum dot in a specific state [54]. In chapter 4 we combine the PT-MPO with an established many-body tensor network method to compute the dynamics and multi-time correlations of chains of general open quantum systems [68]. Furthermore, we propose a method to study the thermalisation and resulting effective temperature of subsystems even when their coupling to the rest of the chain and the environment is strong. We exemplify this by studying an XYZ Heisenberg spin chain in both equilibrium and non-equilibrium scenarios. In chapter 5 we exploit time-translational invariance of the system-environment coupling to construct a time-translational invariant PT-MPO, which allows efficient computation of steady states even in non-equilibrium scenarios. Finally we conclude and briefly discuss future directions in chapter 6.

Chapter 2

Background

In this chapter we introduce the concepts and formalisms that form the basis for the rest of this thesis. We begin with the general formulation of open quantum systems and a brief discussion of the most commonly applied concepts such as the evolution of the reduced density matrix and the dynamical map. The limitations of these concepts then motivate the introduction of the so called *process tensor formalism* [67] in section 2.1.4 as an alternative approach for the description of general open quantum systems. After a brief introduction to tensor networks in section 2.2, we discuss the construction of the *process tensor* in *matrix product operator* form (PT-MPO), which combines the computational efficiency of tensor network methods with the conceptual advantages of the process tensor formalism for the description of general open quantum systems. The PT-MPO will play an important role in all subsequent chapters.

2.1. Open quantum systems

2.1.1. General formulation

Most generally, the field of open quantum systems seeks to describe properties of a quantum system, called *the open system* or simply *the system*, which is part of a larger quantum system, called *the total system* [8, 69]. The part of the total system that is not the open system is called *the environment*. Typically, the open system is a small system of central interest, such as the electronic exciton states of a single quantum dot. The environment is on the other hand typically a large system comprising a continuum of states, such as the lattice phonon modes that couple to the exciton of the quantum dot. In principle there are however no restrictions on the sizes of the respective Hilbert spaces. Also, the border between environment and open system is a choice and as such physically arbitrary and only a matter of the intention of the theoretical study. The total Hilbert space $\mathcal{H}$ is assumed to be the product of the open system and the environment spaces, i.e. $\mathcal{H} = \mathcal{H}^{\mathrm{S}} \otimes \mathcal{H}^{\mathrm{E}}$. Most commonly one separates the total Hamiltonian

$$\hat{H}(t) = \hat{H}^{\mathrm{S}}(t) + \hat{H}^{\mathrm{E}}(t) + \hat{H}^{\mathrm{I}}(t), \tag{2.1}$$

into a pure system $H^{\mathrm{S}}(t) \in \mathcal{B}(\mathcal{H}^{\mathrm{S}})$, a pure environment $H^{\mathrm{E}}(t) \in \mathcal{B}(\mathcal{H}^{\mathrm{E}})$, and an interaction part $H^{\mathrm{I}}(t) \in \mathcal{B}(\mathcal{H}^{\mathrm{S}} \otimes \mathcal{H}^{\mathrm{E}})$. The expression $\mathcal{B}(\mathcal{H})$ denotes the set of bounded linear operators on the Hilbert space $\mathcal{H}$. One often allows that the total Hamiltonian is explicitly time dependent, which signals that the total system itself need not be closed in

the strictest sense, because for example, energy is then not necessarily conserved. From the point of view of the field of open quantum systems a total system of the form in equation (2.1) is, however, considered quasi-closed in the sense that its overall evolution is unitary. However, in most applications the interaction and environment Hamiltonian are not explicitly time dependent, i.e. $\hat{H}^{\mathrm{I}}(t) = \hat{H}^{\mathrm{I}}$ and $\hat{H}^{\mathrm{E}}(t) = \hat{H}^{\mathrm{E}}$. To differentiate between certain classes of environments, we call a time independent environment with an infinite number of degrees of freedom a *reservoir* and we call an initially thermalised reservoir a *bath*.

For some open quantum systems it is possible to directly study the total system analytically, such as the independent boson model [14, 70]. For most physical scenarios of interest, however, the entirety of the system and environment is too complex to allow for a direct treatment. Thus the general approach in the field of open quantum systems is to derive some effective equations of motion (EOM) for the quantities of interest. The canonical approach is to find EOM that describe the evolution of the reduced density matrix $\rho^{\mathrm{S}}(t)$ of the open system for a given initial total state ρ_0. As a starting point for such an approach let us consider the EOM for the total system in the form of the von Neumann equation (in units of $\hbar = 1$)

$$\frac{\mathrm{d}}{\mathrm{d}t}\rho(t) = -i\left[\hat{H}(t), \rho(t)\right]. \tag{2.2}$$

Let us assume that $\rho(t)$ is a solution of this equation for the initial state $\rho(0) = \rho_0$ with $\rho_0 \in \mathcal{B}(\mathcal{H}^{\mathrm{S}} \otimes \mathcal{H}^{\mathrm{E}})$. We can then define a one parameter family of density matrices

$$\rho^{\mathrm{S}}(t) := \mathrm{Tr}_{\mathrm{E}}\left\{\rho(t)\right\}, \tag{2.3}$$

where $\mathrm{Tr}_{\mathrm{E}}\,\cdot$ denotes the partial trace over the environment Hilbert space. This one parameter family is called *the evolution of the reduced density matrix* $\rho^{\mathrm{S}}(t)$, or in short, the *reduced dynamics*. Most approaches assume that the initial state is a product state with respect to the system and environment Hilbert spaces, i.e. $\rho_0 = \rho_0^{\mathrm{S}} \otimes \rho_0^{\mathrm{E}}$. In this case one can further straightforwardly define the so called *dynamical map* Λ_0^t, which maps any initial system state ρ_0^{S} to the reduced density matrix at later time t,

$$\Lambda_0^t \rho_0^{\mathrm{S}} \equiv \Lambda_0^t[\rho_0^{\mathrm{S}}] = \rho^{\mathrm{S}}(t). \tag{2.4}$$

These two related objects, namely the evolution of the reduced density matrix $\rho^{\mathrm{S}}(t)$ and the dynamical map Λ_0^t, are the focus of most studies in the literature. It is therefore vital to have a good understanding of how these quantities relate to experiments. For this, let us assume we run an experiment with good control over a single small quantum system that is in contact with some complicated environment. To measure the reduced dynamics of the system $\rho^{\mathrm{S}}(t)$, we need to repeatedly prepare the system and environment in the state ρ_0 and then perform quantum state tomography on the system at time t. In many experiments the initial state ρ_0 is the steady state of the total system and the evolution originates from a unitary protocol associated with some system Hamiltonian $\hat{H}^{\mathrm{S}}(t)$ starting at the initial time $t = 0$. To obtain the dynamical map Λ_0^t, on the other hand, we need to not only prepare a single initial product state, but even repeatedly prepare a product state for different system basis states $\left\{\rho_0^{\mathrm{E}} \otimes \rho_0^{\mathrm{S},\alpha}\right\}_\alpha$ and then perform full quantum state tomography at time t for each state $\rho_0^{\mathrm{S},\alpha}$. Conversely, knowing $\rho^{\mathrm{S}}(t)$ or even Λ_0^t encodes all expectation values that one could measure from the system in such a prepare-evolve-measure type protocol.

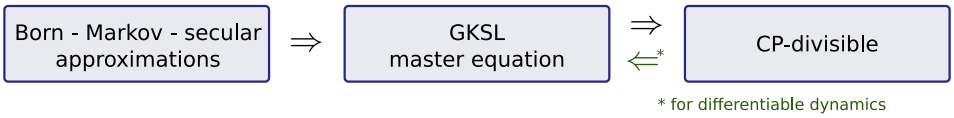

Figure 2.1: Schematic summary of some "Markovian" concepts and their relation. The Born, Markov and secular approximations always result in equations of motion in GKSL form. Also, any GKSL master equation results in CP-divisible dynamics, and any differentiable CP-divisible dynamics can be described by a GKSL master equation.

However, not all properties of an open system can be measured in a prepare-evolve-measure type experiment. In many experiments the observed quantities are related to multi-time correlations, such as the fluorescence and absorption spectra in molecular spectroscopy [71], and bunching and anti-bunching of photons in quantum optics experiments [10]. Also, in the context of quantum information protocols, one is often interested in predicting the state of the system after multiple interactions with additional ancillary systems [72]. With the exception of very special circumstances (on which we will comment in section 2.1.3) neither the reduced dynamics $\rho^{\mathrm{S}}(t)$ nor the dynamical map Λ_0^t encode multi-time correlations or how the system will react to multiple interactions with an ancilla. This also means that any property one defines solely on the basis of the reduced dynamics $\rho^{\mathrm{S}}(t)$ or the dynamical map Λ_0^t is only a statement about expectation values of prepare-evolve-measure type experiments described above. There is no a priori guarantee that any such property would persist in a different context in which, for example, an extra ancillary system interacts with the open system at multiple times.

Therefore, to completely characterise general open quantum systems a different approach is necessary. In section 2.1.4 we briefly introduce such an approach brought forward by Pollock *et al.* which will form the conceptual basis for all following chapters of this thesis. To relate this alternative approach to the canonical methods we first briefly review some important concepts and results of the reduced dynamics paradigm in the following sections 2.1.2 and 2.1.3.

2.1.2. Quantum Markov processes

Obtaining the reduced dynamics for an open quantum system as described above is in general a difficult task. There are, however, many open systems where the approximate EOM for the reduced dynamics $\rho^{\mathrm{S}}(t)$ take a simple time-local form. This is the case if at all times $t_1 > 0$ the EOM for $\rho^{\mathrm{S}}(t)$ at that time t_1 only depend on its current state $\rho^{\mathrm{S}}(t_1)$, but not on its history $\rho^{\mathrm{S}}(t')$ with $t_1 > t' \geq 0$. Such open quantum systems are informally often said to be *Markovian*, referring to a quantum equivalent of the concept for classical stochastic processes. Generic open systems are not Markovian because in general there exist processes in which the system influences the environment and then the environment acts back on the system with some time delay.

To make these informal statements more concrete, we now discuss three related concepts, namely completely positive divisibility, the Gorini–Kossakowski–Sudarshan–Lindblad master equation, and the Born-Markov and secular approximations. Figure 2.1 shows an overview sketch of how these concepts relate to each other. Finally, we briefly discuss the use of the term "Markovian" in a quantum context.

CP-divisibility: A dynamical map Λ_0^t is called *completely positive divisible* [73, 74] (CP-divisible) if and only if for all times $t_2 \geq t_1 \geq 0$, there exists a completely positive and trace preserving (CPTP) map [72] $\Theta_{t_1}^{t_2}$ such that

$$\Lambda_0^{t_2} = \Theta_{t_1}^{t_2} \, \Lambda_0^{t_1}, \tag{2.5}$$

where $\Theta_{t_1}^{t_2} \, \Lambda_0^{t_1}$ is to be understood as a composition, i.e. $\Theta_{t_1}^{t_2} \, \Lambda_0^{t_1} \, \rho_0^{\mathrm{S}} = \Theta_{t_1}^{t_2}\big[\Lambda_0^{t_1}\big(\rho_0^{\mathrm{S}}\big)\big]$. We note that often no distinction is made between the maps Λ and Θ in the literature. We make this distinction here to emphasise their different operational meaning and call the latter the *generalised dynamical map* Θ [66]. While Λ_0^t can be measured in an prepare-evolve-measure type experiment, this is not true for $\Theta_{t'}^t$. The map $\Theta_{t'}^t$ is in general different from the map $\Phi_{t'}^t$ that one would measure in an experiment in which one performs measurements at time t after a system state preparation at time t' [75]. As an example, consider a CP-divisible process which evolves any initial state into a completely mixed state by the time $t_a > 0$ and then continues the evolution unitarily. Such a unitary evolution could be implemented by decoupling the environment from the system at time t_a, i.e. $H^{\mathrm{I}}(t) = 0$ for $t > t_a$. Then, *any* unitary map would qualify as an appropriate $\Theta_{t_1}^{t_2}$ for $t_2 > t_1 > t_a$ in the sense of the above definition of CP-divisibility, while a measurement of $\Phi_{t_1}^{t_2}$ would reveal the specific unitary of the protocol.

GKSL master equation: A dynamical map is said to admit a *Gorini–Kossakowski–Sudarshan–Lindblad* (GKSL) master equation if and only if it is the solution to EOM of the form

$$\begin{aligned}\frac{\mathrm{d}}{\mathrm{d}t}\rho^{\mathrm{S}}(t) = &- i\left[\hat{H}^{\mathrm{eff}}(t), \rho^{\mathrm{S}}(t)\right] \\ &+ \sum_{k=1}^{d^2-1} \gamma_k(t)\left(\hat{A}_k^\dagger(t)\rho^{\mathrm{S}}(t)\hat{A}_k(t) - \frac{1}{2}\left\{\hat{A}_k^\dagger(t)\hat{A}_k(t), \rho^{\mathrm{S}}(t)\right\}\right),\end{aligned} \tag{2.6}$$

where $d = \dim(\mathcal{H}^{\mathrm{S}})$ is the dimension of the system Hilbert space, $\hat{H}^{\mathrm{eff}}(t) \in \mathcal{B}(\mathcal{H}^{\mathrm{S}})$ is an effective Hamiltonian, $\hat{A}_k \in \mathcal{B}(\mathcal{H}^{\mathrm{S}})$ are traceless orthonormal operators, and $\gamma_k(t) \geq 0$ are positive real numbers. Any dynamical map that admits a GKSL master equation is CP-divisible. The reverse is also true when we consider only differentiable CP-divisible processes, i.e. processes for which $\lim_{\epsilon\to 0^+}\left(\Theta_t^{t+\epsilon}/\epsilon\right)$ is well defined for all $t > 0$ [73, 76–79]. While this informs us under what circumstances a dynamical map admits such a time-local GKSL master equation, there is still the question of how to obtain an explicit GKSL master equation for a specific microscopic model given in terms of $\hat{H}^{\mathrm{S}}(t)$, $\hat{H}^{\mathrm{I}}(t)$, $\hat{H}^{\mathrm{E}}(t)$, and an initial environment state ρ_0^{E}. The most commonly applied method to achieve this is to perform a particular set of approximations, which we briefly discuss next.

Born, Markov and secular approximations: The Born, Markov and secular approximations are a sequence of approximations that are guaranteed to result in effective EOM of the reduced dynamics in a GKSL form [8]. They are often applied to microscopic models in the field of quantum optics. First, the *Born approximation* assumes that during the entire evolution the environment is only altered in such a way that as far as the effective EOM for the reduced dynamics are concerned the total state can be assumed to be in a product state of the form $\rho(t) = \rho^{\mathrm{S}}(t) \otimes \rho_0^{\mathrm{E}}$. Intuitively this approximation may be justified for large and weakly coupled environments. It does, however,

not assume that the environment truly stays in its initial state, or that a product state would be a good approximation to the total state at later times—it rather assumes that it does not make a significant difference to the EOM whether the true total state or this product state enters into the calculation. Consider an open system in which the total initial state is a pure state and the environment causes the system to obtain a fully mixed state after some time. Then the system and environment must be maximally entangled because the entire state is still pure. However, even in such a scenario the Born approximation might still be justified. Second, the *Markov approximation* assumes that the processes in which the system perturbs the environment that then acts back on the system are much faster than the system evolution itself. Therefore the most important contributions from such processes enter the EOM as time-local terms. And third, the *secular approximation* is a type of rotating wave approximation in which fast rotating terms in the effective EOM of the reduced dynamics are neglected. We refer the reader to the canonical literature on the topic [8] for further details.

Quantum Markovianity: The definition of CP-divisibility is most commonly accepted as a definition for the word "Markovian" in a quantum context, but it is not generally agreed upon in the field. As explained in a review article [11] by the authors of a related seminal paper [74] CP-divisibility can be understood as a quantum version of classical divisibility, which—for one-time probabilities—is equivalent to classical Markovianity. Even for classical processes, divisibility does not in general imply Markovianity, because to judge the latter the knowledge of all multi-time correlations is necessary [11, 75, 80]. Thus CP-divisibility appears to be an appropriate definition of quantum Markovianity for one-time probabilities, i.e. for any observable that is measurable in a prepare-evolve-measure type experiment as discussed in the previous section 2.1.1. In case one intends to classify open quantum systems with respect to their multi-time correlations (which are in general not encoded in the dynamical map) other concepts are necessary. It is unsurprising that CP-divisibility, whose definition is based solely on the dynamical map cannot classify open quantum systems with respect to observables that are not encoded in the dynamical map. A review by Li, Hall and Wiseman [66] summarises the most commonly used definitions that are refereed to as "Markovian" at various places in the literature and presents a hierarchy of which definitions imply which others. This shows that caution is in order when the term "Markovian" is used in a quantum context. In the review [66] the authors argue "that there is no single concept that deserves the name quantum Markovianity", and advocate to "regard quantum Markovianity as very much context-dependent".

In this thesis we do not rely on any particular definition of Markovianity because all our core results do not rely on any approximation that could be considered "Markovian". However, we use the term *non-Markovian* as a synonym for "general" whenever we want to stress that we do *not* assume Markovianity (which is thus independent of the exact definition). We use the term *Markovian* to hint at approximations that might be considered "Markovian" by some authors, and we call an open quantum system *not Markovian* if we want to point out that it significantly contradicts a particular definition of Markovianity. For the use of the terms *Markovian* and *not Markovian* we specify, if relevant, their meaning in a given context.

2.1.3. The quantum regression formula

As argued above in section 2.1.1, there is no a priori reason to assume that the dynamical map would encode the information necessary to predict multi-time correlations. In fact, there exist examples even for CP-divisible processes that show that there is measurable information encoded in multi-time correlations which is not present in the dynamical map [75]. The scenario outlined above following the definition of CP-divisibility in equation (2.5) is one such example. There, the map $\Phi_{t_1}^{t_2}$ can be understood as a two-time correlation that is not obtainable through the dynamical map. It has been shown by Lax [81] that one may obtain, however, approximate two-time correlations from the EOM for the reduced dynamics under certain assumptions. A common formulation of Lax's result for CP-divisible processes is that

$$\left\langle \hat{A}(t_2)\hat{B}(t_1)\right\rangle \simeq \mathrm{Tr}_{\mathrm{S}}\left\{\hat{A}\,\Theta_{t_1}^{t_2}\left[\hat{B}\,\Theta_0^{t_1}\left(\rho_0^{\mathrm{S}}\right)\right]\right\}, \tag{2.7}$$

where $\hat{A}(t_2)$ and $\hat{B}(t_1)$ are system operators in the Heisenberg picture at times $t_2 \geq t_1 \geq 0$, and $\Theta_{t_1}^{t_2}$ is the generalised dynamical map as defined in equation (2.5). We call Eq. (2.7) the *quantum regression formula* (QRF).

The key idea behind this formula is that the EOM for the matrix $\hat{X} := \hat{B}\,\Theta_0^{t_1}\left(\rho_0^{\mathrm{S}}\right) = \hat{B}\rho^{\mathrm{S}}(t_1)$ starting at time t_1 are (due to linearity) the same EOM as for the reduced dynamics of a system in an experiment that has been prepared at time t_1. While this statement is true, it is however in general *not* true that the generalised dynamical map $\Theta_{t_1}^{t_2}$ corresponds to the EOM of such an experiment. Thus for $t_1 > 0$ the QRF is in general an additional approximation on top of any other approximation that may have been made in order to obtain the generalised dynamical map. This is exemplified by the model of an harmonic oscillator experiencing random thermal forces, which leads to the correct EOM for the reduced dynamics in a weak coupling limit when employing the Born, Markov and secular approximations, but fails to predict correct two-time correlations in the same limit [82]. Despite the ongoing discussion about exact criteria for the validity of the quantum regression formula [82–86], it should be noted that its usefulness in many scenarios (in particular in a quantum optics context) is generally undisputed. It is, however, important to appreciate the approximate nature of this formula, especially when considering multi-time correlations of general (i.e. "non-Markovian") open quantum systems.

2.1.4. The process tensor

In sections 2.1.1 to 2.1.3 we have seen that the canonical approach to describe open quantum systems in terms of the reduced dynamics is in general only suitable for the description of single time correlations in prepare-evolve-measure type experiments. In many experiments the observed quantities are however related to multi-time correlations. Furthermore, the dynamical map approach is in many cases ill equipped to describe scenarios with initially correlated states. The most relevant initial states for experiments are however equilibrium or steady states, which generically show entanglement between the system and environment. In view of these demands a different approach to describe open quantum systems seems necessary. We will now give a brief introduction to the so called *process tensor formalism* [67] which allows us to address these challenges.

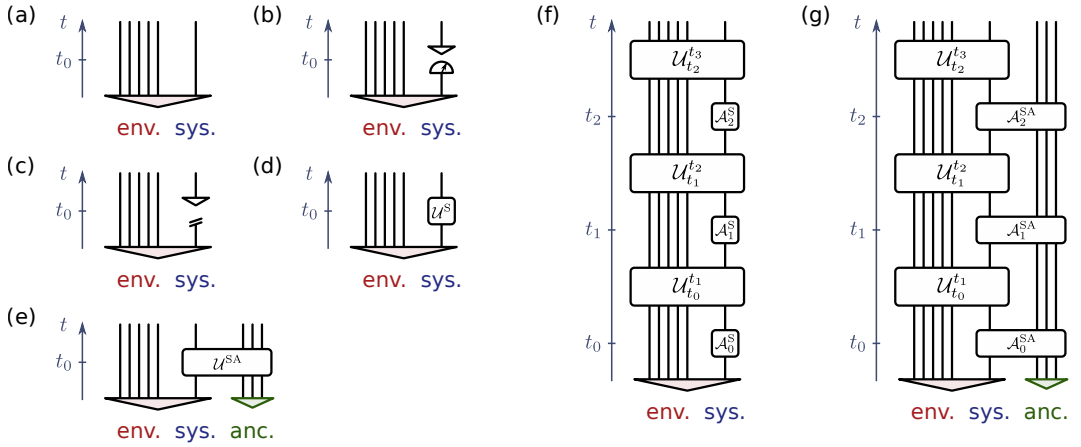

Figure 2.2: Quantum circuits of the environment (env.), system (sys.), and ancillar (anc.) showing various different interventions at a single time (a-e) and multiple times (f-g). The panels show quantum circuits to: (a) make no intervention, (b) perform full quantum state tomography and re-preparation, (c) discard and re-prepare the system state, (d) apply a unitary system gate $\mathcal{U}^{\mathrm{S}}$, (e) apply a unitary system-ancilla gate $\mathcal{U}^{\mathrm{SA}}$, (f) apply a series of CP maps $\mathcal{A}_n^{\mathrm{S}}$ on the system, and (g) apply a series of CP maps $\mathcal{A}_n^{\mathrm{SA}}$ on the system and ancilla.

The process tensor formalism takes an operational approach to describe open quantum systems. This means that the emphasis of this approach lies on the question of how one would obtain the described quantities in an experiment, or similarly: "What quantities of an open quantum system are experimentally accessible?" Thus, the aim is to describe an open quantum system with a mathematical object that stands in a one-to-one relation to the experimentally accessible quantities. This means that both every experimentally accessible quantity should be extractable from the mathematical object *and* the entire mathematical object can be constructed from experimental observations alone. The so called *process tensor*, which we introduce in the following, is such a mathematical object.

To motivate and construct the process tensor we will first ask the question: "What is the set of all possible experiments on an open quantum system?" To answer this question we assume that we have perfect access to the system, but no direct access to the environment. This means that we assume that we can perform any experimentally possible intervention on the system at any time. Possible interventions include projective measurements, the application of gates to the system together with additional ancillas, as well as the preparation of the system in any state at any time. For simplicity we consider that these interventions happen instantaneously (i.e much faster than any other evolution) and only at a finite set of time slots $\{t_n\}_{n\in\{0,\dots,N\}}$. In principle this could be generalised to continuous interventions by considering the limit of an infinite set of times. For simplicity, however, we will omit such an analysis.

It is well known from quantum information theory that any intervention can be described by a CPTP map [72]. Even more generally, we could allow for experiments with interventions corresponding to specific outcomes of measurements. Such interventions are represented by completely positive (CP) maps which may decrease the trace of the input state. Thus, for our purposes, any experiment is a finite set of CP maps $\{\mathcal{A}_n\}_{n\in\{0,\dots,N-1\}}$ that act on the system and possibly any number of additional ancillas at the times $\{t_n\}_{n\in\{0,\dots,N-1\}}$. We visualise this by drawing exemplary quantum circuits

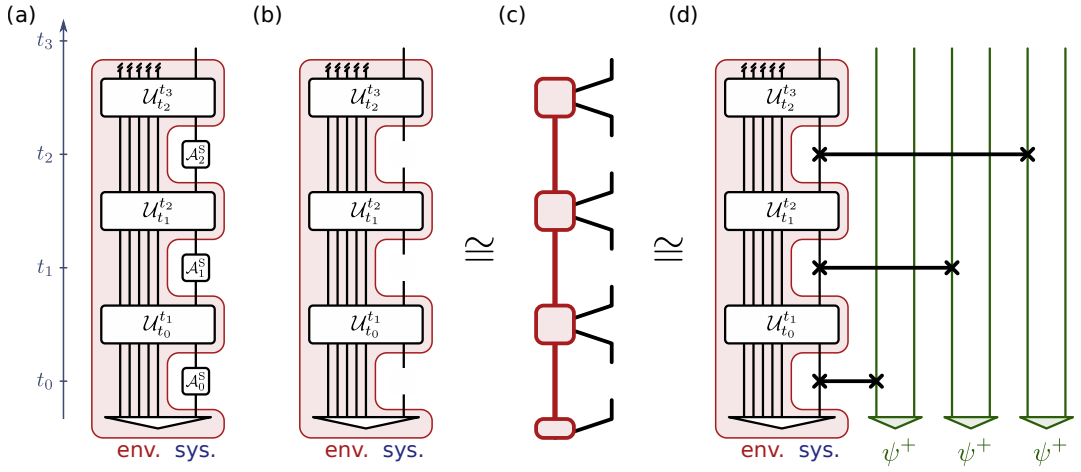

Figure 2.3: Various representations of the process tensor. (a) A quantum circuit with a sequence of three interventions. (b) A tensor network re-interpretation of the quantum circuit, excluding the interventions. (c) A tensor network representation in a matrix product operator form. (d) A many-body representation employing the Choi-Jamiołkowski isomorphism.

in Fig. 2.2. In these figures the environment Hilbert space $\mathcal{H}^{\mathrm{E}}$ is symbolically represented with five lines although in many practical cases the environment might include an infinite number of subsystems such as the continuum of bosonic field modes of the free electro-magnetic field. Note that by drawing the initial total state as a single triangle across the environment and the system, we symbolise that it might not be a separable state.

Figures 2.2(a-e) show examples for possible interventions at time t_0. We can perform full quantum state tomography (Fig. 2.2b) or simply discard the system state (Fig. 2.2c) before preparing it in a new state. We can apply a unitary operation on the system alone (Fig. 2.2d) or include additional ancilla systems (Fig. 2.2e). Also, we can choose not to perform any operation (Fig. 2.2a), which corresponds to the identity map on the system. Considering the most general case for multiple times $\{t_n\}_{n\in\{0,\dots,N-1\}}$ we draw Fig. 2.2f which shows the quantum circuit for an experiment with a set of interventions on the system $\{\mathcal{A}_n^{\mathrm{S}}\}_{n\in\{0,\dots,N-1\}}$ for $N=3$. Also, Fig. 2.2g shows the analogous quantum circuit for interventions $\{\mathcal{A}_n^{\mathrm{SA}}\}_{n\in\{0,\dots,N-1\}}$ that act on both the system and additional ancillas. Between any two adjacent interventions the total system evolves unitarily with

$$\mathcal{U}_{t_n}^{t_{n+1}} = \overleftarrow{\mathbf{T}} \exp\left(\int_{t_n}^{t_{n+1}} \mathcal{L}(t)\,\mathrm{d}t\right), \tag{2.8}$$

where $\overleftarrow{\mathbf{T}}$ denotes time ordering, and $\mathcal{L}(t)\cdot = -i\left[\hat{H}(t),\cdot\right]$ is the Liouvillian of the total Hamiltonian.

We are now in a position to define the process tensor. The process tensor $\mathcal{T}_{0:N}$ is defined to be the map from the set of all intervention sequences $\mathbf{A}_{0:N-1}^{\mathrm{S}} = \{\mathcal{A}_n^{\mathrm{S}}\}_{n\in\{0,\dots,N-1\}}$ to the (possibly sub-normalised) final reduced state of the system

$$\rho^{\mathrm{S}}(t_N) = \mathcal{T}_{0:N}\left[\mathbf{A}_{0:N-1}^{\mathrm{S}}\right]. \tag{2.9}$$

In reference [67] Pollock *et al.* prove that the process tensor exists for every open quantum system and that it is in an one-to-one relation to the set of all operationally

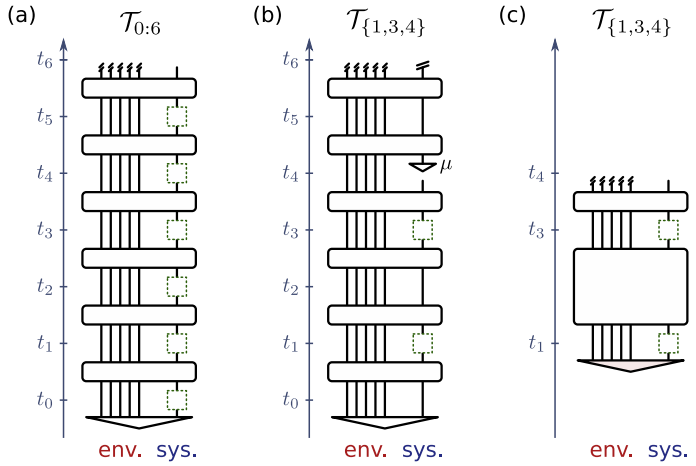

Figure 2.4: Quantum circuits showing the construction of the process tensor $\mathcal{T}_{1,3,4}$ contained in $\mathcal{T}_{0:6}$. (a) The process tensor $\mathcal{T}_{0:6}$. (b) The construction of $\mathcal{T}_{1,3,4}$ from $\mathcal{T}_{0:6}$. For this we insert identities at t_0, t_2, t_5, prepare any normalised state μ at time t_4, and trace over the last time step t_6. (c) The resulting process tensor $\mathcal{T}_{1,3,4}$ for time steps 1, 3, and 4.

accessible quantities in the sense of the above description. The process tensor $\mathcal{T}_{0:N}$ is not only a map but indeed a tensor (i.e. a multi-linear map) with the total dimension of d^{4N+2}, where $d = \dim\left(\mathcal{H}^{\mathrm{S}}\right)$ is the Hilbert space dimension of the system. Pollock *et al.* further show that it obeys the following three key properties:

1. *Linearity.* For any two intervention sequences $\mathbf{A}^{\mathrm{S}}_{0:N-1}, \mathbf{B}^{\mathrm{S}}_{0:N-1}$ and two real numbers $a, b \in \mathbb{R}$: $\mathcal{T}_{0:N}\left[a\mathbf{A}^{\mathrm{S}}_{0:N-1} + b\mathbf{B}^{\mathrm{S}}_{0:N-1}\right] = a\mathcal{T}_{0:N}\left[\mathbf{A}^{\mathrm{S}}_{0:N-1}\right] + b\mathcal{T}_{0:N}\left[\mathbf{B}^{\mathrm{S}}_{0:N-1}\right]$.
2. *Complete positivity.* When the controls act on the system and ancillas (A) then the final reduced system-ancillas state $\left(\mathcal{T}_{0:N} \otimes \mathcal{I}^{\mathrm{A}}\right)\left[\mathbf{A}^{\mathrm{SA}}_{0:N-1}\right] = \rho^{\mathrm{SA}}(t_N) \geq 0$ is positive. The map $\mathcal{I}^{\mathrm{A}}$ denotes the identity process on the ancillas.
3. *Containment.* If the full process tensor $\mathcal{T}_{0:N}$ for the time steps $\{t_n\}_{n\in\{0,\ldots,N\}}$ is known then one can compute the process tensor $\mathcal{T}_D$ for any subset of time steps $\{t_n\}_{n\in D}$ with $D \subseteq \{0, 1, \ldots, N\}$.

Graphically, the red shaded area in Fig. 2.3a might be loosely identified as the process tensor $\mathcal{T}_{0:N}$. It is important to note, however, that the process tensor does *not* include the entire explicit information about the environment's dynamics shown under the red shaded area. Instead, the process tensor includes only the information relevant to the system and it may be constructed from the quantum circuit shown in Fig. 2.3a in two equivalent ways. First, we can construct the process tensor by reinterpreting the quantum circuit as a tensor network shown in Fig. 2.3b. Note that the relevant outer tensor network legs of the process tensor have the dimension of the system Liouville space. We will discuss tensor networks and this approach to the process tensor in the sections 2.2 and 2.3 below. Second, we can construct the process tensor by means of the Choi-Jamiołkowski isomorphism (CJI) [87] as described in [67] and depicted in Fig. 2.3d. Analogous to the canonical application of the CJI in which a quantum channel is mapped onto a two-body state, we can map the process tensor to a many-body state, called the *Choi representation* of the process tensor by performing swap operations with pairs of ancillas at each time step. For this, the ancillas are initially in the state $\psi^+ = |\psi^+\rangle\langle\psi^+|$ with $|\psi^+\rangle = \sqrt{1/d}\sum_{i=1}^{d} |i\rangle \otimes |i\rangle$, where $\{|i\rangle\}_{i\in\{1,\ldots,d\}}$ is a set

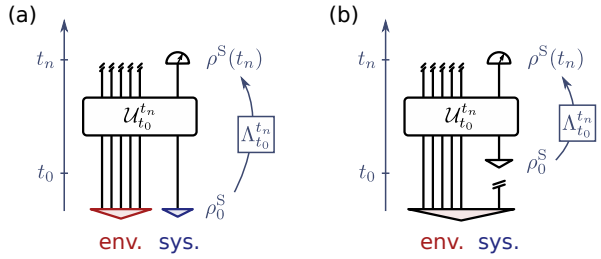

Figure 2.5: Quantum circuits for the measurement of the dynamical map $\Lambda_{t_0}^{t_n}$. (a) A quantum circuit for the measurement of the dynamical map starting in an uncorrelated initial state. (b) A quantum circuit for the measurement of the dynamical map, explicitly including the necessary preparation of the system state.

of basis states and $d = \dim(\mathcal{H}^{\mathrm{S}})$. In this construction the final many-body state of the ancillas together with the final system state carry the exact same information as the original process tensor and can thus be used to compute the outcome of any intervention sequence.

The process tensor $\mathcal{T}_D$ for a subset of time steps $D \subseteq \{t_0, t_1, \ldots, t_N\}$ can be computed by applying identities and trace operations to the full process tensor $\mathcal{T}_{0:N}$. Let t_M be the latest time slot in the set D. In order to remove any of the earlier time slots t_m with $m < M$ one simply inserts an identity control at that time t_m. All the later time slots in the process tensor can be removed by first, inserting any state at time t_M, second, applying any trace preserving control operations at times t_p with $M < p < N$, and third, tracing over the final state at time t_N. We draw exemplary quantum circuits for this procedure in Fig. 2.4.

Connections to the dynamical map

To create a connection to the more common approaches to open quantum systems we now discuss the notion of dynamical maps $\Lambda_{t_0}^{t_n}$ and generalised dynamical maps $\Theta_{t_k}^{t_n}$ from an operational perspective. In a first step, drawing this connection amounts to answering the question of "How would the dynamical map be inferred from an experiment?" As defined in Eq. (2.4) the dynamical map $\Lambda_{t_0}^{t_n}$ maps any initial system state ρ_0^{S} to the reduced system state $\rho^{\mathrm{S}}(t_n) := \mathrm{Tr}_{\mathrm{E}}\, \rho(t_n)$ assuming that the total initial state $\rho(0) = \rho_0^{\mathrm{S}} \otimes \rho_0^{\mathrm{E}}$ is uncorrelated. To measure the data for the construction of $\Lambda_{t_0}^{t_n}$ it is thus necessary to prepare the system in several different states and to perform quantum state tomography for each of them at the later time t_n. Because we can safely assume that $\Lambda_{t_0}^{t_n}$ is linear it is sufficient to do this for a basis set of system states. We can draw the corresponding quantum circuit in two equivalent ways. In Fig. 2.5a we draw the initial state as a product, while in Fig. 2.5b we explicitly include the preparation procedure of the initial system state. Although Fig. 2.5a might appear to be the more suitable quantum circuit, we draw Fig. 2.5b to point out explicitly that there is a state preparation involved in the experimental process at time t_0. Both figures show that the dynamical map as defined above constitutes a quantum channel because there is a (freely choosable) input state ρ_0^{S}, a quantum circuit that processes it and an output state $\rho^{\mathrm{S}}(t_n)$. As a consequence the dynamical map $\Lambda_{t_0}^{t_n}$ is guaranteed to be a CPTP map as expected. We can describe this scenario in terms of the process tensor $\mathcal{T}_{\{0,n\}}$ by

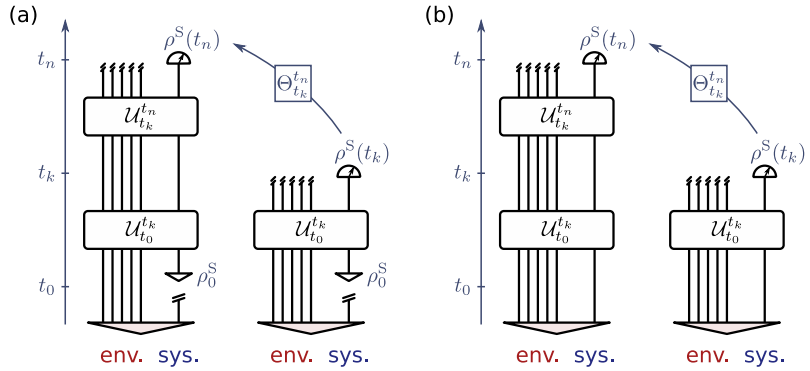

Figure 2.6: Quantum circuits for the measurement of the generalised dynamical map $\Theta^{t_n}_{t_k}$. (a) Quantum circuits that show the meaning of $\Theta^{t_n}_{t_k}$ conditioned on the preparation of the initial system state ρ^{S}_0. (b) Quantum circuits that show the meaning of $\Theta^{t_n}_{t_k}$ for an initially correlated state. In both cases $\Theta^{t_n}_{t_k}$ relates a system *output state* at time t_k with another system *output state* at time t_n. Therefore the map $\Theta^{t_n}_{t_k}$ does *not* constitute a quantum channel.

choosing $\mathcal{A}_0 : \rho^{\mathrm{S}} \mapsto \rho^{\mathrm{S}}_0$, which results in

$$\rho^{\mathrm{S}}(t_n) = \mathcal{T}_{\{0,n\}}\left[\mathcal{A}_0\right]. \tag{2.10}$$

To explicitly construct the dynamical map $\Lambda^{t_n}_{t_0}$ from the process tensor we consider the completely positive map $A : \rho^{\mathrm{S}}_0 \mapsto \left(\rho^{\mathrm{S}} \mapsto \rho^{\mathrm{S}}_0\right)$, which maps the state ρ^{S}_0 to the preparation intervention that maps any state ρ^{S} to ρ^{S}_0. The dynamical map can then be expressed as $\Lambda^{t_n}_{t_0} = \mathcal{T}_{\{0,n\}} \circ A$. Because the composition preserves complete positivity and $\mathcal{T}_{\{0,n\}}$ is a completely positive map [67], this proofs that also $\Lambda^{t_n}_{t_0}$ is completely positive.

The dynamical map $\Lambda^{t_n}_{t_0}$ for $n \in \{0, 1, \ldots, N\}$ only describes the map of the system state starting from time t_0 at which the initial preparation of the system takes place. Another map that is often considered in the literature is the map $\Theta^{t_n}_{t_k}$ that maps the reduced system state $\rho^{\mathrm{S}}(t_k)$ at time t_k to the state $\rho^{\mathrm{S}}(t_n)$ at time t_n. It is important to appreciate the conceptual difference this map compared to $\Lambda^{t_n}_{t_0}$, which is apparent when taking an operational point of view. To understand this in more detail we consider two cases. In Fig. 2.6a we include an intervention to prepare the system's initial state in ρ^{S}_0. In contrast to that Fig. 2.6b shows the case in which the total initial state is some fixed state $\rho(0) = \rho_0$ which is not necessarily a product state. In both cases we can see that the map $\Theta^{t_n}_{t_k}$ maps an *output* state $\rho^{\mathrm{S}}(t_k)$ to an *output* state $\rho^{\mathrm{S}}(t_n)$. Thus $\Theta^{t_n}_{t_k}$ as defined above is in general *not* a quantum channel and it is *not* necessarily CPTP. Also, from an operational point of view, in the case of an initially correlated state the map $\Theta^{t_n}_{t_k}$ only maps *one* state, namely $\rho^{\mathrm{S}}(t_k)$, to one other state, namely $\rho^{\mathrm{S}}(t_k)$, and not a set of states to another set of states because the total initial state is fixed. Although it is mathematically straightforward to define the map $\Theta^{t_n}_{t_k}$, this shows that its operational meaning is in fact quite limited.

If one is interested in addressing questions such as "What is the evolution of the system between time t_k and time t_n?" in an operationally meaningful way one thus needs to consider an alternative protocol. For this one could consider a setup in which after some initial preparation of the system in state ρ^{S}_0 at time t_0 one prepares the system again in some state ρ^{S}_k at time t_k before finally performing measurements at time t_n.

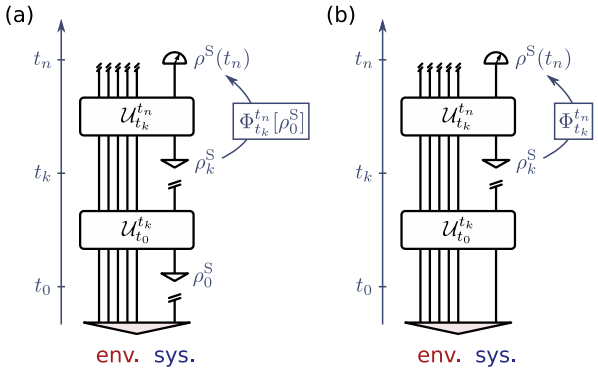

Figure 2.7: Quantum circuits for the measurement of the operational dynamical map $\Phi_{t_k}^{t_n}$. (a) Quantum circuits for the measurement of $\Phi_{t_k}^{t_n}[\rho_0^{\mathrm{S}}]$ conditioned on the preparation of the initial system state ρ_0^{S}. (b) Quantum circuits for the measurement of $\Phi_{t_k}^{t_n}$ for an initially correlated state. In both cases $\Phi_{t_k}^{t_n}$ relates an system input state at time t_k with system output state at time t_n. The map $\Phi_{t_k}^{t_n}$ always constitutes a quantum channel.

Figure 2.7a shows the corresponding quantum circuit. We see that the map $\Phi_{t_k}^{t_n}$ maps the input states at time t_k to the output states at t_n and that these input and outputs are connected through a single quantum circuit. Therefore this map represents a quantum channel and is CPTP. We can also see, however, that the quantum circuit and thus also the map $\Phi_{t_k}^{t_n}$ might depend explicitly on the initial input state ρ_0^{S}, i.e.

$$\rho^{\mathrm{S}}(t_n) = \Phi_{t_k}^{t_n}[\rho_0^{\mathrm{S}}]\left(\rho_k^{\mathrm{S}}\right). \tag{2.11}$$

In terms of the process tensor $\mathcal{T}_{\{0,k,n\}}$ this setup can be expressed by choosing $\mathcal{A}_0 : \rho^{\mathrm{S}} \mapsto \rho_0^{\mathrm{S}}$ and $\mathcal{A}_k : \rho^{\mathrm{S}} \mapsto \rho_k^{\mathrm{S}}$ for which

$$\rho^{\mathrm{S}}(t_n) = \mathcal{T}_{\{0,k,n\}}\left[\mathcal{A}_0, \mathcal{A}_k\right]. \tag{2.12}$$

Finally, we note that the process tensor bears similarity (or is even equivalent) to the Feynman-Vernon influence functional [49, 57, 88], the so called *quantum comb* [89], and the so called *process matrix* [90]. The benefit of the process tensor approach lies not in the mathematical framework alone, but in the insight that the process tensor (or equivalently the quantum comb, etc.) stands in a one-to-one relation to experimentally accessible quantities and is thus a suitable object for the complete characterisation of general open quantum systems. While this is conceptually very useful, from a practical perspective the process tensor suffers from exponential scaling with the number of considered time steps N, which severely limits its applicability in numerical simulations. We can see by virtue of the Choi-Jamiołkowski isomorphism in Fig. 2.3d that this exponential scaling is analogous to the exponential scaling of many-body systems. It thus seems natural that the methods developed to tackle the exponential scaling in many-body systems may be of practical use to dealing with process tensors for the description of general open quantum systems. One such approach is the description of many-body systems in terms of tensor networks. We give a brief introduction to tensor networks in the next section 2.2 and then discuss how these methods can be used to create a numerically efficient representation of the process tensor in section 2.3.

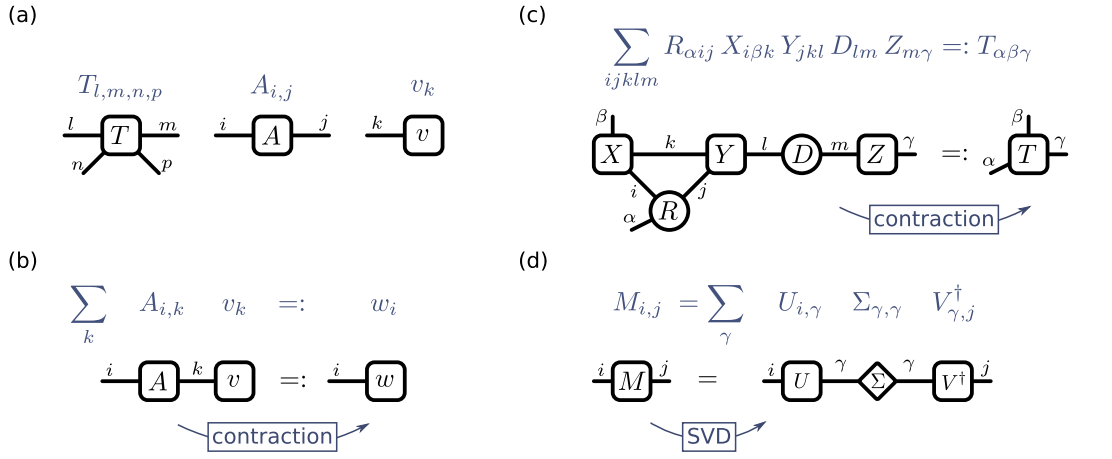

Figure 2.8: Exemplary tensor network diagrams. (a) Tensor diagrams for the 4-rank tensor T, the matrix A, and the vector v. (b) Tensor network representing the contraction of a matrix A and vector v. (c) Tensor network diagram representing the contraction of several 3-rank and 2-rank tensors. (d) Tensor network diagram representing a singular value decomposition (SVD).

2.2. Tensor networks

As pointed out in the previous section process tensors suffer from the same exponential growth as many-body quantum systems. Tensor network methods attempt to address this difficulty by representing large objects such as the total many-body state or the total unitary evolution operator as a collection of many smaller objects that represent the physically most relevant part of the state or operator. In this work, we will use tensor network methods for tackling both many-body quantum systems and general open quantum systems. We thus give a brief introduction to the topic. For a more comprehensive introduction we refer the reader to the review texts by U. Schöllwock [50] and R. Orus [51].

2.2.1. Diagrammatic representation

Let us start by introducing the diagrammatic representation of tensor networks. The mathematical object of a tensor is represented as a square (or possibly any other shape such as a circle or triangle) with several lines—called *legs*—attached to it. For our purposes a tensor is a multidimensional generalisation of a matrix[1]. Each leg represents one index of a tensor. For example, a matrix is represented by a square with two legs (2-rank tensor) and a vector by a square with one leg (1-rank tensor). In general, it matters which leg is which and so the legs are equipped with a label if necessary (see Fig. 2.8a). Joining legs in the diagram represents a multiplication and summation over the dimension of the legs analogous to the a repeated index in the Einstein convention. In Fig. 2.8b we can see that joining one leg of the vector v with one leg of the matrix A gives a 1-rank tensor, i.e. a vector, as expected. The same is also possible for multiple tensors of larger ranks as exemplified in Fig. 2.8c. Legs that join two tensors need to

[1] A mathematically more rigorous definition of a n-rank tensor is: a multilinear map from the tensor product of n vector spaces over the field K to K. The definition as a multidimensional generalisation of a matrix follows for finite dimensional vector spaces after the choice of a basis. It can be shown that the operations performed on tensor networks are independent of this choice.

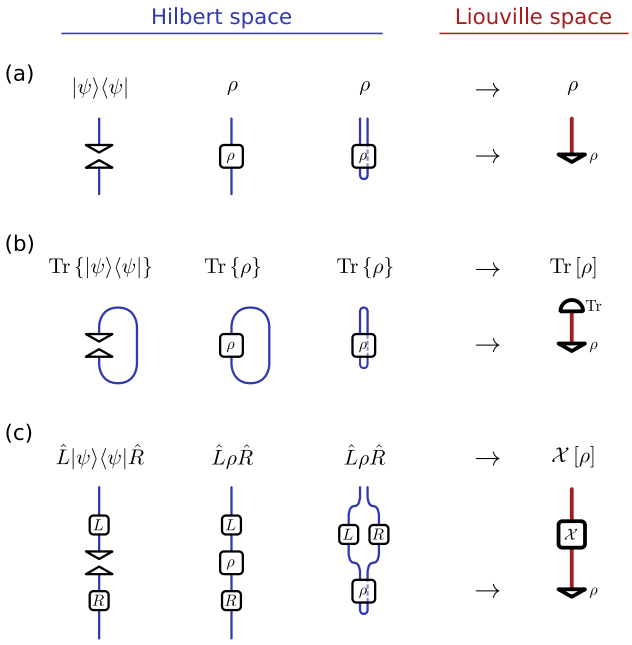

Figure 2.9: Tensor networks for various operations on a quantum state in Hilbert space and Liouville space representations. (a) The tensor network representations of a state. (b) The tensor network representations of the trace of a state. (c) The tensor network representations of an operation on a state. The thin blue lines are legs with the Hilbert space dimension d, whereas the thick red lines have the Liouville space dimension d^2.

have the same dimension on both ends[2]. This process of calculating the resulting tensor from two or more tensors by performing the multiplications and summations is called *contraction*. Legs that are connected to other legs are termed *internal legs*, and legs that are not connected are termed *open legs*.

Tensor networks in Liouville space: Most commonly, tensor networks represent the wave functions of pure states and the unitary operations that act on these wave functions. For the purpose of dealing with open quantum systems we will instead mostly work in Liouville space and draw tensor networks that represent density matrices and so called *super-operators* that map density matrices to density matrices. This results in tensor networks of similar shape, however, with legs of the squared dimension (d^2 instead of d). Figure 2.9 shows a table for a few example tensor networks in both the Hilbert space representation and the Liouville space representation.

2.2.2. Truncated singular value decomposition

Let us assume we want to represent a wave function of a spin chain with N spins. Choosing a basis for a single site $|\phi_n\rangle_{n\in 1,\dots,d}$ allows us to write any wave function $|\psi\rangle$ of

[2] In the more rigorous definition of tensors as multilinear maps, the internal legs must join vector spaces with their covector spaces.

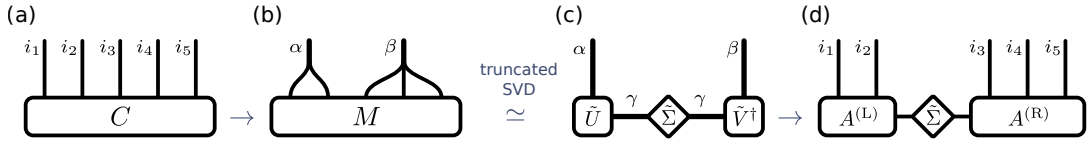

Figure 2.10: Compression of a tensor network representation of a 5-site chain. (a) The full 5-rank tensor C representing a 5-site chain. (b) The matrix M after grouping indices $\alpha := (i_1, i_2)$ and $\beta := (i_3, i_4, i_5)$. (c) The truncated singular value decomposition (SVD) of the matrix M. (d) The compressed tensor network representation of the 5-site chain with the restored indices $i_1 \dots i_5$.

the entire chain[3] as

$$|\psi\rangle = \sum_{i_1,i_2,\dots,i_N}^{d} C_{i_1,i_2,\dots,i_N} |\phi_{i_1}\rangle \otimes |\phi_{i_2}\rangle \otimes \cdots \otimes |\phi_{i_N}\rangle, \tag{2.13}$$

where the d^N coefficients $C_{i_1,i_2,\dots,i_N}$ carry all information of the state. These coefficients constitute a N-rank tensor which we represent in diagrammatic form in Fig. 2.10a. This tensor, however, still scales exponentially with the number of spins N and there is so far no advantage in expressing the state in this form. To represent a state of a spin-1/2 chain with 30 sites like this takes 8 GB of memory and a chain with 50 sites would already take 8192 TB of memory, etc. The essential benefit of tensor network algorithms comes from the idea of approximating large rank tensors like this as a network of many lower rank tensors.

The generic approach to split a large tensor into several smaller tensors is to perform a singular value decomposition (SVD). The SVD of a matrix $M \in \mathbb{C}^{m\times n}$ consists of matrices with mutually orthonormal column vectors[4] $U \in \mathbb{C}^{m\times r}$ and $V \in \mathbb{C}^{n\times r}$, and the diagonal matrix $\Sigma \in \mathbb{R}_+^{r\times r}$, with $r \leq \min(m, n)$ such that $M = U\Sigma V^\dagger$. This decomposition is exact, not unique, and exists for any matrix $M \in \mathbb{C}^{m\times n}$. The values in Σ are called *the singular values of* M, are unique, non-negative, and typically sorted in decreasing order such that $\Sigma_{ii} \geq \Sigma_{kk}$ for $i > k$. Figure 2.8d shows the tensor network diagram of such an SVD.

We can decompose the full spin chain tensor (Fig. 2.10a) into a chain of 2-rank and 3-rank tensors (Fig. 2.11a) by repeated applications of SVDs. To understand this process we start by splitting the chain into two parts: a left part with sites $\{1, \dots, K\}$ and a right part with sites $\{K + 1, \dots, N\}$. For this, we express the total state $|\psi\rangle$ in terms of a basis for the left $|\phi_\alpha^{(\mathrm{L})}\rangle$ and right $|\phi_\beta^{(\mathrm{R})}\rangle$

$$|\psi\rangle = \sum_{\alpha,\beta} M_{\alpha,\beta} |\phi_\alpha^{(\mathrm{L})}\rangle \otimes |\phi_\beta^{(\mathrm{R})}\rangle. \tag{2.14}$$

Here α are the indices that join all left indices $\{i_1, \dots, i_K\}$ and thus run from 1 to d^K. The index β is defined analogously. Because M is a matrix we can perform an SVD, which will yield the matrices $U \in \mathbb{C}^{m\times r}$, $V \in \mathbb{C}^{n\times r}$, and $\Sigma \in \mathbb{R}_+^{r\times r}$, with

[3] The many body wave function need not be made from copies of the same system. We could also consider lattices of systems with different Hilbert spaces. For this we would choose a different basis for each site.

[4] The matrices $U \in \mathbb{C}^{m\times r}$ and $V \in \mathbb{C}^{n\times r}$ can be extended to be unitary matrices $\bar{U} \in \mathbb{C}^{m\times m}$ and $\bar{V} \in \mathbb{C}^{n\times n}$ by attaching sets of basis vectors as columns for the missing subspaces.

$m = d^K$, $n = d^{N-K}$, and $r \leq \min(d^K, d^{N-K})$ as described above. We express this diagrammatically in Fig. 2.10(b-c).

Because the column vectors of U and V are orthonormal, their application to the left and right basis vectors yields sets of orthonormal states $|\varphi_\gamma^{(\mathrm{L})}\rangle$ and $|\varphi_\gamma^{(\mathrm{R})}\rangle$ with $\gamma \in \{1, \ldots, r\}$. Because Σ is a diagonal matrix we can express the total state as

$$|\psi\rangle = \sum_\gamma \sigma_\gamma \, |\varphi_\gamma^{(\mathrm{L})}\rangle \otimes |\varphi_\gamma^{(\mathrm{R})}\rangle, \tag{2.15}$$

which can be identified as the Schmidt decomposition of the state $|\psi\rangle$, with $\sigma_\gamma := \Sigma_{\gamma\gamma}$. For a normalised state the sum of the squared singular values must be unity, i.e. $\sum_\gamma \sigma_\gamma^2 = 1$. We can see that the singular values λ_γ have a physical meaning: If only one singular value is non-zero then the total state can be written as a product state, which amounts to an unentangled state. If all singular values are non-zero and equal to each other then $|\psi\rangle$ is a maximally entangled state. Most generic states are however in neither category but instead show some distribution of larger and smaller singular values. In such cases one can approximate the total state by discarding the smallest singular values, i.e. one only keeps the $\chi \leq r$ largest singular values. For this one replaces the matrices U, V, and Σ with the truncated matrices $\tilde{U} \in \mathbb{C}^{m\times\chi}$, $\tilde{V} \in \mathbb{C}^{n\times\chi}$, and $\tilde{\Sigma} \in \mathbb{R}_+^{\chi\times\chi}$. In this context, such a truncation of singular values may be understood as the neglect of weakly entangled contributions to the state. More generally (and regardless of what the matrix M represents from a physical perspective) one may understand this as an approximation of the matrix M with $\tilde{M} = \tilde{U}\tilde{\Sigma}\tilde{V}^\dagger$ for which $\left\|M - \tilde{M}\right\|_\mathrm{F} = \left\|\Sigma - \tilde{\Sigma}\right\|_\mathrm{F} = \left\|\Sigma - \tilde{\Sigma}\right\|_2$, where $\|\cdot\|_\mathrm{F}$ denotes the Frobenius norm and $\|\cdot\|_2$ denotes the 2-norm. After the truncation process, we recover the original open legs by splitting the indices α into $\{i_1, \ldots, i_K\}$ and β into $\{i_{K+1}, \ldots, i_N\}$ as shown diagrammatically in Fig. 2.10(c-d). The internal leg connecting the two tensors that represent the left and right part of the chain is call *the bond*, and its dimension χ is called *the bond dimension*.

This process of combining indices, performing an SVD, truncating the singular values, and finally splitting the indices again could now be performed on the resulting left and right parts of the chain and so on, to then eventually yield a tensor network of the form shown in Fig. 2.11a. In practice, however, one would like to avoid dealing with the full tensor C throughout the computation. Thus, most tensor network methods start the computation with an initial state that allows for a direct representation as a tensor network with many low rank tensors (such as a product state) and then evolves this state while maintaining its general decomposed form. Maintaining the decomposed form while keeping the bond dimensions low typically requires the truncation of singular values like explained above. The bond dimensions then enter the computation as a convergence parameter. While there exist some rigorous statements about the accuracy of such computations for specific scenarios [51], in practice, one performs a variational analysis to estimate the accuracy of the computation. For this, one repeats the computation with a series of increasing bond dimensions until the physical quantity of interest ceases to show any significant change.

2.2.3. Matrix products (MPS/MPO)

The tensor networks shown in Fig. 2.11 are said to be in the form of a *matrix product state* (MPS) [91, 92]. This form derives its name from interpreting the 3-rank tensors A_n

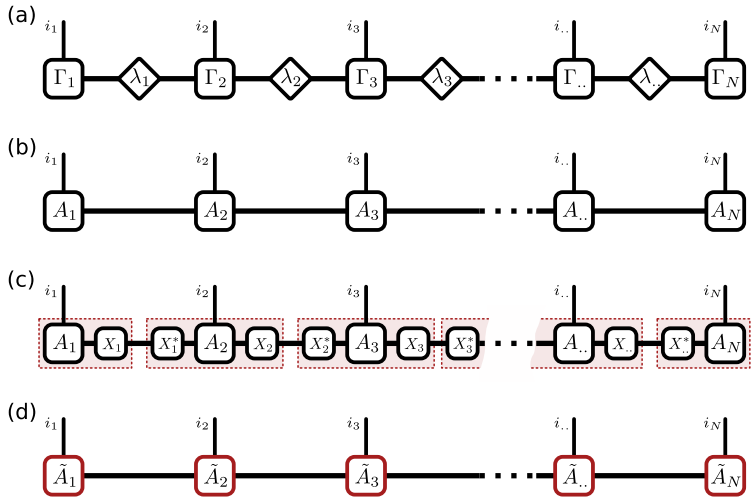

Figure 2.11: A matrix product state (MPS) for N sites in different gauges. (a) An MPS in Vidal gauge (given that the λ matrices are diagonal and correspond to the Schmidt coefficients). (b) The same MPS as in (a), but in a different gauge with $A_n = \Gamma_n \lambda_n$. (c) The same MPS as in (b), but with inserted identities $\mathbb{1} = X_1 X_1^* = \ldots = X_N X_N^*$. (d) The same MPS as in (b), but in a different gauge with $\tilde{A}_n = X_{n-1}^* A_n X_n$.

in Fig. 2.11b as a collection of d_n matrices $\left\{A_n^{i_n}\right\}_{i_n \in \{1,\ldots,d_n\}}$, where d_n is the dimension of the local Hilbert space at site n. The coefficients of the total chain state with respect to a choice of local basis states for a specific index $\vec{i} = (i_1, i_2, \ldots, i_N)$ can be expressed as the product of these matrices

$$\psi_{\vec{i}} = \prod_{n=1}^{N} A_n^{i_n}, \tag{2.16}$$

where the first and last factors $A_1^{i_1}$ and $A_N^{i_N}$ are in fact row and column vectors, respectively. Matrix product states have proven to be particularly powerful in representing states of 1D many-body systems when the correlations among the sites decay rapidly with distance. Intuitively, non-negligible long range correlations across the chain would correspond to singular values that cannot be truncated, which would make a large bond dimension necessary to represent the state accurately.

The representation of a many-body state as an MPS of the form in Fig. 2.11a or Fig. 2.11b is not unique. One may, for example, contract the λ_n matrices into the neighbouring Γ_n matrices by replacing: $\Gamma_n \rightsquigarrow A_n = \Gamma_n \lambda_n$ and $\lambda_n \rightsquigarrow \tilde{\lambda}_n = \mathbb{1}$. In this case the $\tilde{\lambda}_n$ matrices could be omitted entirely, as shown in Fig. 2.11b. More generally, any internal leg of a tensor network can be replaced by the application of some invertible matrix X and its inverse X^{-1} as shown in Fig. 2.11c, resulting in different representations of the same total tensor. Specific choices of the representation are called *canonical forms* or *gauges* in the literature [51]. This is an important aspect of tensor networks because most truncation protocols only act on pairs of neighbouring sites. Depending on the gauge, the tensors of two neighbouring sites might reveal or conceal the weak correlations between sites further down the left and right parts of the chain and thus might lead to a more or less efficient compression of the data. A particularly intuitive canonical MPS form is the so called *Vidal form* [93], sometimes simply referred to as *the canonical form*. An MPS is in Vidal form if at each bond K the matrix λ_K is diagonal

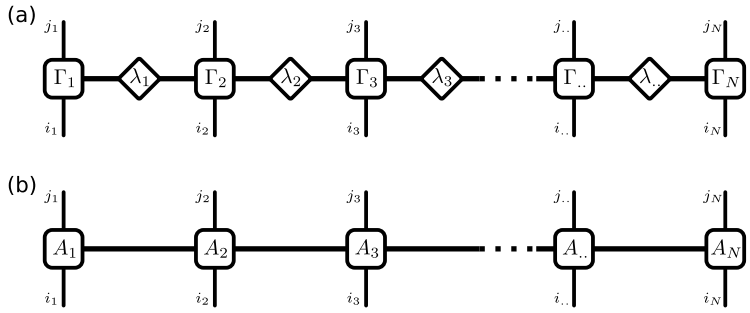

Figure 2.12: A matrix product operator (MPS) for N sites in different gauges. (a) An MPO in Vidal gauge (given that the λ matrices are diagonal and correspond to the singular values of the entire left and right part of the tensor network). (b) The same MPO as in (a), but in a different gauge with $A_n = \Gamma_n \lambda_n$.

and corresponds to the Schmidt coefficients of the Schmidt decomposition of the entire chain into sites $\{1, \ldots, K\}$ and $\{K+1, \ldots, N\}$. In this case the λ matrices that contain the singular values are unique and allow for the physical interpretation as explained in the previous section.

The idea to represent multi-site states in MPS form can be generalised to chains of operators and even higher rank tensors. For chains of operators, the corresponding tensor network as shown in Fig. 2.12 is said to be of *matrix product operator* form (MPO) [94]. We will see in section 2.3 that the process tensor may be brought into MPO form in Liouville space, i.e. the process tensor is a chain of (possibly correlated) super-operators.

There exist numerous tensor network methods that employ matrix product states and matrix product operators in various forms, such as the *density matrix renormalisation group* (DMRG) [95, 96], the *time dependent variational principle* (TDVP) [97, 98], and *time evolving block decimation* (TEBD) [93, 99–101]. Time evolving block decimation is a method that is particularly useful for the study of the explicit time evolution of a chain of systems governed by a Hamiltonian with only on-site and nearest neighbour interactions. In preparation for chapter 4—in which we extend this method to chains of general open quantum systems—we now give a brief introduction to this widely applied approach.

2.2.4. Time evolving block decimation

The time evolving block decimation (TEBD) method evolves an MPS in Vidal form in small discrete time steps δt by applying propagators to neighbouring sites [93, 99]. Suppose we have a total Hamiltonian for a chain of N sites in the form

$$\hat{H}_{\text{chain}} = \sum_{n=1}^{N} \hat{H}_n + \sum_{n=1}^{N-1} \hat{J}_{n,n+1}, \tag{2.17}$$

where the on-site Hamiltonians $\hat{H}_n$ act only on site n and the nearest neighbour terms $\hat{J}_{n,n+1}$ act only on two neighbouring sites n and $n+1$. As a first step we absorb the on-site Hamiltonians into the nearest neighbour terms such that

$$\hat{H}_{\text{chain}} = \sum_{n=1}^{N-1} \hat{K}_{n,n+1}, \tag{2.18}$$

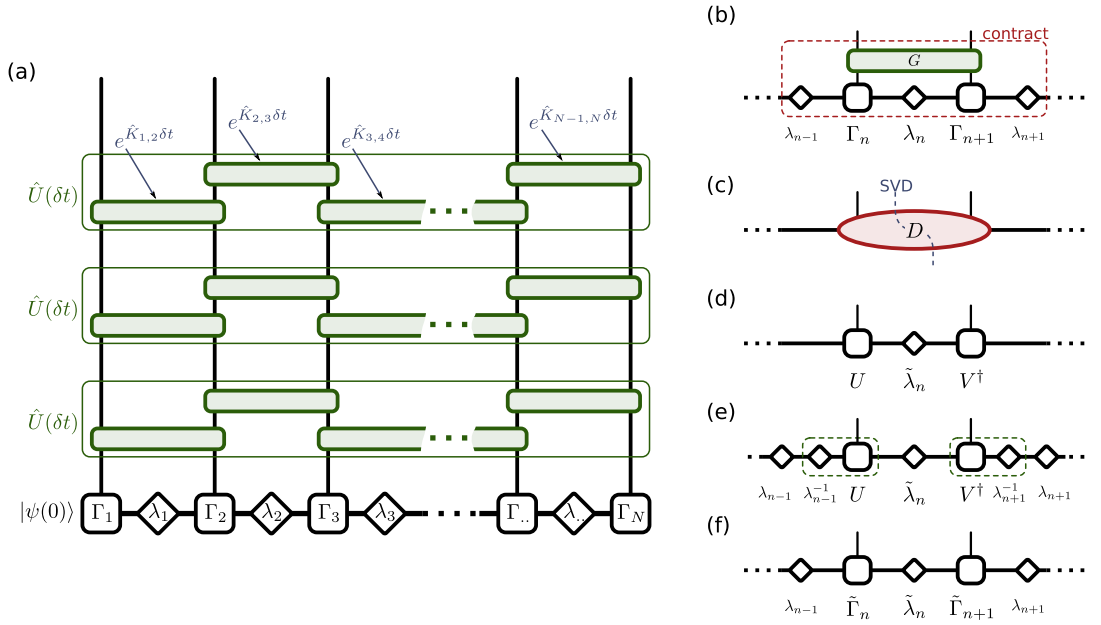

Figure 2.13: Tensor networks for the construction and contraction the TEBD method. (a) The full TEBD tensor network for three time steps of an N-site chain. (b-f) Contraction and decomposition sequence for the application of a two-site gate G.

with

$$\hat{K}_{n,n+1} := \hat{J}_{n,n+1} + \begin{cases} \hat{H}_1 + \frac{1}{2}\hat{H}_2 & \text{for } n = 1 \\ \frac{1}{2}\hat{H}_{N-1} + \hat{H}_N & \text{for } n = N-1 \\ \frac{1}{2}\hat{H}_n + \frac{1}{2}\hat{H}_{n+1} & \text{otherwise.} \end{cases} \tag{2.19}$$

We can then express the entire unitary propagator for a time step δt as

$$\hat{U}(\delta t) = \exp\left(i\hat{H}_{\text{chain}}\delta t\right) = \exp\left(i\sum_{n=1}^{N-1}\hat{K}_{n,n+1}\delta t\right). \tag{2.20}$$

A Suzuki-Trotter expansion [102] of the propagator to first order in δt yields

$$\hat{U}(\delta t) = \prod_{n\,\text{odd}} e^{\hat{K}_{n,n+1}\delta t} \prod_{p\,\text{even}} e^{\hat{K}_{p,p+1}\delta t} + \mathcal{O}(\delta t^2). \tag{2.21}$$

We may neglect the higher order terms $\mathcal{O}(\delta t^2)$ whenever the time step δt is chosen small enough such that for all $n \in \{1, \ldots, N-2\}$:

$$\frac{1}{2}\left[\hat{K}_{n,n+1}, \hat{K}_{n+1,n+2}\right]\delta t^2 \ll \left(\hat{K}_{n,n+1} + \hat{K}_{n+1,n+2}\right)\delta t. \tag{2.22}$$

Because each operator $e^{\hat{K}_{n,n+1}\delta t}$ in Eq. (2.21) acts only on neighbouring sites n and $n+1$, we can approximate the total unitary propagator as a product of two-body gates. Figure 2.13a shows the full tensor network for a TEBD simulation for three time steps. It represents the state of the chain after three time steps for an initial state $|\psi\rangle$ expressed as an MPS in Vidal form. To compute the final chain state explicitly the tensors need to be contracted. A direct contraction of the propagators with the initial state, however, would not conserve the representation of the state in MPS form and

lead to an exponentially growing memory requirement with every time step. Therefore, the TEBD method involves a specific sequence of operations to ensure that the state at later times continues to be an MPS in Vidal form. Figures 2.13(b-f) show the operations for applying a two body gate $G = e^{\hat{K}_{n,n+1}\delta t}$, which are:

(b-c) Contraction:
$D := \lambda_{n-1}\Gamma_n G \lambda_n \Gamma_n \lambda_{n+1}$

(c-d) Truncated singular value decomposition:
$U\Sigma V^\dagger :\simeq D$ and $\tilde{\lambda}_n := \Sigma$

(d-e) Insert identities:
$\lambda_{n-1}\lambda_{n-1}^{-1} = \mathbb{1}$ and $\lambda_{n+1}^{-1}\lambda_{n+1} = \mathbb{1}$

(e-f) Contraction:
$\tilde{\Gamma}_n := \lambda_{n-1}^{-1} U$ and $\tilde{\Gamma}_{n+1} := V^\dagger \lambda_{n+1}^{-1}$

This sequence of operations is local, i.e. it only involves tensors of the chain at sites n and $n+1$, and it conserves the Vidal form of the MPS. Due to the pairwise independence of the two-body gates in each layer (odd and even bond layers) this algorithm is also well suited for high performance parallel computing.

Finally we mention that besides the use of higher order Suzuki-Trotter expansions in Eq. (2.21), TEBD can be generalised in various ways. The TEBD method has been generalised to tackle chains with closed boundary conditions [101], chains with long range interaction terms [103], and chains of "Markovian" open quantum systems [100], i.e. systems whose dynamics is governed by a GKSL master equation. In addition to these generalisations, we will introduce a novel method in chapter 4 that generalises TEBD to chains of *general* open quantum systems, i.e also including systems whose dynamics might not admit a description with a GKSL master equation.

2.3. The process tensor in MPO form

While the process tensor is a versatile object for the description of general open quantum systems it generically scales exponentially with the number of time steps which impedes its numerical applicability. In this section we will show how to efficiently represent and compute process tensors for a large class of open quantum systems by employing tensor network methods. This opens up a wide range of potential applications that may benefit from the flexibility of the process tensor while keeping the computational requirements at a moderate level.

The key idea is to find an efficient tensor network representation of the process tensor for a given interaction Hamiltonian. The choice of a suitable tensor network relies on the internal structure of the process tensor. A process tensor may have an efficient representation as an MPO (i.e. showing only linear scaling with the number of time steps) if the correlations over time have a finite range. This is analogous to 1D many-body systems for which an MPS representation is suitable if the spatial correlations are localised to some finite distance. In many cases, it is thus possible to systematically discard negligible correlations and express the process tensor in a matrix product operator form (PT-MPO). For different environments different methods for the construction of a PT-MPO exist [45, 49, 52–58, 104]. For linearly coupled Gaussian bosonic environments one can directly construct a tensor network that yields a PT-MPO [49, 52, 54, 104].

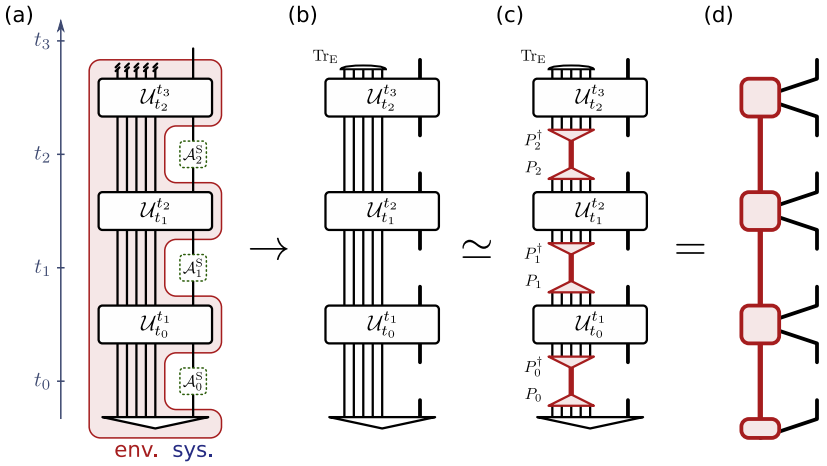

Figure 2.14: Tensor network construction of a PT-MPO. (a) A quantum circuit with a sequence of three interventions. (b) A tensor network re-interpretation of the quantum circuit, excluding the interventions. (c) Application of projection operators $P_n P_n^\dagger$ onto the physically most relevant environment subspace. (d) A process tensor in MPO form.

Other approaches allow the construction of PT-MPOs for any environment that can be approximated by a finite set of independent degrees of freedom [55, 57], or allow an explicit tensor network representation [45, 53, 56, 58]. It is also possible to construct PT-MPOs directly from experimental measurements [28].

Before we briefly discuss some of these methods below, we first comment on a few properties of process tensor representations in general and the MPO representation in particular. As mentioned in section 2.1.4 we can interpret the quantum circuit in Fig. 2.14a as a tensor network. The full process tensor is then a $(2N+1)$-rank tensor where each leg is of the dimension of the Liouville space d^2. The representation shown in Fig. 2.14b is readily in an MPO form that consists of the total Liouville propagators for each time interval. The bond dimension of this particular MPO representation is the full Liouville space of the environment, which in most cases is prohibitively large for any practical numerical application. Conceptually, a more efficient representation of the process tensor may be thought to be the MPO that results from inserting suitable isometries P_n and $P_n^\dagger$ which project the total environment Liouvillian space to the most relevant subspace as shown in Fig. 2.14c. The isometries $P_n \in \mathbb{C}^{E\times\chi_n}$ and $P_n^\dagger \in \mathbb{C}^{\chi_n\times E}$ must have the property that $P_n^\dagger P_n = \mathbb{1}_{\chi_n}$, where E is the dimension of the total environment Liouville space and χ_n is the dimension of the relevant subspace. From a practical perspective however, this is not a viable approach because it would still require the explicit representation of the total Liouville propagator.

The Choi representation of the process tensor as a many-body state (see Fig. 2.3d) is equivalent to the direct approach of reinterpreting the quantum circuit as a tensor network up to appropriate reordering of legs and a rescaling of the input legs with a factor $1/d$. This is because in a tensor network interpretation the two body state ψ^+ can be rewritten as an identity matrix of dimension $d^2 \times d^2$ divided by d, i.e. $\psi^+ = \mathbb{1}_{d^2}/d$. Because the Choi representation is a many body state with unity trace, we expect that the total trace of the direct process tensor representation is d^N. In order to keep the numbers in all tensors involved at the order 1 it is thus advisable to rescale all tensors for the purpose of the computation with the factor $1/d$ to fit the Choi representation.

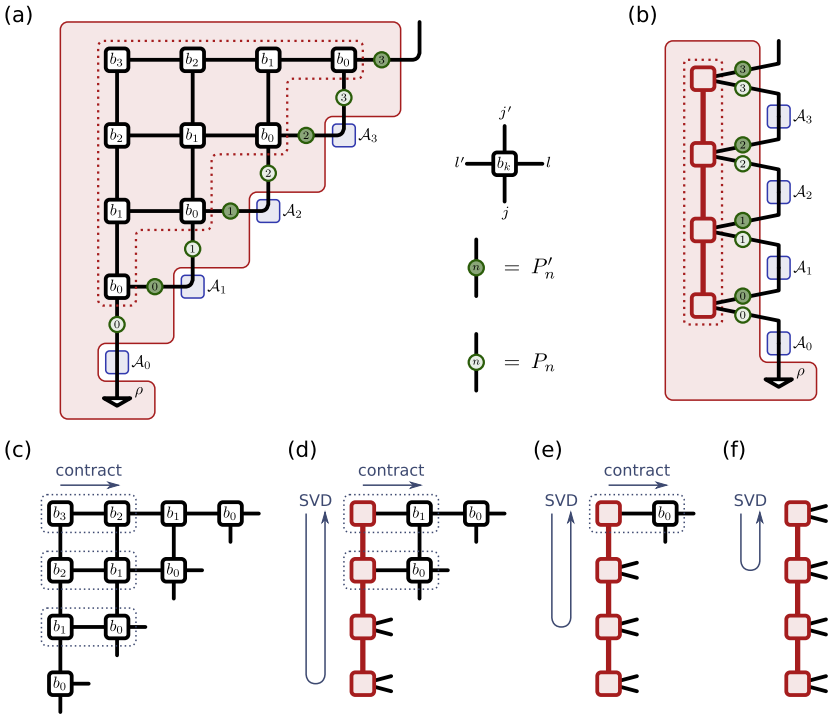

Figure 2.15: Tensor networks for the process tensor time evolving matrix product operator (PT-TEMPO) method. (a) Tensor network representation of Eq. (2.29) for the reduced density matrix after 4 time steps, with additionally inserted system interventions $\mathcal{A}_n$. (b) Tensor network for the reduced density matrix after 4 time steps employing the PT-MPO of $\tilde{\mathcal{T}}_{0:4}$ (encircled by the red dotted line). (c-f) Contraction and decomposition sequence for the computation of the PT-MPO of $\tilde{\mathcal{T}}_{0:4}$.

However, because the direct representation is more suitable for most applications we will always consider the direct representation (and not the Choi representation) unless explicitly stated otherwise.

2.3.1. Time evolving matrix product operator

The time evolving matrix product operator (TEMPO) method is a tensor network method for simulating the reduced dynamics of open quantum systems with Gaussian bosonic environments [47, 52]. It is based on the Feynman-Vernon influence functional [88] and, like the quasi adiabatic propagator path integral method (QUAPI) [43, 44], uses an augmented density tensor to capture memory effects of the bath. The TEMPO method can be modified to yield the full process tensor by reordering its contraction sequence. In the following we explain the construction of the TEMPO tensor network as presented in the methods sections of reference [47] and then present a contraction strategy to obtain the PT-MPO as suggested by Jørgensen and Pollock in reference [49].

Construction of the TEMPO tensor network: The most general form of the total Hamiltonian that we consider is (in units of $\hbar = 1$)

$$\hat{H}(t) = \hat{H}^{\mathrm{S}}(t) + \underbrace{\hat{S}\sum_k \left(g_k \hat{a}_k + g_k^* \hat{a}_k^\dagger\right)}_{\hat{H}^{\mathrm{I}}} + \underbrace{\sum_k \omega_k \hat{a}_k^\dagger \hat{a}_k}_{\hat{H}^{\mathrm{E}}}, \tag{2.23}$$

where $\hat{a}_k$ ($\hat{a}_k^\dagger$) are bosonic creation (annihilation) operators. The environment interaction is fully characterised by the system coupling operator $\hat{S} \in \mathcal{B}\left(\mathcal{H}^{\mathrm{S}}\right)$ and the spectral density $J(\omega)$, which is defined as

$$J(\omega) = \sum_k |g_k|^2 \delta(\omega - \omega_k). \tag{2.24}$$

The exact dynamics of the total system is given by the von Neumann equation

$$\frac{\mathrm{d}}{\mathrm{d}t}\rho(t) = -i\left[\hat{H}, \rho(t)\right] = \mathcal{L}\rho(t) \tag{2.25}$$

and its formal solution is

$$\rho(t) = \overleftarrow{\mathbf{T}} e^{\int_0^t \mathrm{d}t' \mathcal{L}(t')} \rho(0), \tag{2.26}$$

where $\mathcal{L}(t) \cdot = -i\left[\hat{H}(t), \cdot\right]$ is the Liouvillian super operator for $\hat{H}(t)$. We can split up the total time evolution into N time steps of length $\delta t = t/N$ and consider only the reduced system state by performing the partial trace Tr_{E} over the environment degrees of freedom

$$\rho^{\mathrm{S}}(t) = \mathrm{Tr}_{\mathrm{E}}\left\{\overleftarrow{\mathbf{T}} e^{\int_0^t \mathrm{d}t' \mathcal{L}(t')} \rho(0)\right\} = \mathrm{Tr}_{\mathrm{E}}\left\{\prod_{n=0}^{N-1}\left(\overleftarrow{\mathbf{T}}\, e^{\int_{t_n}^{t_{n+1}} \mathrm{d}t' \mathcal{L}(t')}\right)\rho(0)\right\}, \tag{2.27}$$

where $\overleftarrow{\mathbf{T}}$ denotes time ordering from right to left. Next, we approximate the propagator for a time step δt by a symmetrised second order Trotter splitting [102] as

$$\overleftarrow{\mathbf{T}} e^{\int_{t_n}^{t_{n+1}} \mathrm{d}t' \mathcal{L}(t')} = \left(\overleftarrow{\mathbf{T}} e^{\int_{t_{n+1/2\delta t}}^{t_{n+1}} \mathrm{d}t' \mathcal{L}^{\mathrm{S}}(t')}\right)\left(e^{\delta t \mathcal{L}^{\mathrm{IE}}}\right)\left(\overleftarrow{\mathbf{T}} e^{\int_{t_n}^{t_{n+1/2\delta t}} \mathrm{d}t' \mathcal{L}^{\mathrm{S}}(t')}\right) + \mathcal{O}(\delta t^3), \tag{2.28}$$

where the Liouvillians $\mathcal{L}^{\mathrm{S}}(t)$ and $\mathcal{L}^{\mathrm{IE}}$ correspond to the system $\hat{H}^{\mathrm{S}}(t)$ and the environment-interaction parts $\hat{H}^{\mathrm{I}} + \hat{H}^{\mathrm{E}}$, respectively.

To continue, we assume that the initial state is a product state $\rho(0) = \rho_0^{\mathrm{S}} \otimes \rho_0^{\mathrm{E}}$, with an Gaussian initial environment state ρ_0^{E}, which we choose to be the thermal state at temperature T for simplicity. We work in a basis such that $\hat{S}_{\alpha,\beta} = \delta_{\alpha,\beta}\hat{S}_{\alpha,\beta}$ is diagonal and we write operators and density matrices in Liouville space.

Inserting Eq. (2.28) into Eq. (2.27), omitting the higher order $\mathcal{O}(\delta t^3)$ terms, and performing the trace over the environment leads to a discretised version of the Feynman-Vernon influence functionals [52]. With this, we can write down the expression for the system density matrix at time t explicitly as

$$\rho_{j_N}(t) = \sum_{j_0, j_1, \ldots j_{N-1}}\left[\prod_{n=1}^{N-1} P'_n(j_{n+1}, j_n)\left(\prod_{k=0}^{n-1} I_k(j_n, j_{n-k})\right) P_n(j_n, j_{n-1})\right]\rho_{j_0}(0), \tag{2.29}$$

where $I_k(j, j')$ are the influence functions and $P_{j,j'}$ is the system propagator

$$P'_n(j, j') := \left[\overleftarrow{\mathbf{T}} e^{\int_{t_n+\delta t/2}^{t_n+\delta t} \mathrm{d}t' \mathcal{L}^{\mathrm{S}}(t')}\right]_{j,j'} \quad \text{and} \quad P_n(j, j') := \left[\overleftarrow{\mathbf{T}} e^{\int_{t_n}^{t_n+\delta t/2} \mathrm{d}t' \mathcal{L}^{\mathrm{S}}(t')}\right]_{j,j'}. \tag{2.30}$$

The influence functions are defined as

$$I_k(j, j') := \exp\left[-\mathcal{S}_j^-\left(\mathcal{S}_{j'}^- \mathrm{Re}\left[\eta_k\right] + i\mathcal{S}_{j'}^+ \mathrm{Im}\left[\eta_k\right]\right)\right], \tag{2.31}$$

with

$$\eta_k = \begin{cases} \int_0^{\delta t} \mathrm{d}t' \int_0^{t'} \mathrm{d}t'' C(t'-t'') & k = 0 \\ \int_{k\delta t}^{(k+1)\delta t} \mathrm{d}t' \int_0^{\delta t} \mathrm{d}t'' C(t'-t'') & k \neq 0 \end{cases} \tag{2.32}$$

and the environment correlation function

$$C(t) = \int_0^\infty \mathrm{d}\omega J(\omega) \left[\coth\left(\frac{\omega}{2T}\right) \cos(\omega t) - i \, \sin(\omega t) \right]. \tag{2.33}$$

The super-operators $\mathcal{S}^- \cdot := \left[\hat{S}, \cdot\right]$ and $\mathcal{S}^+ \cdot := \left\{\hat{S}, \cdot\right\}$ are the commutator and anti-commutator for the coupling operator $\hat{S}$, respectively. Because the basis is chosen such that $\hat{S}$ is diagonal, the super-operators $\mathcal{S}^\pm$ are diagonal too, and $S_j^\mp := [S^\mp]_{j,j}$ denote these diagonal entries.

To express Eq.(2.29) as a tensor network we define the tensors b_k to be

$$[b_k]_{j,j',l,l'} := I_k(j,j')\delta_{j,l}\delta_{j',l'} \tag{2.34}$$

and draw them as indicated in Fig. 2.15a. With this definition it is straightforward to check that the tensor network depicted in Fig. 2.15a represents Eq. (2.29). The b_k tensors at the left and top of the diagram are defined without the l respective l' legs for which we simply omit the corresponding Kronecker deltas $\delta_{j,l}$ and $\delta_{j',l'}$ in definition (2.34). With this we have successfully constructed a tensor network that represents the system density matrix at time t. The original TEMPO algorithm suggests that this tensor network is contracted line by line while performing horizontal SVD truncation sweeps [47]. For many physically relevant environments the correlation function $C(t)$ rapidly decays to zero for times longer than some maximal correlation time $\tau_{\max}$. In such cases one may omit all b_k tensors in the tensor network for which $k > \tau_{\max}/\delta t =: K_{\max}$. Employing the zip-up algorithm introduced in [105] this method can be implemented with a total computational cost scaling as $\mathcal{O}(N\,\chi^3 D^3\,K_{\max})$, where χ is the bond dimension of the boundary MPS during contraction and D is the Liouville space dimension.

Extraction of the process tensor: To see how this tensor network links to the process tensor we include additional interventions $\mathcal{A}_n$ to the picture, which we draw as blue squares in Fig. 2.15a. The tensor network in Fig. 2.15a now represents the final state $\rho^{\mathrm{S}}(t_N)$ for any intervention sequence $\mathbf{A}_{0:N-1}$. We know from section 2.1.4 that the process tensor is the unique multilinear map with this property. We can thus conclude that the tensor network within the red shaded area in Fig. 2.15 (excluding the interventions $\mathcal{A}_0, \mathcal{A}_1, \ldots$) *must* be a representation of the desired process tensor $\mathcal{T}_{0:N}$.

As we will see later, it is often advantageous to consider the slightly smaller part of this tensor network shown as dotted area in Figs. 2.15a and 2.15b, which excludes the initial state ρ_0^{S} and the system propagators P_n and P'_n. This corresponds to the process tensor $\tilde{\mathcal{T}}_{0:N}$ for an initially uncorrelated state and a total Hamiltonian $\tilde{H} = \hat{H}^{\mathrm{I}} + \hat{H}^{\mathrm{E}}$ without any contribution from the system Hamiltonian. From this perspective the final state is then

$$\rho^{\mathrm{S}}(t_N) = \mathcal{T}_{0:N}\Big[\{\mathcal{A}_0, \mathcal{A}_1, \ldots, \mathcal{A}_{N-1}\}\Big] = P'_{N-1}\tilde{\mathcal{T}}_{0:N}\Big[\{\tilde{\mathcal{A}}_0, \tilde{\mathcal{A}}_1, \ldots, \tilde{\mathcal{A}}_{N-1}\}\Big], \tag{2.35}$$

with $\tilde{\mathcal{A}}_n = P_n \circ \mathcal{A}_n \circ P'_{n-1}$ and $\tilde{\mathcal{A}}_0 : \rho^{\mathrm{S}} \mapsto \mathcal{A}_0\left[P_0\left(\rho_0^{\mathrm{S}}\right)\right]$. This means that the evolution due to the system part of the Hamiltonian can be realised as a discrete set of interventions

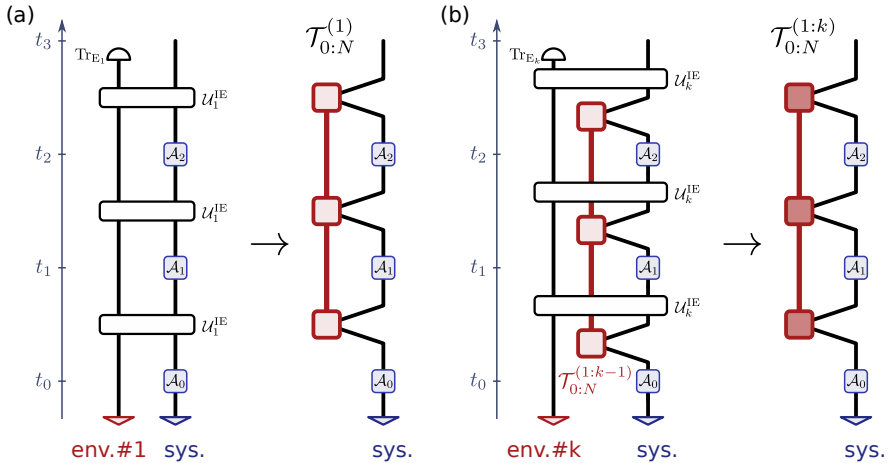

Figure 2.16: Tensor networks for the automatic compression of environments (ACE). (a) Tensor network construction for a PT-MPO of a single environment. (b) Tensor network construction of a PT-MPO for k environments given the PT-MPO for $k-1$ environments.

when the time steps δt are chosen small enough such that the higher order terms in Eq. (2.28) can be neglected.

To compute $\tilde{\mathcal{T}}_{0:N}$ from the tensor network shown in Fig. 2.15c, Jørgensen and Pollock suggest to contract the network column by column with appropriate SVD sweeps during the process [49]. We depict this procedure graphically in Figs. 2.15(c-f). This algorithm scales similarly to the original TEMPO method as $\mathcal{O}(N\,\chi^3 D^3\,K_{\max})$, where χ is the bond dimension of the PT-MPO. Both the original TEMPO and the modified process tensor TEMPO (PT-TEMPO) are available as part of our open source python package OQuPy [104].

2.3.2. Automatic compression of environments

While the TEMPO method is restricted to Gaussian bosonic baths, an alternative method, called *automatic compression of environments* (ACE), allows the construction of PT-MPOs for any environment that can be approximated by a finite set of small independent parts [55]. ACE has been used to calculate PT-MPOs for bosonic environments with non-Gaussian initial states as well as for fermion, spin baths and combinations thereof.

The key idea of ACE is to construct the process tensors for each environment part individually before combining them into one PT-MPO. For this the Hamiltonian must be of the form

$$\hat{H}(t) = \hat{H}^{\mathrm{S}}(t) + \sum_{k}^{K} \left(\hat{H}_k^{\mathrm{I}} + \hat{H}_k^{\mathrm{E}} \right), \tag{2.36}$$

where $\hat{H}_k^{\mathrm{I}} \in \mathcal{B}\left(\mathcal{H}^{\mathrm{S}} \otimes \mathcal{H}_k^{\mathrm{E}}\right)$ and $\hat{H}_k^{\mathrm{E}} \in \mathcal{B}\left(\mathcal{H}_k^{\mathrm{E}}\right)$ are the interaction and environment Hamiltonians of the k^{th} environment. We assume that the Hilbert space dimension $d_k = \dim\left(\mathcal{H}_k^{\mathrm{E}}\right)$ for each environment is small or can be truncated to some small effective dimension. Given that the system Hilbert space dimension is small as well (i.e. allowing exact numerical diagonalisation) it is straight forward to explicitly construct the propagators $\mathcal{U}_k^{\mathrm{IE}} = \exp\left(\mathcal{L}_k^{\mathrm{IE}} \delta t\right)$, with $\mathcal{L}_k^{\mathrm{IE}} \cdot = \left[\hat{H}_k^{\mathrm{I}} + \hat{H}_k^{\mathrm{E}}, \cdot\right]$. In order to obtain the process

tensor $\tilde{\mathcal{T}}_{0:N}$ for the total Hamiltonian excluding the pure system part $\tilde{H} = \hat{H}(t) - \hat{H}^{\mathrm{S}}(t)$, we start by constructing the process tensor $\mathcal{T}^{(1)}_{0:N}$ for the first environment as shown in Fig. 2.16a. For this, one constructs the appropriate tensor network (including the environment's initial state and trace operation) and performs SVD truncations to obtain a compressed PT-MPO. Then, one sequentially includes all other environments yielding PT-MPOs for $\mathcal{T}^{(1)}_{0:N} \to \mathcal{T}^{(1:2)}_{0:N} \to \mathcal{T}^{(1:3)}_{0:N} \to \cdots \to \mathcal{T}^{(1:K)}_{0:N} = \tilde{\mathcal{T}}_{0:N}$ as shown in Fig.2.16b. For more details on this method we refer the reader to reference [55].

With these methods we are prepared to construct PT-MPOs for a large range of different environments. In the rest of this thesis we will employ these PT-MPOs in various different scenarios.

Chapter 3

Optimal Control of General Open Quantum Systems

Equipped with a versatile set of tools for the theory of open quantum systems we now turn to one of the primary fields of its application: quantum information technology. The protocols of quantum information applications often consider a closed quantum system as the ideal scenario [72]. Physical implementations of these protocols are however never truly isolated and thus the influence of the environment has to be taken into account. The performance of most quantum applications crucially hinges on how close the physical implementation reflects the ideal closed scenario. Even a slight fidelity improvement of the quantum protocols can lead to a considerable increase in performance.

There exist various approaches to improve the fidelity of quantum information applications, such as the design of particularly well isolated systems [106–108], the use of topologically protected states [109, 110], and the application of quantum error correction protocols [111]. Optimal control theory augments these approaches by searching for protocols that achieve the highest fidelity of a process for a given experimental setup [59, 60]. For this, it is necessary to be able to accurately compute the dynamics of the system under the influence of the environment. Most of the research on control for open quantum systems has been carried out in a Markovian limit where one assumes a weak system-environment coupling and environment correlations that are short compared to the timescale of the system evolution. However, in many solid-state devices and other systems these assumptions break down [16–19, 112] and a non-Markovian description becomes necessary. Furthermore, it has been shown that non-Markovian effects can, in fact, improve the fidelity of quantum operations due to the possible information backflow from the environment to the system [113–115]. The simulation of general open quantum systems is, however, a computationally challenging task, which hampers progress on the design of optimal control procedures that may take advantage of these effects.

There are several methods available that can be applied for the optimisation of various specific non-Markovian scenarios [39–44, 116–130]. The most common approach is to assume that the environment can be modelled with extra noise qubits which couple strongly to the system and weakly to some Markovian environment [116, 120, 126]. Another method involves repeatedly solving the hierarchical equations of motion

(HEOM) [42, 122, 123, 130], which performs well for environments with a spectral density that can be approximated with a small number of Lorentzians. A similar approach would be possible with other numerically exact methods, such as the quasi adiabatic path integral (QUAPI) [43, 44] or the time evolving density operator with orthogonal polynomials (TEDOPA) [39, 40]. A major impediment to the use of these methods for optimal control applications is, however, that they are computationally intensive and the entire calculation needs to be restarted as a whole for each iteration step of the optimisation.

In this chapter[1] we introduce a general method based on the PT-MPO that makes an efficient numerical exploration of control procedures for non-Markovian open quantum systems possible [54]. The key insight is that, based on an appropriate Trotterisation of the system and environment as shown in section 2.3.1, the PT-MPO for the environment interaction can be computed independently of any specific control protocol for the system. Thus the computation of the PT-MPO has to be performed only once for a given environment. This enables us to repeatedly compute the reduced dynamics for various sets of control parameters at very low computational cost, which we can use to optimise control procedures with respect to any chosen aspect of the system evolution, taking full account of non-Markovian effects. After a detailed introduction to the proposed method in section 3.1, we illustrate it by optimising the shape of a laser pulse to prepare a quantum dot in a specific state in section 3.2. For this we completely map out the state preparation fidelity for a two dimensional parameter space of chirped pulses. Furthermore, we apply a differential evolution algorithm to find an optimised laser pulse in a 35 dimensional parameter space to simultaneously drive five detuned quantum dots to the equator of the Bloch sphere.

3.1. Exploring control procedures using PT-MPOs

The most general scenario that we consider is a total Hamiltonian of the form

$$\hat{H}(t, \{c_k\}) = \hat{H}^{\mathrm{S}}(t, \{c_k\}) + \hat{H}^{\mathrm{I}} + \hat{H}^{\mathrm{E}}, \tag{3.1}$$

where $\hat{H}^{\mathrm{S}}(t, \{c_k\})$ is an explicitly time dependent system Hamiltonian that is parametrised by a set of real control variables $\{c_k\}_{k\in\{1,\dots,K\}}$. The interaction and environment Hamiltonians $\hat{H}^{\mathrm{I}}$ and $\hat{H}^{\mathrm{E}}$ are assumed to be independent of these control parameters. This reflects the typical experimental scenario in which the experimenter has control over some time dependent protocol (such as the length and detuning of a laser pulse) that manipulates the system of interest (such as the electronic state of a quantum dot), but has no direct control over the environment (such as the vibrational states that couple to the quantum dot). In the simplest case the aim is to optimise the choice of control parameters $\{c_k\}$ such that for a given initial system state ρ_0^{S} the final state $\rho_{\mathrm{final}}^{\mathrm{S}} := \rho^{\mathrm{S}}(t_{\mathrm{final}})$ is as close as possible to a given target state $\rho_{\mathrm{target}}^{\mathrm{S}}$. More generally, one might seek for optimal control parameters that not only optimise the protocol for a specific given initial state, but also for all other possible initial states. This means that the choice of control parameters should bring the resulting dynamical map $\Lambda_{t_0}^{t_{\mathrm{final}}}$ as close as possible to a given target map Ξ_{target}. The optimisation of protocols is a particularly challenging task when the environment interaction does not permit a time-local effective description of the reduced dynamics.

[1] This chapter is based on an early draft (from the 13th of November, 2020) of the publication [54]. That draft had been written exclusively by the author of the present work.

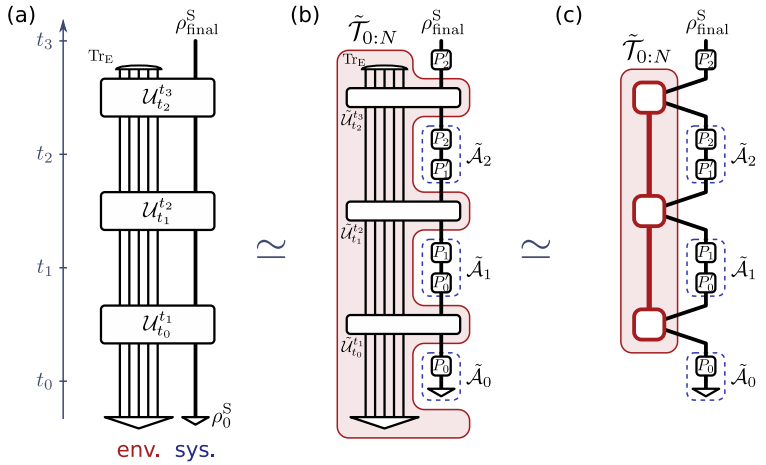

Figure 3.1: Quantum circuits and tensor networks for the PT-MPO approach to optimal control of general open quantum systems. (a) Full quantum circuit for the system and environment for three time steps. (b) Trotter splitting of the system and environment interaction parts. (c) The PT-MPO of the environment interaction part with an appropriate system intervention sequence.

To address that challenge we propose to use a Trotter splitting of the system and environment parts to then compute the PT-MPO for the environment interaction independently of the system Hamiltonian. Upon a suitable choice of the Trotterisation time step δt we may then use the PT-MPO to compute the reduced dynamics (or dynamical map) for a large set of different system control protocols at very little computational cost. Employing standard numerical local [131] and global optimisation procedures (such as basin-hopping [132] or differential evolution [133]) this enables us to optimise control procedures for non-Markovian open quantum systems efficiently.

Trotterisation of system and environment parts: We separate the system and environment interaction parts of the total evolution by performing a Suzuki-Trotter expansion similar to the procedure presented in section 2.3.1, but not restricted to Gaussian bosonic environments. The total evolution of system and environment from time t_n to $t_{n+1} = t_n + \delta t$ is given by the unitary super-operator

$$\mathcal{U}_{t_n}^{t_{n+1}} = \overleftarrow{\mathbf{T}} e^{\int_{t_n}^{t_{n+1}} \mathrm{d}t' \mathcal{L}(t', \{c_k\})}, \tag{3.2}$$

where $\overleftarrow{\mathbf{T}}$ denotes time ordering from right to left and $\mathcal{L}(t, \{c_k\})\cdot := -i\left[\hat{H}(t, \{c_k\}), \cdot\right]$ is the total Liouvillian. A symmetrised second order Suzuki-Trotter expansion [102] yields the same expression as in section 2.3.1

$$\mathcal{U}_{t_n}^{t_{n+1}} = \underbrace{\left(\overleftarrow{\mathbf{T}} e^{\int_{t_{n+1/2\delta t}}^{t_{n+1}} \mathrm{d}t' \mathcal{L}^{\mathrm{S}}(t', \{c_k\})}\right)}_{=:P'_n} \underbrace{\left(e^{\delta t \mathcal{L}^{\mathrm{IE}}}\right)}_{=:\tilde{\mathcal{U}}_{t_n}^{t_{n+1}}} \underbrace{\left(\overleftarrow{\mathbf{T}} e^{\int_{t_n}^{t_{n+1/2\delta t}} \mathrm{d}t' \mathcal{L}^{\mathrm{S}}(t', \{c_k\})}\right)}_{=:P_n} + \mathcal{O}(\delta t^3), \tag{3.3}$$

where $\mathcal{L}^{\mathrm{S}}(t', \{c_k\})$ and $\mathcal{L}^{\mathrm{IE}}$ are the system and environment interaction Liouvillians, respectively. Upon the choice of a small enough time step δt such that

$$\frac{1}{2}\left[\hat{H}^{\mathrm{S}}(t, \{c_k\}), \hat{H}^{\mathrm{I}}\right] \delta t^2 \ll \left(\hat{H}^{\mathrm{S}}(t, \{c_k\}) + \hat{H}^{\mathrm{I}}\right) \delta t, \tag{3.4}$$

we can omit the higher order terms $\mathcal{O}(\delta t^3)$ in Eq. (3.3). Figures 3.1a and 3.1b show the corresponding quantum circuits for an evolution of three time steps. Upon inspection of Fig. 3.1b we can identify the red shaded region comprising the propagators $\tilde{\mathcal{U}}_{t_n}^{t_{n+1}} = e^{\delta t \mathcal{L}^{\mathrm{IE}}}$ to be the process tensor $\tilde{\mathcal{T}}_{0:N}$ with respect to a total Hamiltonian

$$\tilde{H} := \hat{H}(t, \{c_k\}) - \hat{H}^{\mathrm{S}}(t, \{c_k\}) = \hat{H}^{\mathrm{I}} + \hat{H}^{\mathrm{E}}, \tag{3.5}$$

which is independent of the system control parameters $\{c_k\}$.

Computation of the PT-MPO for the environment part: To take advantage of the Trotterised evolution we compute the process tensor $\tilde{\mathcal{T}}_{0:N}$ in a matrix product operator form (PT-MPO) with respect to $\tilde{H}$ from Eq. 3.5. This step is limited to environments for which there exists an efficient representation of the process tensor in MPO form and an adequate method to obtain such a PT-MPO is available. The PT-TEMPO and ACE methods introduced in section 2.3 already cover a large class of relevant environment interactions, but other methods [28, 45, 53, 56–58] may also be applied. We note that the PT-MPO is a particular representation of a physically meaningful object (the process tensor) and thus the details of *how* an appropriate PT-MPO for a specific environment is obtained is not relevant to its application. The only ambiguity lies in the gauge of the MPO representation, which if considered relevant, can be removed by demanding a particular canonical form, such as the Vidal form.

Extraction of the reduced dynamics: Assuming that we have access to a PT-MPO of $\tilde{\mathcal{T}}_{0:N}$ with $t_N = t_{\mathrm{final}}$ we can compute the final state

$$\rho^{\mathrm{S}}_{\mathrm{final}} = \rho^{\mathrm{S}}(t_N) = P'_{N-1} \tilde{\mathcal{T}}_{0:N} \left[\{\tilde{\mathcal{A}}_0, \tilde{\mathcal{A}}_1, \ldots, \tilde{\mathcal{A}}_{N-1}\} \right], \tag{3.6}$$

for any choice of control parameters $\{c_k\}$ and initial state ρ^{S}_0 by contracting the PT-MPO with the appropriate intervention sequence $\tilde{\mathcal{A}}_0 : \rho^{\mathrm{S}} \mapsto P_0(\rho^{\mathrm{S}}_0)$ and $\tilde{\mathcal{A}}_n = P_n \circ P'_{n-1}$ as shown in Fig. 3.1c. For small time steps δt the system propagators P_n and P'_n may be approximated as

$$P_n = \overleftarrow{\mathbf{T}} \exp\left[\int_{t_n}^{t_n + \delta t/2} \mathrm{d}t' \mathcal{L}^{\mathrm{S}}\left(t', \{c_k\}\right) \right] \simeq \exp\left[\mathcal{L}^{\mathrm{S}}\left(t_n + \frac{1}{4}\delta t, \{c_k\} \right) \frac{\delta t}{2} \right] \tag{3.7}$$

and

$$P'_n = \overleftarrow{\mathbf{T}} \exp\left[\int_{t_n + \delta t/2}^{t_n + \delta t} \mathrm{d}t' \mathcal{L}^{\mathrm{S}}\left(t', \{c_k\}\right) \right] \simeq \exp\left[\mathcal{L}^{\mathrm{S}}\left(t_n + \frac{3}{4}\delta t, \{c_k\} \right) \frac{\delta t}{2} \right]. \tag{3.8}$$

We can thus write a 0^{th}-order oracle routine $\phi : \mathbb{R}^K \to \mathbb{R}_+, \{c_k\} \mapsto d_T\left(\rho^{\mathrm{S}}_{\mathrm{final}}, \rho^{\mathrm{S}}_{\mathrm{target}}\right)$ that takes a set of control parameters $\{c_k\}_{k \in \{1,\ldots,K\}}$ and returns the trace distance d_T of the final state to a given target state. We can then use any optimisation method suitable for 0^{th}-order oracles to find control parameters that minimise ϕ.

Scaling of the computational cost: The computation time of this method is typically dominated by the contraction of the PT-MPO with the system propagators (assuming that the bond dimension of the PT-MPO is significantly larger than the system Liouville dimension). The contraction sequence as indicated in Fig. 3.1 can be implemented with a computational cost scaling as $\mathcal{O}(\chi_P^2 D^2)$ for each time step, where χ_P is

the bond dimension of the PT-MPO and D is the system Liouville space dimension. An optimisation process that takes M oracle calls thus involves $C + \mathcal{O}(NM\chi_P^2 D^2)$ operations, where C is the number of operations necessary for the initial one-time computation of the PT-MPO.

We consider the TEMPO method to compare the scaling of this approach to the brute force approach of starting afresh for each given trial control parameter set. We choose the TEMPO method because in its original form it requires the full computation for every trial system Hamiltonian, but in the modified (PT-TEMPO) form may also yield a PT-MPO. As mentioned in section 2.3.1 the TEMPO method in its original form scales as $\mathcal{O}(N\,\chi_A^3 D^3\,K_{\max})$, where χ_A is the bond dimension necessary to accurately represent the intermediate MPS of the computation, and $\delta t K_{\max}$ is the time scale at which the environment correlation function decays to zero. The modified form that yields a PT-MPO scales similarly as $\mathcal{O}(N\,\chi_P^3 D^3\,K_{\max})$, where the bond dimension of the PT-MPO χ_P is not necessarily equal to the bond dimension required in the original TEMPO computation χ_A. They are, however, typically of similar magnitude, such that $\chi := \chi_P \simeq \chi_A$. Overall, we thus find that the proposed PT-MPO approach for the search of control parameters scales as $\mathcal{O}(N\,\chi^3 D^3\,K_{\max}) + \mathcal{O}(M\,N\,\chi^2 D^2)$ compared to the direct TEMPO approach which scales as $\mathcal{O}(M\,N\,\chi^3 D^3\,K_{\max})$. Considering that the number of oracle calls is typically very large ($M \gtrsim 1000$) this suggests a speed-up that scales as $\mathcal{O}(\chi\,D\,K_{\max})$.

Optimisation of dynamical maps: To optimise a protocol with respect to a target dynamical map Ξ_{target}, we need to be able to compute the resulting dynamical map $\Lambda_{t_0}^{t_{\text{final}}}$ for any set of control parameters. We can compute the map by either repeatedly computing the final state for a set of initial basis states, or by omitting the insertion of an initial state in the tensor network and leaving the corresponding leg open during the contraction sequence. Upon a suitable choice of a distance measure $d\left(\Xi_{\text{target}}, \Lambda_{t_0}^{t_{\text{final}}}\right)$, the proposed strategy for the optimisation of dynamical maps is analogous to the above described process for the optimisation of specific final states.

3.2. Optimised laser pulses for a quantum dot

We now demonstrate the performance of the PT-MPO approach introduced above by applying it to a quantum dot that is strongly coupled to its phonon environment and driven by a configurable laser pulse. Below, we completely map out the performance of the laser pulse for a two dimensional parameter space (see Fig. 3.3) and we perform a global search with the differential evolution algorithm [133] on a 35 dimensional parameter space (see Fig. 3.4).

Figure 3.2 shows a sketch of an experimental setup to drive exciton transitions in a quantum dot with a shaped laser pulse. The pulse shaper consists of a pair of diffraction gratings, lenses, and a spatial light modulator (SLM). We choose to parametrise the system Hamiltonian in a way that emulates this particular experimental setup to ensure that the resulting optimised protocol is indeed experimentally feasible. We consider the ground state and the exciton state of the quantum dot and denote them with $|\downarrow\rangle$ and $|\uparrow\rangle$ respectively. Under the rotating wave approximation the system Hamiltonian (with $\hbar = 1$) is

$$\hat{H}_S(t) = \frac{\omega_{\uparrow\downarrow}}{2}\hat{\sigma}_z + \frac{\Omega(t)}{2}e^{-i\omega_0 t}\hat{\sigma}^+ + \frac{\Omega^*(t)}{2}e^{i\omega_0 t}\hat{\sigma}^-, \tag{3.9}$$

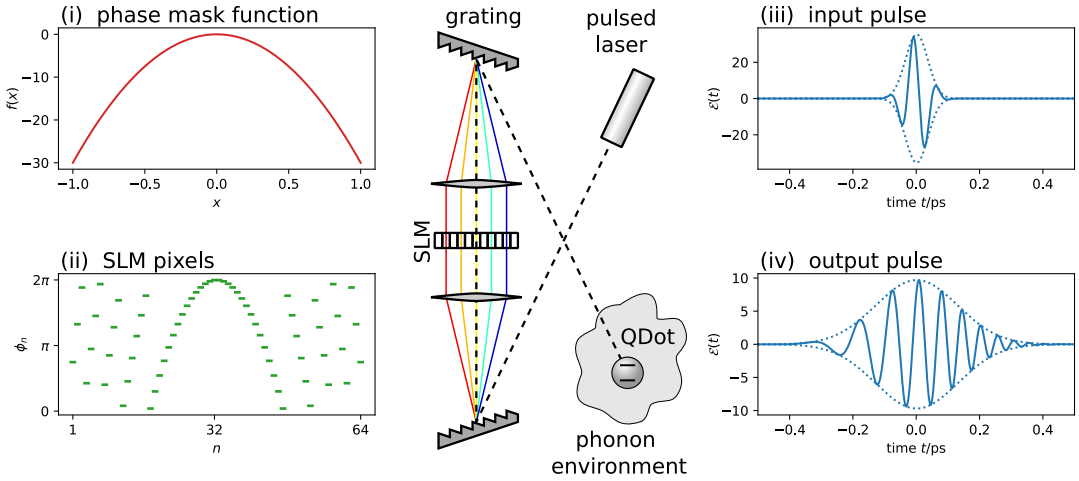

Figure 3.2: Sketch of the experimental setup to drive a quantum dot (QDot) with a shaped laser pulse. The pulse form can be modified with a spatial light modulator (SLM). The insets show (i) the phase mask function, (ii) the SLM pixel phase shifts, (iii) the input pulse, and (iv) the output pulse.

where $\Omega(t)$ is the positive frequency part of the classical electrical field amplitude, ω_0 is the laser carrier frequency and $\omega_{\uparrow\downarrow}$ is the exciton energy. Also, $\hat{\sigma}_z$ is the Pauli matrix, $\hat{\sigma}^+ = |\uparrow\rangle\langle\downarrow|$, and $\hat{\sigma}^- = |\downarrow\rangle\langle\uparrow|$. The quantum dot couples strongly to its phonon environment such that the total Hamiltonian has the form

$$\hat{H}(t, \{c_k\}) = \hat{H}^{\mathrm{S}}(t, \{c_k\}) + \underbrace{\hat{S} \sum_k \left(g_i \hat{a}_i + g_i^* \hat{a}_i^\dagger \right)}_{\hat{H}^{\mathrm{I}}} + \underbrace{\sum_i \omega_i \hat{a}_i^\dagger \hat{a}_i}_{\hat{H}^{\mathrm{E}}}, \tag{3.10}$$

with the coupling operator $\hat{S} = \hat{\sigma}_z/2$ and a super-ohmic spectral density

$$J(\omega) := \sum_i |g_i|^2 \, \delta(\omega_i - \omega) = 2\alpha \, \frac{\omega^3}{\omega_c^2} \, \exp\left(-\frac{\omega^2}{\omega_c^2} \right). \tag{3.11}$$

We choose realistic values for the unit-less coupling constant $\alpha = 0.126$ and cut-off frequency $\omega_c = 3.04\,\mathrm{ps}^{-1}$ [18, 134]. The initial state is assumed to be the product of the quantum dot ground state $|\downarrow\rangle$ and the thermal state of the environment at $T = 1.0\,\mathrm{K}$. We note that the environment auto-correlation function dies off only after about 2.5 ps, which renders a Markovian approach invalid at comparable and shorter timescales.

For convenience, we transform the system Hamiltonian into the frame of the exciton transition, such that

$$\hat{H}_{\mathrm{S}}(t) = \frac{\mathcal{E}(t)}{2} \hat{\sigma}^+ + \frac{\mathcal{E}^*(t)}{2} \hat{\sigma}^-, \tag{3.12}$$

where $\mathcal{E}(t) = \Omega(t) \exp(-i\Delta t)$ is the positive frequency part of the electric field in the rotating frame, and $\Delta = \omega_0 - \omega_{\uparrow\downarrow}$ is the detuning of the carrier frequency of the input pulse with respect to resonance. The input pulse (before it enters the pulse shaper) is assumed to be Gaussian, i.e. $\mathcal{E}_{\mathrm{in}}(t) \propto \tau^{-1} \exp\left(-t^2/\tau^2\right) \exp\left(-i\Delta t\right)$, with an input pulse duration τ assumed to be between 30 fs and 300 fs. The pair of diffraction gratings and appropriate lenses allow the spatial separation of the frequency components of the input pulse, with an approximately linear relationship between frequency and position

at the SLM. Therefore each SLM pixel modifies a particular frequency range of the pulse. We further assume that the pulse also has a finite spatial width with a Gaussian profile which results in a finite spot size for each frequency part at the SLM. Assuming that each SLM pixel can induce a phase shift ϕ_n to its corresponding frequency Ω_n the output pulse $\mathcal{E}(t) \propto (h * \mathcal{E}_{\text{in}})(t)$ is a convolution with the pulse shaper's impulse response function

$$h(t) \propto \operatorname{sinc}\left(\frac{\delta\Omega_p\, t}{2}\right) e^{-\frac{\delta\Omega_s^2 t^2}{4}} \sum_{n\in\text{pixels}} e^{i(\Omega_n t+\phi_n)}, \tag{3.13}$$

where $\delta\Omega_p$ is the pixel width and $\delta\Omega_s$ is the spot size in terms of their corresponding frequency range [135, 136]. We assume 512 SLM pixels centred at the pulse carrier frequency and evenly spaced over a frequency range of $2\pi \times 128.0\,\text{ps}^{-1}$. Also, we assume that the spot size of the pulse covers about two pixels, i.e. $\delta\Omega_s = 2.0 \times \delta\Omega_p$.

The setup described here leads to 515 open experimental parameters to modify the laser pulse, namely, the initial pulse length τ, the initial pulse detuning Δ, the pulse area Θ, and one phase shift ϕ_n for each of the 512 SLM pixels. Instead of directly using the 512 parameters on the SLM, we use a continuous phase mask function $f(x)$ on the interval $x \in [-1, 1]$, where -1 is mapped to most red detuned pixel and 1 is mapped to the most blue detuned pixel of the SLM. Then, the phase shift ϕ_n of pixel n is $\phi_n = 2\pi\,\text{frac}(f(x(n))/2\pi) \in [0, 2\pi)$, where $x(n) = (n - 256)/256$ and $\text{frac}(y) = y - \lfloor y \rfloor$ denotes the fractional part. Figure 3.2 shows an example for the phase mask function $f(x)$ the resulting pixel phase shifts ϕ_n and the corresponding input and output laser pulse to achieve a chirped laser pulse.

To study the dynamics of the quantum dot as a function of these experimental parameters we employ the PT-MPO approach introduced above for which we first compute the PT-MPO with respect to $\tilde{H} = \hat{H}^{\text{I}} + \hat{H}^{\text{E}}$. For this we choose the PT-TEMPO method with a time step of 10 fs and a memory time of 2.5 ps. Furthermore we employ a relative singular value truncation, i.e. we truncate singular values that are smaller than $10^{-6.5}$ relative to the largest value. With this, the computation of the process tensor takes approximately 167 s, while the application of a system Hamiltonian to this process tensor takes only 1.7 s on a single core of an Intel I7 (8th Gen) processor. For comparison, a original TEMPO computation leading to a comparable accuracy of the result takes approximately 230 s for each run.

Preparation of $|y+\rangle$: As a first example we apply a laser pulse to drive the quantum dot from its ground state $|\downarrow\rangle$ to the $|y+\rangle = (|\uparrow\rangle + i|\downarrow\rangle)/\sqrt{2}$ state. For simplicity we pick a two dimensional parameter space, for which we fix the initial pulse length to $\tau = 50\,\text{fs}$ and the pulse area to $\Theta = 10\,\pi$. We also fix the shape of the phase mask function to a downward facing parabola $f(x) = \Phi - 1300\,x^2$ with a central phase shift Φ. This parabola results in a broadened and chirped output laser pulse that starts blue detuned and ends red detuned with respect to its carrier frequency. The central phase shift simply induces an overall phase which rotates the x-y coordinate system. Applying our method we can easily map out the trace distance of the final state to the $|y+\rangle$ target state, as a function of the two open parameters $\Delta \in [-50, 50]\,\text{ps}^{-1}$ and $\Phi \in [-\pi, \pi]$. Figure 3.3a shows the results of 201×81 full non-Markovian simulations corresponding to the different parameter sets. Employing the PT-MPO approach the entire computation takes less than 8 hours on a single core of an Intel i7 processor, while it would take

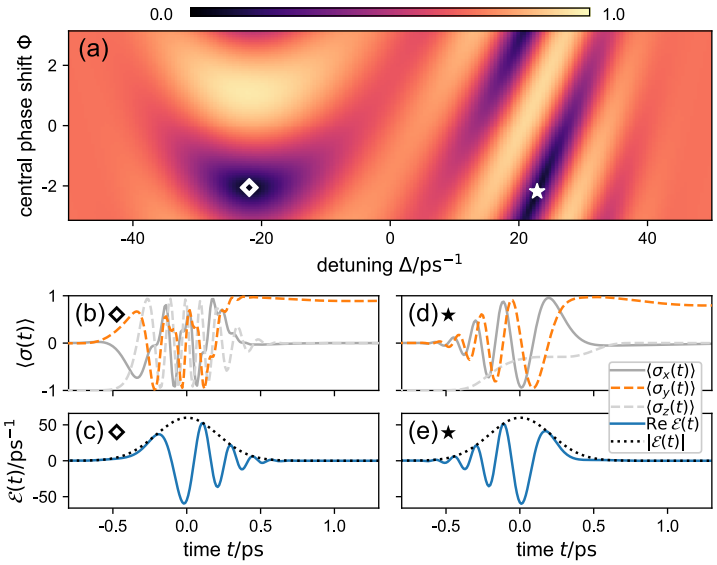

Figure 3.3: The dynamics of a quantum dot as a function of the detuning and overall phase of a chirped laser pulse. (a) A heat map indicating the trace distance of the final state to the target state $|y+\rangle$. (b-e) Dynamics of the quantum dot and the electric field for the laser pulse parameters marked with the symbols $\diamond$ and $\star$ in (a) respectively.

approximately 1040 hours or 43 days employing the original TEMPO method. We find two local minima on this landscape which are marked by a star and a diamond in Fig. 3.3a. The laser pulse that corresponds to the star parameter set is a chirped pulse that starts strongly detuned and finishes on resonance. This can be thought of as an interrupted adiabatic rapid passage, which has the advantage of being almost independent of a possibly inaccurate pulse area, but has the disadvantage to be sensitive towards the detuning of the pulse. The laser pulse that corresponds to the diamond parameters, on the other hand, starts on resonance and ends strongly red detuned. In this case the fidelity of the protocol is sensitively dependent on the pulse area, but tolerant towards detuning inaccuracies, similar to a simple $\pi/2$-pulse.

Manipulating an ensemble of five detuned quantum dots: As a second example to demonstrate the performance of the PT-MPO approach we consider an ensemble of five detuned quantum dots and aim to find an optimal laser pulse to simultaneously drive them to the equator of the Bloch sphere. The detunings of the quantum dots relative to the middle dot are chosen to be $[-10, -5, 0, 5, 10]\,\mathrm{ps}^{-1}$. We perform a global optimisation search employing the differential evolution algorithm on 35 pulse parameters. We parametrise the phase mask function by splitting it up into 32 segments and assigning one parameter to the slope of each segment. In addition to these 32 parameters we also optimise over all three input pulse parameters τ, Δ and Θ. To avoid extra oscillations in the time domain, the phase mask function is smoothed out with a 3rd order spline. We expect that a short $\pi/2$-pulse will successfully drive the states of the quantum dots close to the equator of the Bloch sphere. This is because the shorter the pulse is, the broader is its frequency distribution, leading to a suppressed detuning dependency. We employ differential evolution with a population size of eight parameter sets per dimension, where we set one element of the initial population to a simple 100 fs $\pi/2$-pulse and chose the rest randomly.

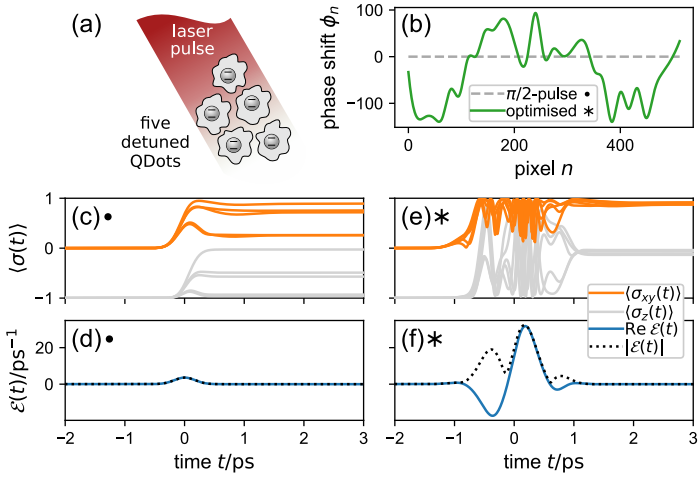

Figure 3.4: Optimisation of a laser pulse driving an ensemble of five quantum dots. (a) A sketch of the quantum dot ensemble taking the place of the single quantum dot in the setup from Fig. 3.2. (b) The phase mask function for the initial laser pulse (simple $\pi/2$-pulse) and the optimal laser pulse. (c-f) Dynamics of the quantum dot and the electric field for the initial and the optimal laser pulse denoted with • and $*$ respectively. The pulse length of both pulses prior to the pulse shaper is 245 fs, the pulse areas for the initial pulse and the optimised pulse are $0.5 \times \pi$ and $7.56 \times \pi$ respectively. The plots in (c) and (e) show the expectation values $\langle S_{xy}(t)\rangle = \sqrt{\langle S_x(t)\rangle^2 + \langle S_y(t)\rangle^2}$ for all five quantum dots.

The differential evolution algorithm employed 10 400 ensemble simulations, which each entailed the computation of the full non-Markovian dynamics of 5 independent quantum dots. Using the PT-MPO approach on all four cores of an Intel i7 processor this took only about 11 hours, while the same computation would have taken more than a month with the original TEMPO method. The result of this optimisation is shown in the right column of Fig. 3.4. Surprisingly, the algorithm found an unexpected pulse form that leads to a root mean square (RMS) distance to the equator of the Bloch sphere of 0.10, which is significantly better than the performance of a $\pi/2$-pulse with the same initial pulse duration of $\tau = 245$ fs (see left column of Fig. 3.4). Also, it performs slightly better than the shortest $\pi/2$-pulse with $\tau = 30$ fs, which yields a RMS distance of 0.12. However, we note that, unlike the $\pi/2$-pulse, the performance of the optimised pulse is sensitively dependent on the exact detuning of the individual quantum dots.

3.3. Conclusion and outlook

We have shown that the PT-MPO approach makes optimal control of non-Markovian open quantum systems a feasible task. It is limited to small system sizes and environments for which an efficient PT-MPO representation may be obtained.

We note that the control parameters that enter into the protocol are classical variables, and thus the scenarios considered in this chapter are about optimal *classical* control of open quantum systems. However, the method may readily be used to study control sequences in which the control parameters exhibit a quantum nature. For this one may consider, for example, the quantum circuit presented in Fig. 3.5a in which three additional ancilla systems interact unitarily with the open system. In such a case one may be interested in finding an optimal collective initial ancilla state σ for a given target state of the system. This may be formulated as the tensor network shown in Fig. 3.5b

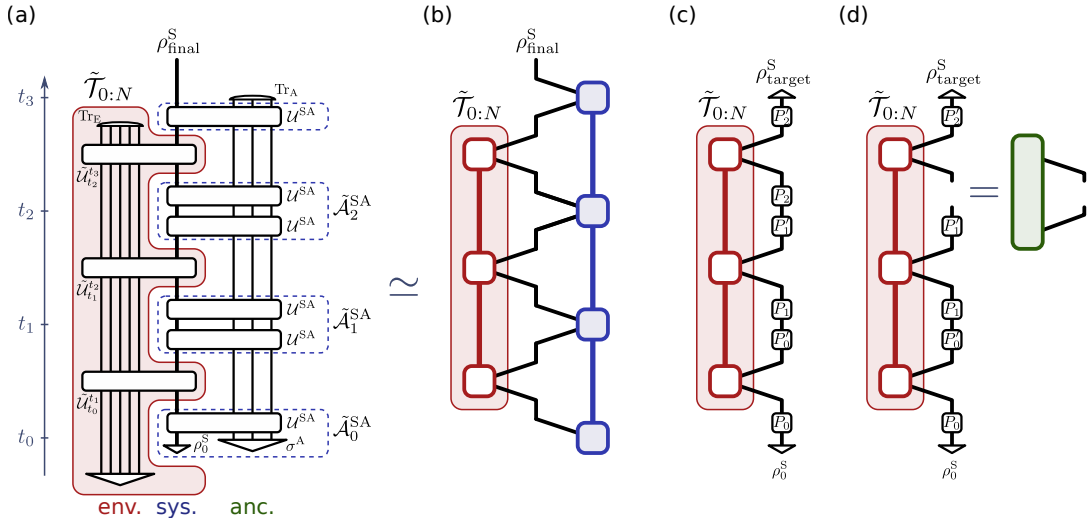

Figure 3.5: Quantum circuits and tensor networks for the "quantum control" of a process (a-b) and the derivative of the fidelity of a process (c-d). (a) Quantum circuit for a process controlled by an initial ancilla state σ^A. (b) Tensor network representation of a process controlled by an initial ancilla state, employing the PT-MPO of $\tilde{\mathcal{T}}_{0:N}$. (c) Tensor network representation of the fidelity of the final state (with respect to the target state $\rho^{\mathrm{S}}_{\mathrm{target}}$). (d) Derivative of the fidelity with respect to the system propagator at the second time step.

and contracted for many different trial states σ without the need to recompute the PT-MPO representing the environment interaction.

Finally we note that the efficiency of the optimisation can be significantly improved further by using the tensor network shown in Fig. 3.5c to compute the first derivative (i.e. the Jacobian) of the fidelity with respect to the control parameters [137]. Due to the linearity of tensor networks, the derivative of a tensor network with respect to one of its parts is equal to the same tensor network without that part. Figure 3.5c shows a tensor network that represents the fidelity for a given control parameter set. The tensor network shown in Fig. 3.5d is thus the Jacobian of the fidelity with respect to the system propagator P_2 at time t_2. Using an efficient contraction strategy one may compute the Jacobians with respect to all system propagators and then use of the chain rule to compute the Jacobian with respect to the control parameters. The resulting 1^{st}-order oracle in conjunction with suitable optimisation algorithms may then further drastically improve the performance of the search for optimal control parameters.

Chapter 4

Chains of General Open Quantum Systems

In the previous chapters we have seen that the PT-MPO is a versatile tool for dealing with general open quantum systems, even when the coupling to the environment is strong. The exponential growth of complexity with memory time of such non-Markovian open quantum systems is analogous to the complexity growth of many-body quantum systems on lattices with the number of sites. We have seen that using tensor network methods to represent the process tensor in MPO form allows us to tackle that growth with memory time for small systems. There is, however, even a range of interesting physical scenarios that include both many-body quantum systems *and* strongly coupled structured environments [61–65]. Such scenarios are of importance for fundamental research, such as the study of strong coupling quantum thermodynamics [21–24, 26, 27], as well as technological and biological applications [3–5, 25, 138–140]. However, almost all currently available methods for the study of many-body quantum systems only consider closed or Markovian dynamics, while methods for the study of non-Markovian open quantum systems are generically restricted to small system sizes (we briefly review the exceptions in section 4.1 below [39, 40, 141–149]).

In this chapter[1] we introduce a numerical method that enables the computation of the dynamics and multi-time correlations of chains of general open quantum systems. The method is based on a combination of the PT-MPO approach and the time evolving block decimation method (TEBD) [93, 99, 100, 150]. After introducing the key idea of the method in section 4.1 we present a more detailed derivation in section 4.2. Equipped with this, we suggest to employ the fluctuation dissipation theorem as a general approach to judge the thermalisation of subsystems of many-body (open) quantum systems in section 4.3. Finally, in section 4.4, we demonstrate the introduced approaches by studying the thermalisation of individual spins of an XYZ Heisenberg spin chain strongly coupled to thermal leads in both equilibrium and non-equilibrium scenarios.

4.1. PT-MPO augmented tensor network methods

The challenge of simulating many-body systems with non-Markovian environments lies in the exponential scaling of both the Hilbert space of the many-body system with

[1] This chapter is based on various drafts of the publication [68].

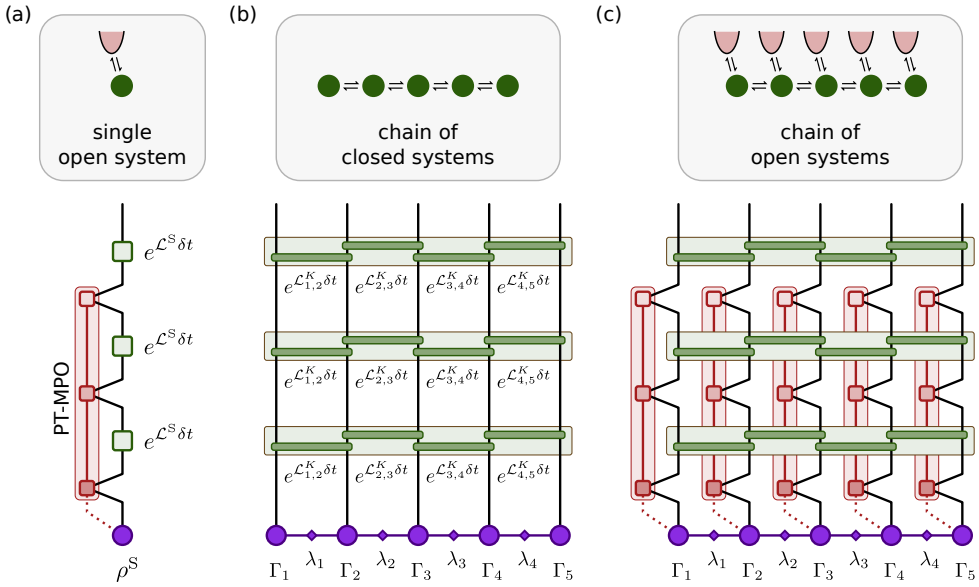

Figure 4.1: Tensor networks for (a) a single open quantum system using the PT-MPO approach, (b) a chain of closed quantum systems using the TEBD method, and (c) a chain of open quantum systems using the PT-MPO augmented TEBD method. The insets on the top of each panel show the connectivity between individual systems (green discs) and individual environments (red cups). The purple parts of the tensor network represent the initial state of the system, the green parts represent the closed system propagators, and the red parts represent the environment interaction.

the number of sites and the complexity of the environments with the degree of non-Markovianity. To tackle these challenges the general approach described in this chapter is to employ the PT-MPO for dealing with the non-Markovian environments and a suitable tensor network method for dealing with the many-body aspect of the problem. In particular, we present a combination of the PT-MPO approach with TEBD to simulate the dynamics and multi-time correlations of chains of open quantum systems. We note however, that the general approach of augmenting many-body tensor network methods with the PT-MPO may also be applicable to other methods such a the time-dependent variational principle (TDVP) [98].

Figure 4.1c shows the combination of the TEBD method (see Fig. 4.1b) with PT-MPOs (see Fig. 4.1a) on each site to include the influence of locally coupled environments. This tensor network is suitable to simulate a chain of systems where each site may couple strongly to its individual environment. We call this tensor network method *PT-MPO augmented TEBD* because for each environment the TEBD method is augmented with one additional leg that connects the site with its PT-MPO. This *augmented leg* thus encodes the correlations of the site with its environment. Figure 4.1c shows the tensor network for a first order Trotterised PT-MPO augmented TEBD tensor network. We present the second order network in Fig. 4.2b alongside a more detailed description of the method in section 4.2 below.

Before presenting the details of the PT-MPO augmented TEBD method, we now give a brief overview of several alternative approaches [39, 40, 141–149]. A method proposed by Suzuki *et al.* [143] is based on the transfer matrix approach and restricted to Gaussian bosonic environments as well as diagonal system-system couplings (with respect to the local system basis). The modular path integral (MPI) method proposed by

Makri [142] is originally based on the same assumptions, but has recently been extended to more general cases [146]. Also recently, Bose and Walters proposed a multi-site decomposition of the tensor network path integral (MS-TNPI) [149], which is similar to the method presented in this chapter, but restricted to Gaussian bosonic environments and comparitively short memory times (only 4 time steps are presented). Furthermore, for the special case where only the end sites couple to environments, a chain mapping technique for Gaussian bosonic environments called *time evolving density matrices using orthogonal polynomials* (TEDOPA) [39, 40] may be used. However, due to artefact reflections from the end of the chain (representing the environment) this method is unsuitable for computing long time dynamics. The approach to periodically reset the environment [144] solves this problem. However, because of the periodic destruction of system-environment correlations this method cannot be used to compute multi-time correlations (see the discussion on the failure of the quantum regression formula in section 2.1.3).

All these alternative approaches attempt to tackle the numerical complexity of both the system-system and the system-environment correlations simultaneously. In contrast to that, the PT-MPO approach tackles these challenges sequentially by first systematically reducing the numerical complexity originating from system-environment correlations before integrating them into the full many-body problem. We expect that this has a considerable positive impact on the performance, and that thus the PT-MPO augmented TEBD method can access a much wider class of problems than any other currently available method.

4.2. Derivation of PT-MPO augmented TEBD

In this section we present details of the PT-MPO augmented TEBD method. The method allows the computation of the dynamics and multi-site multi-time correlations of 1D many-body quantum systems in the presence of strongly coupled and structured environments. We assume a total Hamiltonian of the form

$$\hat{H} = \sum_{n=1}^{N} \left(\hat{H}_n^{\mathrm{S}} + \hat{H}_n^{\mathrm{IE}} \right) + \sum_{n=1}^{N-1} \hat{J}_{n,n+1}, \tag{4.1}$$

as sketched in the inset of Fig. 4.1c. It consists of on-site system Hamiltonians $\hat{H}_n^{\mathrm{S}} \in \mathcal{B}(\mathcal{H}_n^{\mathrm{S}})$, on-site environment interaction parts $\hat{H}_n^{\mathrm{IE}} \in \mathcal{B}(\mathcal{H}_n^{\mathrm{S}} \otimes \mathcal{H}_n^{\mathrm{E}})$, and nearest neighbour coupling terms $\hat{J}_{n,n+1} \in \mathcal{B}(\mathcal{H}_n^{\mathrm{S}} \otimes \mathcal{H}_{n+1}^{\mathrm{S}})$ for each of the N sites. Here, $\mathcal{H}_n^{\mathrm{S}}$ and $\mathcal{H}_n^{\mathrm{E}}$ denote the system and environment Hilbert spaces of the n^{th} site, and $\mathcal{B}(\mathcal{H})$ denotes the set of bounded linear operators on $\mathcal{H}$.

In principle the on-site system Hamiltonians can be completely absorbed in the definition of the on-site environment interactions. However, as we have seen in the previous chapter, it is often useful to separate the pure system part from the interaction part as much as possible. In addition to the total Hamiltonian in Eq. (4.1), we will also allow for on-site time-local dissipative processes described by a local master equation of GKSL form.

In the following we show how to construct the TEBD tensor network augmented with the process tensor approach and present a suitable contraction algorithm. Finally, we will show how to extract the intermediate time chain dynamics as well as multi-site multi-time correlations.

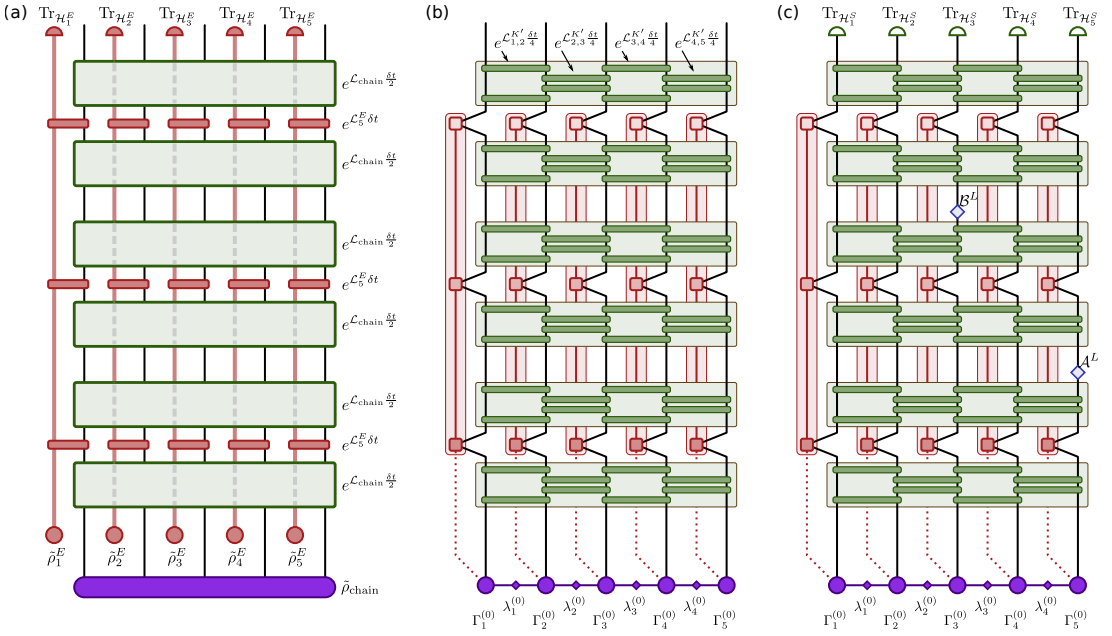

Figure 4.2: Tensor networks combining process tensors and TEBD. (a) Tensor network for three time steps using a second-order Suzuki-Trotter splitting between a 5-site chain and its environments. (b) Full tensor network for a 5-site chain using a second order Suzuki-Trotter splitting in both environment and inter-site coupling. (c) Full tensor network to compute the two time correlation $\left\langle \hat{B}(2\delta t), \hat{A}(1\delta t) \right\rangle$.

4.2.1. Tensor network construction

Like in the previous chapters, the entire following calculation is carried out in Liouville space, i.e. we consider super-operators that act on the space of vectorised density matrices. As a start we consider the formal solution of the von Neumann equation for the total density operator at time t

$$\rho(t) = e^{\mathcal{L}t}\rho(0) \tag{4.2}$$

with the total Liouvillian $\mathcal{L}\cdot = -i[\hat{H}, \cdot\,]$. We can separate this total Liouvillian into a chain and an environment part

$$\mathcal{L} = \mathcal{L}_{\text{chain}} + \sum_n^N \mathcal{L}_n^{\text{IE}}, \tag{4.3}$$

where

$$\mathcal{L}_{\text{chain}} = \sum_n^N \mathcal{L}_n^{\text{S}} + \sum_n^{N-1} \mathcal{L}_{n,n+1}^{J}, \tag{4.4}$$

with each Liouvillian corresponding to a part of the total Hamiltonian in Eq. (4.1). As mentioned above, the system Liouvillians may additionally include dissipative terms, i.e.

$$\mathcal{L}_n^{\text{S}}\cdot = -i[\hat{H}_n^{\text{S}}, \cdot\,] + \sum_k \left(\hat{L}_{n,k}^{\dagger} \cdot \hat{L}_{n,k} - \frac{1}{2}\{\hat{L}_{n,k}^{\dagger}\hat{L}_{n,k}, \cdot\,\} \right), \tag{4.5}$$

with GKSL operators $\hat{L}_{n,k} \in \mathcal{B}(\mathcal{H}_n^{\text{S}})$.

Analogously to the approach taken in the previous chapters, we divide the total propagation into M short time steps δt and perform a second-order Suzuki-Trotter splitting [151] between the chain and the environment terms

$$e^{\mathcal{L}t} = \left[e^{\mathcal{L}\delta t} \right]^M \tag{4.6}$$

$$\simeq \left[e^{\mathcal{L}_{\text{chain}} \frac{\delta t}{2}} e^{\left(\sum_n^N \mathcal{L}_n^{\text{IE}} \delta t\right)} e^{\mathcal{L}_{\text{chain}} \frac{\delta t}{2}} \right]^M \tag{4.7}$$

$$= \left[e^{\mathcal{L}_{\text{chain}} \frac{\delta t}{2}} \left(\prod_n^N e^{\mathcal{L}_n^{\text{IE}} \delta t} \right) e^{\mathcal{L}_{\text{chain}} \frac{\delta t}{2}} \right]^M , \tag{4.8}$$

where the last equality follows from the fact that the $\mathcal{L}_n^{\text{IE}}$ act on different site-environment pairs for different n. For ease of presentation we now apply this propagator to a total initial state that is separable between the chain and each environment, which means that $\rho(0) = \tilde{\rho}_{\text{chain}} \bigotimes_n \tilde{\rho}_n^{\text{E}}$. We comment below how this can be extended to initially correlated states. Let us now consider the reduced chain state, which we obtain by performing the partial traces over all environments, i.e. $\text{Tr}_E := \text{Tr}_{\{\bigotimes_n \mathcal{H}_n^{\text{E}}\}}$. Assuming an initial separable state and the approximated propagator from Eq. (4.8), we show a tensor network in Fig. 4.2a that represents $\rho_{\text{chain}}(t) := \text{Tr}_E \left\{ e^{\mathcal{L}t} \rho(0) \right\}$ for three time steps.

So far, the tensor network in Fig. 4.2a is unsuitable for carrying out a numerical computation. The tensors representing the interaction with the environment (red tensors) explicitly involve the environment Hilbert spaces, and the chain propagators $e^{\mathcal{L}_{\text{chain}} \frac{\delta t}{2}}$ (green tensors) are still assumed to be exact, with a total dimension of $\dim(\mathcal{H}_n^{\text{S}})^{4N}$. This is impractical for any generic environment and any chain of significant length. In the following we present how to construct the tensor network in Fig. 4.2b instead, which is then suitable for an efficient numerical computation.

First, we consider the part of the tensor network that consists of the environment initial state $\tilde{\rho}_n^{\text{E}}$, the interaction propagators $e^{\mathcal{L}_n^{\text{IE}} \delta t}$, and the final environment trace $\text{Tr}_{\mathcal{H}_n^{\text{E}}}$. Together, these tensors constitute a multi-linear map, which is—per definition—the process tensor of the environment interaction Hamiltonian $\hat{H}_n^{\text{IE}}$ with the initial state $\tilde{\rho}_n^{\text{E}}$ [67], as introduced in section 2.1.4. Depending on the type of the environment we then may use one of the methods [45, 49, 52–58, 104] introduced in section 2.3 to construct an efficient representation of the process tensor in MPO form. In Fig. 4.2b we have replaced the full process tensors with the PT-MPOs obtained from any such suitable method. Given that the computation of such a PT-MPO is often numerically involved, it can be beneficial to absorb all pure on-site system terms into $\mathcal{L}_n^{\text{S}}$ and reuse the PT-MPO for any identical occurrences of the $\mathcal{L}_n^{\text{IE}}$ environment interactions.

Next, we consider the chain propagators $e^{\mathcal{L}_{\text{chain}} \frac{\delta t}{2}}$. To decompose these large tensors into smaller tensors, we perform another second-order Suzuki-Trotter splitting (this time among the chain sites), making use of the fact that the chain Hamiltonian only contains on-site and nearest neighbour terms. This leads to a TEBD tensor network for the chain evolution in Liouville space [100, 150], as discussed in section 2.2.4. For this, we first absorb the on-site system Hamiltonians $\hat{H}_n^{\text{S}}$ into the nearest neighbour terms $\hat{J}_{n,n+1}$ by defining $\hat{K}_{n,n+1}$ like in Eq. (2.19) such that $\mathcal{L}_{\text{chain}} = \sum_{n=1}^{N-1} \mathcal{L}_{n,n+1}^K$. In Fig. 4.2b we replace the half time step chain propagators $e^{\mathcal{L}_{\text{chain}} \frac{\delta t}{2}}$ with the second-order Suzuki-Trotter splitting, which is of a similar form as the first-order splitting presented in Eq. (2.21). It consists of two body gates of the form $e^{\mathcal{L}_{n,n+1}^K \frac{\delta t}{4}}$.

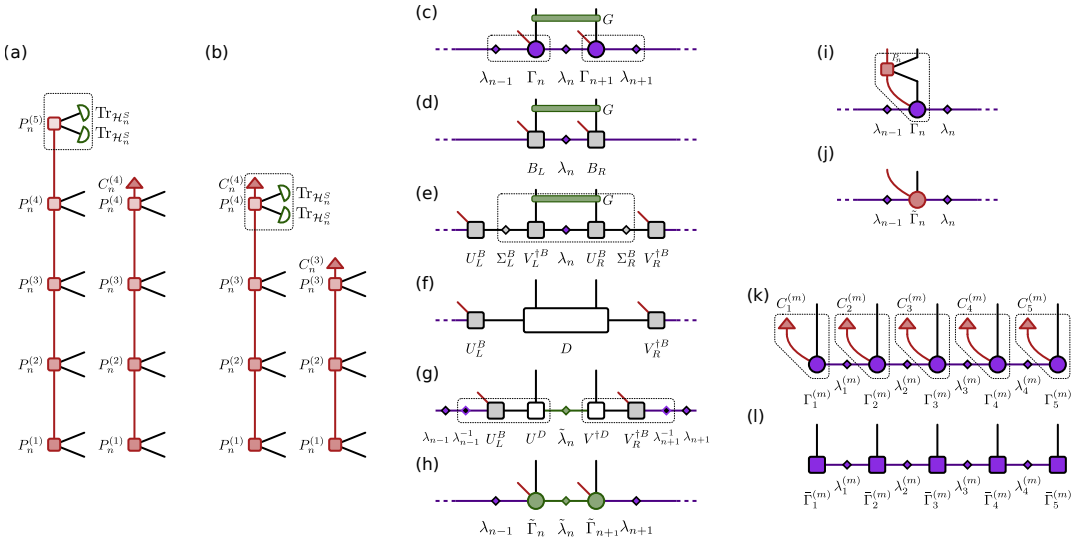

Figure 4.3: Contraction algorithms for the PT-MPO and augmented MPS. (a) Construction of the 4^{th} cap tensor $C_n^{(4)}$ of the PT-MPO at site n. (b) Construction of the 3^{rd} cap tensor $C_n^{(3)}$. (c-h) Contraction and decomposition sequence for the application of a two-site gate G on the augmented MPS. (i-j) Contraction of the augmented MPS with a PT-MPO tensor. (k-l) Contraction of the augmented MPS with the cap tensors, yielding a canonical MPS.

Finally, we insert the initial chain state as a matrix product state (MPS) in Vidal form [99]. Although the pure chain propagation works analogously to TEBD, each of the Γ tensors of the MPS needs to have an extra leg which corresponds to the entanglement of the chain site with its environment. We will call this MPS the *augmented MPS*. For initially uncorrelated chain-environment states the MPS has initially no extra legs. In such cases, we nonetheless include dummy legs of dimension 1. These are indicated with dotted lines in Fig 4.2b. We do this such that the contraction algorithm for the first time step is of the same form as for all later steps, as well as to allow for the case of an initially correlated state [67], for which the dimension of the dotted legs is > 1.

4.2.2. Contraction algorithm

Figure 4.2b shows the full tensor network for three time steps of a 5-site chain. To contract such a network we propose to absorb the tensors into the augmented MPS line by line. This involves two different types of contraction sequences which we describe in the following.

The first type is a contraction of the augmented MPS with the chain propagators, which consist of two-site nearest neighbour gates. We suggest a sequence of operations in Figs. 4.3(c-h). Compared to the canonical TEBD presented in section 2.2.4 above, this sequence includes some additional operations for the augmented legs with the aim of minimising the size of the intermediate tensors involved. Figures 4.3(c-h) show the proposed operations for applying a two body gate $G = e^{\mathcal{L}^{K'}_{n,n+1}\frac{\delta t}{4}}$ to an augmented MPS:

(c-d) Contraction:
$B_L := \lambda_{n-1}\Gamma_n$ and $B_R := \Gamma_{n+1}\lambda_{n+1}$

(d-e) Truncated singular value decomposition:
$U_L^B \Sigma_L^B V_L^{\dagger B} :\simeq B_L$ and $U_R^B \Sigma_R^B V_R^{\dagger B} :\simeq B_R$

(e-f) Contraction:
$D := \Sigma_L^B V_L^{\dagger B} \lambda_n G U_R^B \Sigma_R^B$

(f-g) Truncated singular value decomposition:
$U^D \Sigma^D V^{\dagger D} :\simeq D$ and $\tilde{\lambda}_n := \Sigma^D$

(g) Insert identities:
$\lambda_{n-1}\lambda_{n-1}^{-1} = \mathbb{1}$ and $\lambda_{n+1}^{-1}\lambda_{n+1} = \mathbb{1}$

(g-h) Contraction:
$\tilde{\Gamma}_n := \lambda_{n-1}^{-1} U_L^B U^D$ and $\tilde{\Gamma}_{n+1} := V^{\dagger D} V_R^{\dagger B} \lambda_{n+1}^{-1}$

We propose to use a relative singular value truncation threshold ϵ, i.e. we choose the cut-off χ as large as possible while maintaining the overall truncation error to be $\left\| \Sigma - \tilde{\Sigma} \right\|_2 < \epsilon \max(\Sigma)$, where $\|\cdot\|_2$ denotes the 2-norm and $\tilde{\Sigma}$ are the χ largest singular values.

The other type of operation that occurs when absorbing the tensor network line by line is the contraction of the augmented MPS with the subsequent parts of the PT-MPOs. Figures 4.3(i-j) show the contraction of an augmented MPS site (Γ_n) with a single tensor of a PT-MPO (P_n). This contraction only updates the Γ tensors of the augmented MPS, where the bond legs of the PT-MPOs become the new augmented legs of the augmented MPS.

The method is limited to 1D chains of systems whose state can be well approximated by an MPS of some finite maximal bond dimension χ, as well as environments whose process tensor can be well approximated by an MPO of maximal bond dimension ξ. The computational effort is dominated by performing the singular value decompositions involved in compressing the spatial MPS after the application of the nearest neighbour gates. Employing the extended contraction/SVD sequence described above, reduces the dimension of the largest intermediate matrix from $(\chi\xi d^2)\times(\chi\xi d^2)$ to $(\eta d^2)\times(\eta d^2)$, where d is the system Hilbert space dimension of a single site and η is the intermediate bond dimension that occurs in the step shown in Fig. 4.3(d-e), for which $\chi \lesssim \eta \leq \chi\xi$. The overall simulation of an N site chain for K time steps thus takes $\mathcal{O}(NK\eta^3 d^6)$ operations. We point out that the contraction sequences described above only act locally on a short part of the augmented MPS for each step. This contraction scheme is therefore, like the conventional TEBD algorithm, well suited for parallel computing.

4.2.3. Intermediate chain evolution

As presented thus far, this method would only yield a reduced chain state at the final time step. We can, however, extract the reduced density matrix of the chain for every intermediate time step by temporarily removing the correlations of the augmented MPS with the environment. This can be done using the containment property of process tensors as introduced in section 2.1.4, which allows the generation of process tensors for a smaller set of time slots by tracing over all later times. For this we construct the tensors $C_n^{(m)}$, which we call *cap* tensors, as shown in Figs. 4.3(a-b). Applying these cap tensors to the augmented MPS at time step m, as presented in Figs. 4.3(k-l), removes the augmented leg and yields a canonical MPS that represents the vectorised reduced density matrix of the chain at that time.

4.2.4. Multi-site multi-time correlations

Finally, we show how to compute multi-site multi-time correlations. As an example, we could be interested in the correlation $\left\langle \hat{B}(2\delta t)\hat{A}(1\delta t)\right\rangle$, with $\hat{A}$ and $\hat{B}$ acting on the 5$^{\text{th}}$ and 2$^{\text{nd}}$ spin of a 5-site chain respectively. More generally, we consider all time-ordered correlations C of the form

$$C = \left\langle \prod_{p=1}^{P} \hat{C}_p(m_p\delta t) \right\rangle = \left\langle \hat{C}_P(m_P\delta t)\ \ldots\ \hat{C}_2(m_2\delta t)\,\hat{C}_1(m_1\delta t) \right\rangle, \tag{4.9}$$

with the operator $\hat{C}_p$ acting at the time $m_p\delta t$. Time ordering means that $m_P \geq \ldots \geq m_1$. This can be written as

$$C = \mathrm{Tr}\left[\prod_{p=1}^{P} \left(\mathcal{C}_p^L\, e^{\mathcal{L}(m_p - m_{p-1})\delta t} \right) \rho(0) \right] \tag{4.10}$$

$$= \mathrm{Tr}\left[\prod_{p=1}^{P} \left(\mathcal{C}_p^L [\, e^{\mathcal{L}\delta t}]^{(m_p - m_{p-1})} \right) \rho(0) \right], \tag{4.11}$$

with $m_0 := 0$ and the left acting super-operators $\mathcal{C}_p^L := \hat{C}_p \cdot$. To represent Eq. (4.11) as a tensor network, we replace the full propagators for a single time step $e^{\mathcal{L}\delta t}$ with the same construction as in section 4.2.1 above. This leads to the same tensor network as in Fig. 4.2b, but with additionally inserted super-operators and with additional traces over the chain sites at the top of the network. We exemplify this in Fig. 4.2c for the two-time correlation $\left\langle \hat{B}(2\delta t)\hat{A}(1\delta t)\right\rangle$. Finally, we mention that for anti time-ordered correlations, the operators need to be inserted as right acting super-operators $\mathcal{C}_p^R := \cdot\, \hat{C}_p$ instead.

4.3. Thermalisation of subsystems

With the above method we now have an efficient numerical tool at hand to study the dynamics and multi-time correlations of chains of systems, where each system may couple strongly to a structured environment. A natural question that often arises when studying such open many-body systems is whether a particular subsystem thermalises. Identifying that a subsystem is in thermal equilibrium allows one to link its microscopic state to thermodynamic properties and is thus at the heart of the field of strong coupling quantum thermodynamics [21–24, 26, 27].

One approach to judge whether a subsystem has thermalised is to compare its reduced density matrix with the Gibbs state of some effective local Hamiltonian for that subsystem. This approach works well when the subsystem only couples weakly to the rest of the system. In the weak coupling limit the thermal reduced density matrix of the subsystem is identical to the Gibbs state of the subsystem with respect to the local Hamiltonian. For weak but finite coupling, perturbation theory predicts that the reduced part of the subsystem of the true total Gibbs state deviates from the Gibbs state with respect to the local Hamiltonian at second order in the coupling strength [152]. There exist perturbative methods that—given the total Hamiltonian—allow the computation of the lowest order corrections to the effective local Hamiltonian for the subsystem.

This means that judging the thermalisation of subsystems through the reduced density matrix depends on the ability to compute an appropriate effective local Hamiltonian, which in turn depends on the explicit knowledge of the total Hamiltonian. However, it would be desirable to have access to a method that is capable of judging thermalisation of a subsystem that does not require the explicit knowledge of the total Hamiltonian, but instead only depends on observables of the subsystem. Such a goal cannot be achieved by considering the reduced density matrix of a subsystem alone because *any* density matrix can be expressed as a thermal Gibbs state of some suitably constructed Hamiltonian.

Instead of studying the reduced density matrix, we therefore propose to use two-time correlations of local observables in conjunction with the quantum fluctuation dissipation theorem (FDT) to judge whether a subsystem has thermalised. This can be done without the explicit knowledge of any Hamiltonian[2]. The FDT states that for a thermalised quantum system at temperature T the ratio of the fluctuation and dissipation spectra with respect to any observable $\hat{A}$ must be

$$\frac{S_A(\omega)}{\chi''_A(\omega)} = \coth\left(\frac{\omega}{2T}\right), \tag{4.12}$$

for all frequencies ω [153, 154]. The fluctuation spectrum $S_A(\omega)$ is the Fourier transform of the Keldysh Green's function $S_A(\tau) = \frac{1}{2}\left\langle\{\hat{A}(\tau), \hat{A}(0)\}\right\rangle$ and is also called the symmetrised quantum noise spectral density [155]. Similarly, the dissipation spectrum $\chi''_A(\omega)$ is the imaginary part of the Fourier transformed linear response function $\chi_A(\tau) = i\Theta(\tau)\left\langle[\hat{A}(\tau), \hat{A}(0)]\right\rangle$, which is the retarded Green's function that quantifies the density of states with respect to transitions driven by the operator $\hat{A}$. The FDT is a general result of statistical quantum mechanics and in the form presented above does not involve any approximation. Operationally, the fluctuation and dissipation spectra could be measured by weakly coupling a measuring device to the observable $\hat{A}$ and recording its fluctuations as well as its response to weak perturbations. Here, the weak coupling assumption only applies to the coupling between the operator $\hat{A}$ and the measuring device. No such assumption is made about the coupling of $\hat{A}$ to the rest of the system, and this method is thus suitable to judge the temperature of subsystems even when they couple strongly to the rest of the system.

It is important to note that many commonly applied approaches for open quantum systems, such as time-convolutionless, Nakajima-Zwanzig, and the Gorini-Kossakowski-Sudarshan-Lindblad (GKSL) master equations [8], aim at correctly describing the reduced system dynamics, but in general do not yield the correct multi-time correlations. As mentioned in section 2.1.3, Ford and O'Connell have shown that a GKSL master equation may be adequate to describe thermalisation of the reduced density matrix of a harmonic oscillator experiencing random thermal forces in the weak coupling limit, but leads to incorrect fluctuation and dissipation spectra [82]. For the above proposition to work, it is therefore necessary to have access to a method that can correctly compute multi-time correlations of open quantum systems. The PT-MPO augmented TEBD

[2]The fact that one may judge thermalisation from multi-time correlations but not from the reduced dynamics alone demonstrates the statement made repeatedly in chapter 2, namely that multi-time correlations carry information that is not encoded in the reduced dynamics of an open quantum system alone.

method fulfils that necessity and thus allows the study of thermalisation of subsystems in chains of general open quantum systems.

4.4. XYZ spin chain with thermal leads

To demonstrate the power of the approaches introduced in this chapter we study the thermalisation of individual spins in an XYZ chain with strongly coupled thermal leads. We consider the chain Hamiltonian of the form

$$\hat{H}_{\mathrm{XYZ}} = \sum_{n=1}^{N} \epsilon_n \hat{s}_n^z + \sum_{n=1}^{N-1} \sum_{\gamma\in\{x,y,z\}} J^\gamma \, \hat{s}_n^\gamma \hat{s}_{n+1}^\gamma, \tag{4.13}$$

where $\hat{s}_n^\gamma = \hat{\sigma}_n^\gamma/2$ are the spin-1/2 operators at site n. Throughout this section, we set $\hbar = k_\mathrm{B} = 1$ and express all frequencies and times in units of some characteristic frequency and its inverse. We choose $J^x = 1.3$, $J^y = 0.7$, and $J^z = 1.2$ to break the symmetries of the Heisenberg model, and we start with studying the case of constant $\epsilon_n = 1.0$ for all sites.

4.4.1. Single thermal lead

As a first check we couple only a single bosonic bath at temperature $T = 1.6$ to the first site of a short ($N = 5$) chain and study the steady state and its two-time correlations (see Fig. 4.5e). The bath couples to the chain operator $\hat{s}_1^y$ with

$$\hat{H}_1^{\mathrm{IE}} = \sum_{k=0}^{\infty} \left[\hat{s}_1^y \left(g_k \hat{b}_k^\dagger + g_k^* \hat{b}_k \right) + \omega_k \hat{b}_k^\dagger \hat{b}_k \right], \tag{4.14}$$

where $\hat{b}_k^{(\dagger)}$ are bosonic lowering (raising) bath operators. The g_k parameters are determined by the spectral density $J(\omega) := \sum_k |g_k|^2 \delta(\omega - \omega_k)$, which we choose to be $J(\omega) = 2\alpha\omega \exp(-\omega/\omega_c)$, where α quantifies a dimensionless coupling strength and ω_c is a cut-off frequency which we set to $\omega_c = 4.0$.

To employ the augmented TEBD method to this scenario we first need to compute the PT-MPO for the particular environment at hand. For this we use the PT-TEMPO method [49, 52, 54, 104] as introduced in section 2.3.1. Such a computation has three convergence parameters: the time step δt, the maximal number of memory steps $K_{\max}$, and the relative singular value truncation threshold $\epsilon_{\mathrm{TEMPO}}$. The product $\delta t\, K_{\max}$ is the maximal correlation time of the environment that is included in the computation. For the given spectral density the environment correlation function drops at time $t = 8.0$ below 10^{-3} of its maximum value. Consistent with this, we find the choice of $\delta t = 0.2$, $K_{\max} = 40$, and $\epsilon_{\mathrm{TEMPO}} = 10^{-6}$ to be adequate. We comment on checking the convergence of the simulations in section 4.4.2 below. To allow a study of how the above scenario depends on the coupling strength α, we compute PT-MPOs with a length of 1600 time steps for various values of α using open source package OQuPy [104]. For a coupling strength of $\alpha = 0.32$ the computation takes approximately 4 minutes on a single core of an Intel i7 (8th Gen) processor, resulting in a PT-MPO with a maximal bond dimension of 37.

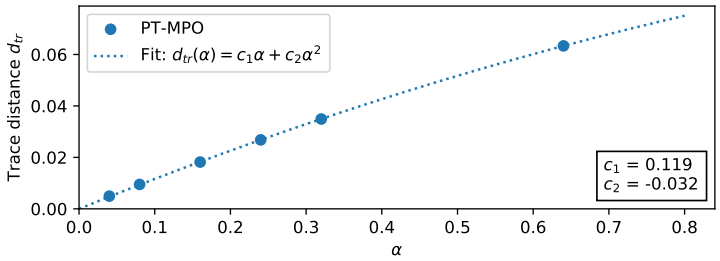

Figure 4.4: Trace distance between the thermal Gibbs state of the closed 5-site spin chain and the approximate steady state of the chain coupled to the bath with varying coupling strength α. A fit shows that this difference is vanishing at a linear order in α (i.e. a quadratic order in bath couplings g_k) in a weak coupling limit.

Reduced steady state: Equipped with the appropriate PT-MPOs for various coupling strengths, we can use the augmented TEBD method to evolve the spin chain from the initial state at time $t_i = 0.0$ to an approximate steady state at time t_{ss}. During the TEBD propagation we use a relative singular value truncation of $\epsilon_{\text{TEBD}} = 10^{-6}$. We find that for all scenarios considered $t_{ss} = 192.0$ (960 steps) is long enough to reach an approximate steady state. For the results presented in the following we chose the initial state of each spin to be $\tilde{\rho}_n^{\text{S}} \propto \exp\left(-\frac{\hat{\sigma}^z}{T}\right)$. As expected, we find the same steady state when starting from other random initial product states.

As mentioned in section 4.3, perturbation theory predicts that in a weak coupling limit the reduced chain density matrix of the full thermal state differs from the Gibbs state of the chain Hamiltonian at a quadratic order in the bath coupling [152]. The dimensionless coupling strength α is proportional to the square of the bath coupling amplitudes $|g_k|^2$, i.e. $\alpha \propto |g_k|^2$. Assuming that the chain thermalises with the bath in the long time limit, we thus expect to find a difference between the reduced steady state and the Gibbs state of the chain Hamiltonian that is proportional to α in a weak coupling limit. Figure 4.4 shows the trace distance for various coupling strengths α. A fit to the data shows that the results are consistent with the expectation.

Two-time correlations: While we can compare the steady state to a known exact result in a weak coupling limit, we lack a reliable reference for finite coupling. However, following the approach suggested in section 4.3 we can check the consistency of two-time correlations with the FDT to validate the thermalisation of the spin chain also at finite coupling strengths.

To compute two-time correlations such as $\left\langle \hat{B}(t_{ss}+\tau)\hat{A}(t_{ss}) \right\rangle$ with respect to some single site operators $\hat{A}$ and $\hat{B}$, we apply the left acting super-operator $\mathcal{A}^L \cdot = \hat{A}\cdot$ to the steady state and compute the expectation value of $\hat{B}$ for all later times up to the final time $t_f = 320.0$. We can thus compute the two time correlations $\langle \hat{\sigma}_n^z(t_{ss}+\tau)\hat{\sigma}_n^z(t_{ss})\rangle$ of spin n for all τ up to $\tau_{\max} := t_f - t_{ss}$ with a single propagation starting from the steady state. It is important to point out that the expression "steady state" refers to the state of the whole (chain and environment) and not just the reduced chain state. Because the two-time auto-correlations of the chain depend on the steady state correlations of the chain with the environment it is vital to continue the propagation from the full augmented MPS at time t_{ss}.

With this, we obtain $\langle \hat{\sigma}_n^z(t_{ss}+\tau)\hat{\sigma}_n^z(t_{ss})\rangle$ for all $\tau \in (0, \tau_{\max})$, which we identify with

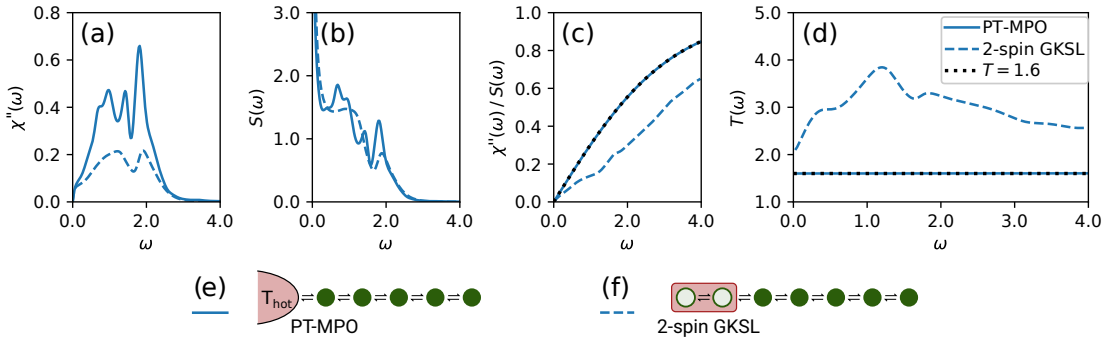

Figure 4.5: The dissipation spectrum (a), fluctuation spectrum (b), their ratio (c), and effective temperature (d) at the steady state for the σ^z observable of the middle spin in the 5-site chain. The solid and dashed lines show the results obtained employing the PT-MPO approach and a 2-spin driving protocol [156–158], respectively. The PT-MPO results overlap with the expected FDT $\tanh(\frac{\omega}{2T})$ (dotted line) in (c) and show no frequency dependence in (d), confirming complete thermalisation. Panel (e) shows a sketch of the 5-site chain coupled to a single bath at temperature $T = 1.6$. Panel (f) shows a sketch of the 5-site chain extended with two additional spins which are driven with a GKSL master equation towards their local Gibbs state.

$\langle \hat{\sigma}_n^z(\tau)\hat{\sigma}_n^z(0)\rangle_{ss}$ at the steady state. Using

$$\langle \hat{\sigma}_n^z(\tau)\hat{\sigma}_n^z(0)\rangle_{ss} = \langle \hat{\sigma}_n^z(0)\hat{\sigma}_n^z(-\tau)\rangle_{ss} \tag{4.15}$$

$$= \langle \hat{\sigma}_n^z(0)\hat{\sigma}_n^z(\tau)\rangle_{ss}^* \tag{4.16}$$

we can construct commutators and anti-commutators for $\tau \in (-\tau_{\max}, \tau_{\max})$ and employ a fast Fourier transformation on this interval to compute the fluctuation and dissipation spectra.

Figures 4.5a and 4.5b show the simulation results for the dissipation and fluctuation spectra for the $\hat{\sigma}^z$ observable of the middle spin of the 5-site chain with a bath coupling strength of $\alpha = 0.32$. Figure 4.5c shows the ratio of the dissipation and fluctuation spectra, which has the shape of a hyperbolic tangent. Inverting the FDT and plotting a frequency dependent effective temperature $T(\omega) = \omega/[2\,\mathrm{artanh}(\chi''(\omega)/S'(\omega)]$ in Fig. 4.5d we can see from the perfectly flat line that the two-time correlations are consistent with the FDT at the expected temperature. We find similar results for all other spins and observables, and no dependency on the chosen initial chain state.

Figure 4.5 also shows the results of a different, widely applied numerical method to study thermodynamic properties of spin chains [156–158]. For this, instead of coupling the first spin to the bosonic environment, we attach two additional spins to the left hand side of the first spin (see Fig.4.5f) and construct a Liouvillian $\mathcal{L}_B$ which drives these two spins towards the Gibbs state of their local Hamiltonian as described in section 2.4 of reference [156]. The two-time correlations obtained using this method strongly deviate from the FDT and are thus incorrect.

4.4.2. Two thermal leads

We now turn to an XYZ spin chain of length $N = 9$ coupled to two thermal leads at different temperatures. Using the PT-MPO augmented TEBD method we couple one bath at temperature $T_H = 1.6$ to the first and one bath at $T_C = 0.8$ to the last spin (see Fig. 4.6e), using the same spectral density and coupling operator as before.

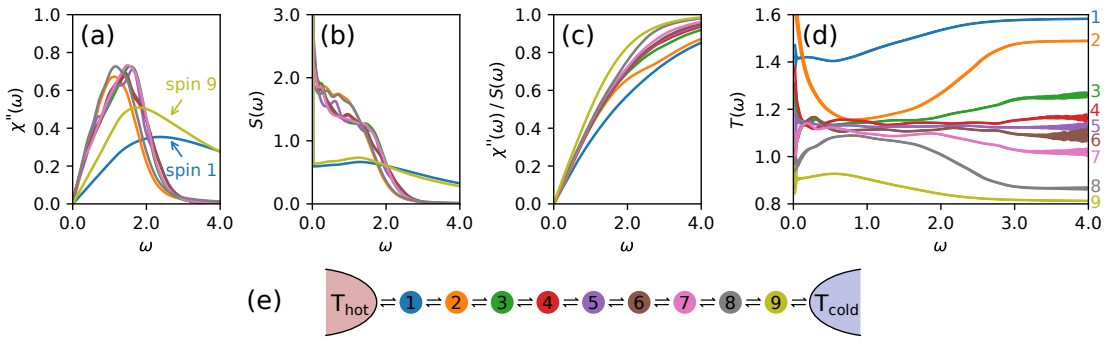

Figure 4.6: The dissipation spectrum (a), fluctuation spectrum (b), their ratio (c), and effective temperature (d) at the steady state for the σ^z observable of each spin in the 9-site spin chain. The thickness of the lines in panel (d) represent an estimate of the numerical error. Panel (e) shows a sketch of the 9-site spin chain placed between a hot ($T_{\text{hot}} = 1.6$) and cold bath ($T_{\text{cold}} = 0.8$).

The propagation from the initial state to the steady state took 8 hours 6 minutes on four cores of an Intel Xeon E5-2695 machine. The propagation after the application of the first $\hat{\sigma}_n^z$ took between 6 hours 37 minutes and 8 hours 39 minutes, depending on the site n to which it was applied. In order to check convergence with respect to the computation parameters, we study the finite difference of our results with respect to altered parameters. We performed simulations substituting $\delta t = 0.2 \to 0.15$, $K_{\max} = 40 \to 30$, $\epsilon_{\text{TEMPO}} = 10^{-6} \to 10^{-5}$ for the process tensor computation; and $\epsilon_{\text{TEBD}} = 10^{-6} \to 10^{-5}$, $t_{ss} = 192.0 \to 160.0$, and $\tau_{\max} = 128.0 \to 160.0$ for the augmented TEBD evolution. We found that the resulting differences are dominated by the variation of ϵ_{TEBD} and we thus consider these differences as an estimate of the numerical error.

Figure 4.6 show the dissipation $\chi''(\omega)$, fluctuation $S(\omega)$, and effective temperature $T(\omega)$ for the $\hat{\sigma}_z$ observable of each spin. The results in Fig. 4.6d show that at a mid frequency range (between roughly 0.5 and 2.0) the inner spins adopt a common intermediate effective temperature, while at higher frequencies (above approximately 3.0) each spin adopts an effective temperature between that of the hot and cold bath depending on its position. In the following we suggest an idea for why this kind of behaviour might arise. For this, we first consider the eigenstates of the closed XYZ spin chain, which consist of a set of delocalised "bulk" states plus localised "surface" states. The surface states are mainly localised at each end of the chain, but reach into the bulk with an exponentially decaying tail. For the chain parameters chosen here the density of states for the closed spin chain slowly vanishes above a frequency of approximately 2.5 (see the supplemental material of reference [68]).

Next, we include the coupling to the environment into our considerations. The strong coupling leads to a significant hybridisation of the chain states with the environment modes. Because the environments couple to the outer spins, they affect the bulk and surface states differently. The delocalised bulk states have an equal and small overlap with the two outer spins and therefore hybridise weakly with both environments. The surface states, on the other hand, have a large overlap with either the first or last spin and thus hybridise strongly with the left or right environment, respectively. In the mid frequency range the density of states for the inner spins is dominated by the weakly hybridised bulk states which, due to their equal overlap with both baths, assume an intermediate effective temperature. For the higher frequencies the density of states are

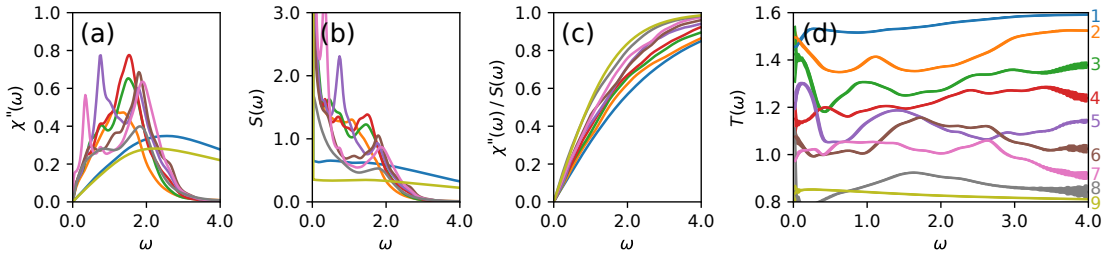

Figure 4.7: The dissipation spectrum (a), fluctuation spectrum (b), their ratio (c), and effective temperature (d) at the steady state for the σ^z observable of each spin in a disordered 9-site spin chain. The spin chain is paced between a hot ($T_{\text{hot}} = 1.6$) and cold bath ($T_{\text{cold}} = 0.8$) and has additional on-site disorder $\epsilon_n = 1 + x_n$, with a random draw $x_n = (0.16, 0.69, 0.33, 0.14, -0.24, 0.47, -0.20, 1.25, 1.48)$ from a uniform distribution in the interval $(-1.6, 1.6)$.

dominated by the strongly hybridised surface states. Because the coupling of a spin with the right and left surface states strongly depends on its position, the effective temperature it adopts depends on its position as well.

We can further test this interpretation of our results by introducing disorder in the chain to destroy the delocalised chain modes. For this, we add random on-site disorder to the chain Hamiltonian by choosing $\epsilon_n = 1 + x_n$, with x_n uniformly distributed in $(-W, W)$, with $W \in \mathbb{R}$. Figure 4.7 shows the results for a random draw with $W = 1.6$. In Fig. 4.7a one can identify several localised modes. For example, there is a peak at a frequency of about 1.9, which is supported by spins 5, 6, and 7, hinting at the existence of a localised mode. Also, one can see in Fig. 4.7d that the disorder destroys the collective common temperature at lower frequencies as expected.

Chapter 5

Long Time Limit of General Open Quantum Systems

So far our study of open quantum systems focused on their explicit time evolution and multi-time correlations following some initial preparation. In many experiments and theoretical studies the main interest lies however in the steady state behaviour. While the methods introduced in the previous chapters allow the study of quasi steady states through a long time evolution, a more direct approach seems desirable.

In cases where the steady state is known to be thermal (i.e. coupled only to a single bath, or to baths at the same temperature), a viable approach is to employ an imaginary time evolution in which the propagation with respect to the total Hamiltonian $\hat{H}$ is taken to be $e^{-\beta\hat{H}}$ instead of $e^{-it\hat{H}}$. An imaginary time evolution adaption of TEMPO has been demonstrated to be a very efficient method to calculate the mean-force Gibbs state of a system coupled strongly to a bosonic environment [159]. However, such an approach only yields the correct steady state density matrix in equilibrium scenarios, but cannot be applied in non-equilibrium scenarios (e.g. coupled to baths at multiple temperatures, or undergoing driving), or for the computation of steady state multi-time correlations. For the case of linearly coupled bosonic environments, the iterative quasi-adiabatic propagator path integral (QUAPI) introduced by Makri and Makarov [43, 44] allows the study of non-equilibrium scenarios and multi-time correlations also in the long time limit. It achieves this by constructing a time translational invariant propagator for the augmented density tensor capturing memory effects of the bath. However, its applicability is limited due to its exponential scaling with memory time.

In this chapter[1] we present some preliminary work on a reformulation of QUAPI that employs tensor network methods to compress the time translational invariant propagator to its physically most relevant parts. It allows us to tackle environments with much longer memory times compared to its original formulation. Unlike the TEMPO method introduced in section 2.3.1, the method introduced below preserves the time translational invariance, making it a suitable numerical method to study long time behaviour. As a first check and demonstration of this method, we study the steady state of the spin-boson model and compare it to known analytical results in the limit of vanishing tunnelling strength. Before presenting the tensor network reformulation of QUAPI in

[1] The work presented in this chapter has been carried out in collaboration with Dominic Gribben.

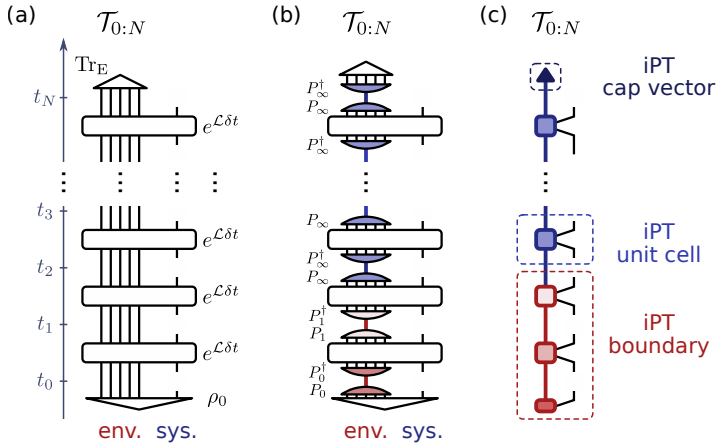

Figure 5.1: Tensor network construction of the infinite process tensor (iPT). (a) Process tensor network for an open quantum system with a constant total Liouvillian $\mathcal{L}$. (b) Process tensor network with projections onto the physically most relevant environment Liouville subspace. (c) Infinite process tensor in MPO form (iPT-MPO). The iPT unit cell may be repeated for the construction of a PT-MPO for any number of time steps N.

section 5.2, we first introduce a time translational invariant adaption of the process tensor—the so called *infinite process tensor* (iPT)—as a general concept in section 5.1. The QUAPI method and its tensor network reformulation yield such an iPT for the special case of a Gaussian bosonic environment. We conclude the chapter with an outlook in section 5.3 on potential applications, improvements, and extensions to the method.

5.1. Infinite process tensors

Although the process tensor formalism is a very powerful concept, one of the drawbacks in its current formulation is the necessity of choosing a finite number of time steps. This is unavoidable in the most general case that allows arbitrarily time dependent environment interactions. However, in most practical scenarios the environment interaction Hamiltonian is constant or at least periodic in time. In these cases it thus seems desirable to find a formulation of the process tensor that reflects the time translational invariance of the environment interaction and thus may represent the process tensor for an infinite number of time steps.

In the following we propose a formulation of such an *infinite process tensor* (iPT). For this, we first consider the simple case of a conventional (finite) process tensor with N equidistant time steps $t_n = n\,\delta t$ for a constant total Hamiltonian $\hat{H}$. Figure 5.1a shows the explicit construction of the process tensor for such a case as introduced in section 2.1.4 above. The methods introduced in chapter 2 allow the computation of an efficient MPO representation for such a process tensor. However, the MPO representations that result from these methods do in general not reflect the time translational structure of the original diagram in Fig. 5.1a. This is analogous to chains of quantum systems with spatially translational invariant Hamiltonians, where boundary effects in general destroy the spatial translational invariance of the chain's MPS. For very long chains a well known approach to solve this problem is to represent the bulk of the chain with a so called infinite MPS for which one chooses an appropriate repeating unit cell [101]. To yield a time translational MPO representation of the process tensor we propose an analogous approach for which one chooses an appropriate unit cell spanning

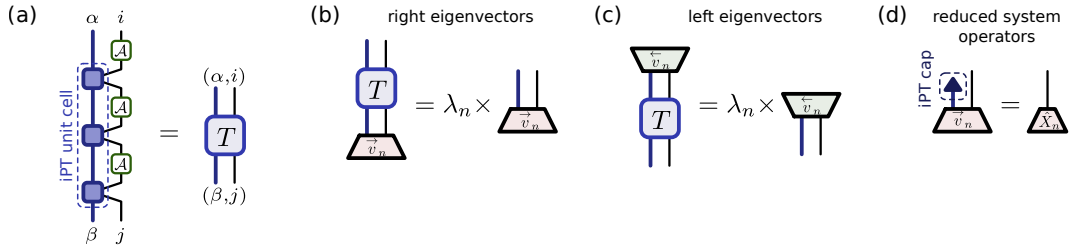

Figure 5.2: Tensor networks for the study of the steady state of a general open quantum system. (a) Construction of the matrix T from the iPT unit cell and the interventions $\mathcal{A}$. (b) Tensor network representation of the right eigenvectors $\vec{v}_n$. (c) Tensor network representation of the left eigenvectors $\overleftarrow{v}_n$. (d) Tensor network construction of the reduced system operator $\hat{X}_n \in \mathcal{B}(\mathcal{H}^{\mathrm{S}})$ from a right eigenvector $\vec{v}_n$.

one or more time steps.

Figure 5.1c shows an MPO representation that consists of an *iPT boundary*, an *iPT unit cell* (in this case of length one) and an *iPT cap vector*. The iPT boundary is a PT-MPO as introduced in section 2.3 for some (freely choosable) number of initial time steps with the constraint that the last MPO bond leg must connect to the first bond leg of the iPT unit cell. The iPT unit cell is an MPO representation of the time translational invariant part of the process tensor and the iPT cap vector is used to terminate the iPT-MPO. Figure 5.1b shows a possible construction of the iPT boundary, the iPT unit cell, and the iPT cap vector by inserting projections $P_n P_n^\dagger$ onto the most relevant environment Liouville subspaces. Given those three parts, one can easily construct a process tensor in MPO form for any number of time steps N by repeating the iPT unit cell. We therefore call this 3-tuple an *infinite process tensor in MPO form* (iPT-MPO).

While the approach outlined in Fig. 5.1b may be helpful conceptually, it is unsuitable for a practical computation due to the initially explicit representation of the full system-environment Liouville propagators. Before we introduce an efficient tensor network method to compute iPT-MPOs for Gaussian bosonic environments in section 5.2, we first analyse several useful properties of the iPT-MPO.

Beside the defining property of an iPT-MPO (which is that it admits the direct construction of a PT-MPO of any length) another useful property is that the iPT unit cell can be used in various ways to study the long time behaviour of open quantum systems. To explore this, let us assume that we have an iPT-MPO with a unit cell of length L which we contract by inserting interventions $\mathcal{A}$ to yield a single 4-rank tensor as shown in Fig. 5.2a. Grouping the output (α, i) and input legs (β, j) yields a square matrix T. The eigenvalues and eigenvectors of this matrix encode various properties of the long time dynamics. Let us consider the left eigenvectors $\overleftarrow{v}_n$ and right eigenvectors $\vec{v}_n$ of T with respect to the eigenvalues λ_n. We can write the eigenvalues in the form

$$\lambda_n = e^{\Gamma_n L \delta t} \tag{5.1}$$

such that the coefficients Γ_n are in close analogy to the eigenvalues of the Liouvillian in a GKSL master equation. The only difference is that here the eigenvectors are proportional to system operators that are augmented with an extra index (i.e. a tensor network leg) which encodes the system-environment correlations. The real and imaginary parts of the coefficients Γ_n correspond to decay rates and oscillation frequencies. In particular, for an open quantum system with a unique steady state, we expect that

there is exactly one eigenvalue with $\Gamma_k = 0$ while $\mathrm{Re}\,[\Gamma_n] < 0$ for all $n \neq k$. In this case the corresponding right eigenvector $\overrightarrow{v}_k$ is proportional to the augmented steady state density matrix, which not only encodes the reduced system steady state, but also its correlations with the environment. It can thus also be used to compute multi-time system correlations at the steady state, analogously to the quasi-steady state augmented MPS in section 4.4.1. We can find the reduced system steady state ρ^{S}_{ss} by contracting the eigenvector with the iPT cap vector (as sketched in Fig. 5.2d). Because eigenvectors can contain an arbitrary multiplicative factor, we must normalise this by multiplying the resulting system operator $\hat{X}_k$ with an appropriately chosen complex number to yield an Hermitian density matrix with unit trace. We will discuss the case of non-unique steady states in the context of the independent boson model in section 5.2.3.

Finally we note that, similarly to the approach in chapter 3, it can be very beneficial to perform a Trotterisation between the pure system part of the evolution and the environment interaction part. In most physically relevant cases the environment interaction part $\hat{H}^{\mathrm{IE}} = \hat{H}^{\mathrm{I}} + \hat{H}^{\mathrm{E}}$ is constant, which admits the construction of an iPT-MPO with an arbitrarily small iPT unit cell. In such cases the same iPT-MPO can be used to study dynamics and correlations for various (also time dependent) system Hamiltonians. For constant or periodic system Hamiltonians one may also employ the eigenvalue analysis explained above if the period coincides with a multiple of the iPT unit cell.

5.2. Gaussian bosonic environments

We now introduce a time translational invariant tensor network reformulation of QUAPI for Gaussian bosonic environments. The QUAPI method takes advantage of the time-translational invariant part of the Feynman-Vernon influence functional which, in fact, constitutes a particular representation of an iPT unit cell as introduced above. The bond dimension of this unit cell, however, grows exponentially with the memory time of the environment, which limits the applicability of this method. In the following we introduce a tensor network reformulation of QUAPI which compresses the vector space that corresponds to that bond dimension, making a much wider range of applications numerically feasible. Due to its similarities with the PT-TEMPO method we call it the *infinite process tensor TEMPO* (iPT-TEMPO) method. While the structure of the PT-TEMPO tensor network relies on the choice of a basis in which the coupling operator is diagonal, this is not the case for iPT-TEMPO. For clarity we will thus introduce iPT-TEMPO independently of any other method and only point out its similarities and differences to QUAPI and PT-TEMPO during that process.

5.2.1. Analytical derivation

The most general form of the total Hamiltonian that we consider in this section is

$$\hat{H}(t) = \hat{H}^{\mathrm{S}}(t) + \underbrace{\hat{S}\hat{F}}_{\hat{H}^{\mathrm{I}}} + \underbrace{\sum_k \omega_k \hat{a}_k^\dagger \hat{a}_k}_{\hat{H}^{\mathrm{E}}}, \tag{5.2}$$

where $\hat{a}_k$ ($\hat{a}_k^\dagger$) are bosonic creation (annihilation) operators, $\hat{S} \in \mathcal{B}\left(\mathcal{H}^{\mathrm{S}}\right)$ is the system coupling operator and $\hat{F} \in \mathcal{B}\left(\mathcal{H}^{\mathrm{E}}\right)$ is an environment field operator which we assume to be linear in $\hat{a}_k$ and $\hat{a}_k^\dagger$. A common example for the field operator is the position coupling

$\hat{F} = \sum_k \left(g_k \hat{a}_k + g_k^* \hat{a}_k^\dagger \right)$ characterised by the spectral density $J(\omega) := \sum_k |g_k|^2 \delta(\omega - \omega_k)$. Analogously to the considerations in section 2.3.1, we construct a process tensor for a total Hamiltonian $\hat{H}' = \hat{H}(t) - \hat{H}^{\mathrm{S}}(t)$ that excludes the pure system part $\hat{H}^{\mathrm{S}}(t)$. If we choose the time steps δt of the process tensor to be small enough, the evolution due to the pure system part can be reinserted as interventions.

In the following derivation we work with super-operators in Liouville space and transform the equations of motion into the interaction picture with respect to the pure environment Hamiltonian $\hat{H}^{\mathrm{E}} = \sum_k \omega_k \hat{a}_k^\dagger \hat{a}_k$, such that the total Hamiltonian becomes $\tilde{H}(t) = \hat{S}(t)\hat{F}(t)$. Formally we can express the process tensor with respect to $\tilde{H}$ for a continuum of time steps as

$$\mathcal{T}_{(0,t)} = \left\langle e^{\int_0^t \tilde{\mathcal{L}}(t')\mathrm{d}t'} \right\rangle_{\mathrm{E}}, \tag{5.3}$$

where $\tilde{\mathcal{L}}(t)\cdot = -i\left[\tilde{H}(t), \cdot\right]$ and $\langle \mathcal{X} \rangle_{\mathrm{E}} \cdot = \mathrm{Tr}_{\mathrm{E}} \left\{ \overleftarrow{\mathbf{T}}\, \mathcal{X} \left(\cdot \otimes \rho_0^{\mathrm{E}} \right) \right\}$ with the initial environment state ρ_0^{E} and time ordering $\overleftarrow{\mathbf{T}}$. Because the super-operators $\tilde{\mathcal{L}}(t')$ act on the total Liouville space (at time t'), the application of the partial trace over the environment results in super-operators that act only on the system Liouville space (also at time t'). Therefore the process tensor in Eq. (5.3) is a product of super-operators acting on the system Liouville space for a continuum of times between $t' = 0$ and $t' = t$. Before we discretise the time steps for the system Liouville space, we first rewrite the continuous process tensor in terms of a cumulant expansion

$$\mathcal{T}_{(0,t)} = \exp\left(\sum_{k=1}^{\infty} \frac{\Phi_k}{k!} \right) \tag{5.4}$$

where Φ^k is the k-th order cumulant of $\int_0^t \tilde{\mathcal{L}}(t')\mathrm{d}t'$ with respect to $\langle \cdot \rangle_{\mathrm{E}}$. The lowest order cumulants are

$$\Phi_1 = \int_0^t \left\langle \tilde{\mathcal{L}}(t') \right\rangle_{\mathrm{E}} \mathrm{d}t', \tag{5.5}$$

$$\Phi_2 = \int_0^t \int_0^t \left\langle \tilde{\mathcal{L}}(t')\tilde{\mathcal{L}}(t'') \right\rangle_{\mathrm{E}} \mathrm{d}t''\mathrm{d}t' - (\Phi_1)^2. \tag{5.6}$$

To continue we assume that the initial environment state ρ_0^{E} is a Gaussian state with a zero mean (i.e. $\Phi_1 = 0$). In this case the only non-zero cumulant is Φ_2 which we divide into discretised time steps

$$\Phi_2 = 2 \int_0^t \int_0^{t'} \left\langle \tilde{\mathcal{L}}(t')\tilde{\mathcal{L}}(t'') \right\rangle_{\mathrm{E}} \mathrm{d}t''\, \mathrm{d}t' \tag{5.7}$$

$$= 2 \sum_{n=0}^{N-1} \int_{n\delta t}^{(n+1)\delta t} \left\{ \sum_{m=0}^{n-1} \int_{m\delta t}^{s(m,t')} \left\langle \tilde{\mathcal{L}}(t')\tilde{\mathcal{L}}(t'') \right\rangle_{\mathrm{E}} \mathrm{d}t'' \right\} \mathrm{d}t' \tag{5.8}$$

with the upper integration bound of the inner integral $s(m,t') := \min\{(m+1)\delta t, t'\}$.

Inserting $\tilde{\mathcal{L}}(t)\cdot = \left[\hat{S}(t)\hat{F}(t), \cdot\right]$ into the time ordered integrand of Eq. (5.8) yields

$$\left\langle \tilde{\mathcal{L}}(t')\tilde{\mathcal{L}}(t'') \right\rangle_{\mathrm{E}} = \mathcal{S}^-(t') \Big(\mathcal{S}^-(t'') \mathrm{Re}\left[C(t',t'')\right] + i\mathcal{S}^+(t'') \mathrm{Im}\left[C(t',t'')\right] \Big) \tag{5.9}$$

with the environment correlation function

$$C(t', t'') = \mathrm{Tr}_{\mathrm{E}} \left\{ \hat{F}(t') \hat{F}(t'') \rho_0^{\mathrm{E}} \right\}, \tag{5.10}$$

and the system commutator $\mathcal{S}^- \cdot = \left[\hat{S}, \cdot \right]$ and anti-commutator $\mathcal{S}^+ \cdot = \left\{ \hat{S}, \cdot \right\}$. The correlation function only depends on the time difference $\tau = t' - t''$, which means that $C(\tau) = C(t'' + \tau, t'')$. For the case that $\hat{F} = \sum_k \left(g_k \hat{a}_k + g_k^* \hat{a}_k^\dagger \right)$ and ρ_0^{E} is the thermal environment state at temperature T the correlation function is

$$C(\tau) = \int_0^\infty \mathrm{d}\omega J(\omega) \left[\coth\left(\frac{\omega}{2T} \right) \cos(\omega\tau) - i \, \sin(\omega\tau) \right]. \tag{5.11}$$

Up until this point the entire derivation is exact. We now make a first simplifying approximation by discretising the time steps of the system super-operators. For each of the time intervals in Eq. (5.8) we approximate the system commutator and anti-commutator at times t' and t'' to act only at the fixed intermediate times $\bar{t}_n := (n + 1/2)\delta t$ and $\bar{t}_m = (m + 1/2)\delta t$. We thus approximate all system operators that connect the time step t_n to time step t_{n+1} in the process tensor with operators acting at time $\bar{t}_n$. The process tensor for the discrete time slots $\{t_n\}_{n \in 0,\ldots,N}$ with $t_n = n\delta t$ can then be written as

$$\mathcal{T}_{0:N} = \prod_{n=0}^{N-1} \prod_{m=0}^{n-1} \mathcal{I}_{n,m} \tag{5.12}$$

with the influence functions

$$\mathcal{I}_{n,m} = \exp\left(\mathcal{S}^-(\bar{t}_n) \left\{ \mathcal{S}^-(\bar{t}_m) \mathrm{Re}\left[\eta_{n-m} \right] + i \mathcal{S}^+(\bar{t}_m) \mathrm{Im}\left[\eta_{n-m} \right] \right\} \right) \tag{5.13}$$

where

$$\eta_k = \begin{cases} \int_0^{\delta t} \int_0^{t'} C(t' - t'') \, \mathrm{d}t'' \mathrm{d}t' & k = 0, \\ \int_{r\delta t}^{(r+1)\delta t} \int_0^{\delta t} C(t' - t'') \, \mathrm{d}t'' \mathrm{d}t' & k > 0. \end{cases} \tag{5.14}$$

We note that the application order of the system commutator and anti-commutator super-operators does not matter, i.e. $\mathcal{S}^-(t)\mathcal{S}^+(t) = \mathcal{S}^+(t)\mathcal{S}^-(t)$, and that thus the execution order of the product in Eq. (5.12) may be chosen freely.

In most relevant physical scenarios the correlation function $C(\tau)$ decays towards zero for large time differences τ and with this the influence functions $\mathcal{I}_{m+k,m}$ decay towards identity operations for large k. We thus now perform a second simplifying approximation by only including influence functions $\mathcal{I}_{m+k,m}$ for k time step differences up to some maximum $K_{\max}$. With this we can write the process tensor for arbitrarily many time steps $N \to \infty$ as

$$\mathcal{T}_{0:\infty} = \prod_{m=0}^{\infty} \prod_{k=0}^{K_{\max}} \mathcal{I}_{m+k,m}. \tag{5.15}$$

Unlike the derivation of QUAPI and TEMPO as presented in their original publications [43, 44, 47], the above derivation of the process tensor did not require the choice of a basis in which the system coupling operator $\hat{S}$ is diagonal. This formulation is therefore straightforwardly extendable to interaction Hamiltonians with multiple non-commuting terms, i.e. $\hat{H}^{\mathrm{I}} = \sum_p \hat{S}_p \hat{F}_p$. Also, the tensor network that we construct in the following does equally not depend on a particular choice of a basis. In contrast to that, an adaptation of the original TEMPO tensor network to an arbitrary choice of the basis would severely change and complicate its tensor network structure as explained in detail in reference [52].

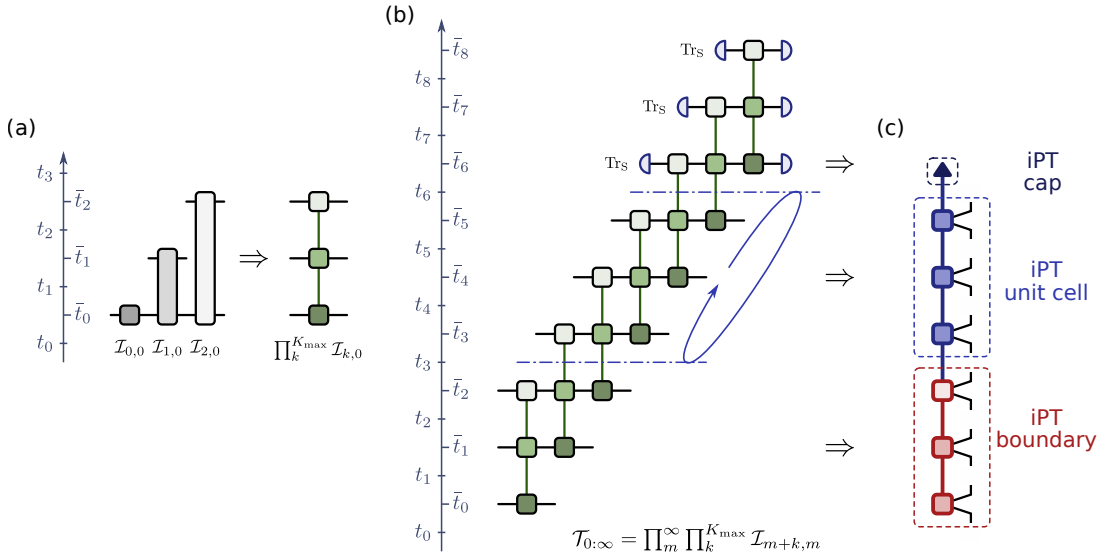

Figure 5.3: Tensor networks for the iPT-TEMPO method. (a) Tensor network of the product of the influence functions $\prod_{k=0}^{K_{\max}} \mathcal{I}_{k,0}$. (b) Tensor network construction of an infinite process tensor using multiple copies of $\prod_{k=0}^{K_{\max}} \mathcal{I}_{k,0}$. (c) The resulting iPT-MPO. The two blue dash-dotted lines in panel (b) indicate a periodic boundary condition.

5.2.2. Tensor network construction

We now express Eq. (5.15) in the form of a tensor network. For this we note that the influence functions $\mathcal{I}_{m+k,m}$ act on different time steps for different m but have otherwise the exact same form for the same time step span k. As a first step we thus construct and contract $\mathcal{I}_{0,0}$, $\mathcal{I}_{1,0}$,..., $\mathcal{I}_{K_{\max},0}$ while performing SVD truncations to compute an MPO representation of $\prod_{k=0}^{K_{\max}} \mathcal{I}_{k,0}$ as shown in Fig. 5.3a. We then construct the full process tensor $\mathcal{T}_{0:\infty}$ by applying this MPO at every time step m as shown in Fig. 5.3b. To find an MPO representation of this infinite process tensor, we choose the iPT boundary and iPT unit cell lengths to be $K_{\max}+1$. The tensor network between the two blue dash-dotted lines in Fig. 5.3b corresponds to the so called *tensor propagator* introduced in the original QUAPI publication, however, without the need to choose the particular basis in which the system coupling operator $\hat{S}$ is diagonal. Also, because QUAPI does not employ any tensor network methods, the tensor propagator grows exponentially with the number of necessary memory time steps $K_{\max}$.

To tackle this problem, we propose to use SVD truncations to compress the bond dimension of the iPT unit cell. The periodic boundary condition implies that during the contraction and SVD truncation the isometries that correspond to the SVD truncation between time step n and $n+1$ must be the same as between $n+K_{\max}+1$ and $n+K_{\max}+2$. Such a contraction then yields a process tensor acting at the times $\bar{t}_n$, which we can redraw in the more familiar form in Fig. 5.3c with timeslots t_n. The construction of a cap tensor can be achieved in two ways. Either one creates an explicit construction of a finite process tensor and traces out the later time steps, as presented in Fig. 5.3b, or one uses the left unit cell eigenvector $\overleftarrow{v}_k$ corresponding to an eigenvalue with $\lambda_k = 1$.

The tensor network construction presented here allows a variety of different contraction algorithms and choices of iPT unit cells resulting in the same iPT, but potentially in different MPO gauges. These may lead to different compression efficiencies which may

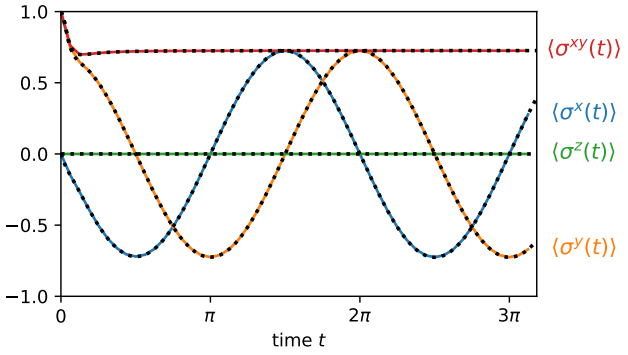

Figure 5.4: Dynamics of the independent boson model at zero temperature with an initial system state $|x+\rangle$. The results using the iPT-MPO (coloured solid lines) match the exact analytical result from Eq. (5.17) (the black dotted lines). The expectation value $\langle\sigma^{xy}(t)\rangle$ is defined as $\langle\sigma^{xy}(t)\rangle := \left(\langle\sigma^{x}(t)\rangle^2 + \langle\sigma^{y}(t)\rangle^2\right)^{1/2}$.

have a strong impact on the computational performance. A more detailed analysis of the efficiency for different contraction algorithms is, however, yet to be carried out. For the results presented in the next section we use a simple contraction algorithm for which we contract the tensor network column by column while performing SVD truncation sweeps with a relative truncation threshold after every contraction.

5.2.3. Spin-boson model

To demonstrate the iPT-TEMPO method we study the dynamics and steady states with respect to a total Hamiltonian of the spin-boson model

$$\hat{H} = \underbrace{\epsilon\frac{\hat{\sigma}^z}{2} + \Delta\frac{\hat{\sigma}^x}{2}}_{\hat{H}^{\mathrm{S}}} + \underbrace{\frac{\hat{\sigma}^z}{2}\sum_k \left(g_k\hat{a}_k + g_k^*\hat{a}_k^\dagger\right)}_{\hat{H}^{\mathrm{I}}} + \underbrace{\sum_k \omega_k\hat{a}_k^\dagger\hat{a}_k}_{\hat{H}^{\mathrm{E}}}. \tag{5.16}$$

We express all frequencies and times in terms of a characteristic frequency and its inverse and set $\hbar = k_B = \epsilon = 1$. Also, we assume that the environment is initially at temperature $T = 1/\beta = 0$ and consider a super-ohmic spectral density of the form

$$J(\omega) = \sum_k |g_k|^2\delta(\omega-\omega_k) = 2\alpha\frac{\omega^3}{\omega_c^2}\,e^{-\frac{\omega}{\omega_c}}$$

with a coupling constant $\alpha = 0.16$ and a cut-off frequency $\omega_c = 4.0$. For a vanishing tunnelling strength $\Delta = 0$, the spin-boson model becomes the so called *independent boson model* (IBM) and admits an exact analytical solution through a polaron transformation. Given a total initial state $\rho(0) = \rho_0^{\mathrm{S}}\otimes\rho_0^{\mathrm{E}}$ where ρ_0^{E} is the environment ground state, the reduced spin evolution for the IBM is

$$\rho^S(t) = \begin{pmatrix} [\rho^S(t)]_{\uparrow\uparrow} & [\rho^S(t)]_{\uparrow\downarrow} \\ [\rho^S(t)]_{\downarrow\uparrow} & [\rho^S(t)]_{\downarrow\downarrow} \end{pmatrix} = \begin{pmatrix} [\rho_0^S]_{\uparrow\uparrow} & [\rho_0^S]_{\uparrow\downarrow}\, e^{-i\epsilon t}\, e^{-\phi(t)} \\ [\rho_0^S]_{\downarrow\uparrow}\, e^{+i\epsilon t}\, e^{-\phi(t)} & [\rho_0^S]_{\downarrow\downarrow} \end{pmatrix} \tag{5.17}$$

with

$$\phi(t) = \int_0^\infty \frac{J(\omega)}{\omega^2}\left(1-\cos(\omega t)\right)\mathrm{d}\omega = 2\alpha\left[1 + \frac{\omega_c^2t^2-1}{(\omega_c^2t^2+1)^2}\right]. \tag{5.18}$$

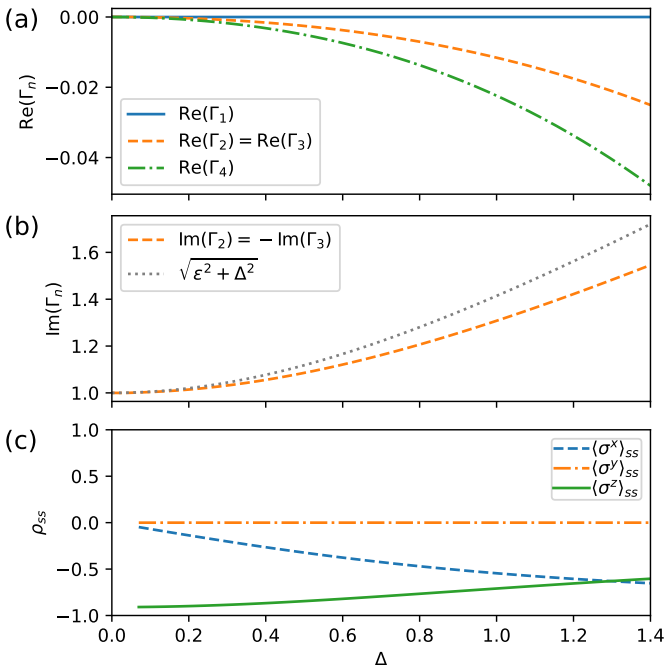

Figure 5.5: Real (a) and imaginary part (b) of the eigenvalue coefficients Γ_n, and the steady state expectation values (c) of the spin-boson model for different tunnelling strengths Δ. The eigenvalue coefficients Γ_n are defined in Eq. (5.1) as $\lambda_n = \exp(\Gamma_n L \delta t)$, where λ_n are the eigenvalues of the contracted iPT unit cell, L is the iPT unit cell length and δt is the time step length.

Following the approach described above, we construct an iPT-MPO for the environment interaction part $\hat{H}' = \hat{H}^{\mathrm{I}} + \hat{H}^{\mathrm{E}}$ and insert the pure system propagators as interventions. The results presented below have been obtained using a time step of $\delta t = \pi/16$, memory steps $K_{\max} = 32$, relative SVD truncation threshold 10^{-7}, and a unit cell of $L = 2\,K_{\max}$. The iPT-TEMPO computation took 43 s on a single core of an Intel i7 (8th Gen) processor, while inserting the system propagators and computing the eigenvectors of the iPT unit cell took less than 0.1 s for each different system Hamiltonian.

As a first check we use the iPT-MPO to compute the spin dynamics for the IBM with an initial state $|x+\rangle = \frac{1}{\sqrt{2}}(|\uparrow\rangle + |\downarrow\rangle)$. Figure 5.4 shows good agreement between the results obtained from the iPT-MPO calculation (coloured solid lines) and the exact results (black dots) following Eq. (5.17). Apart from calculating the explicit time evolution, we can also use the iPT-MPO to study the steady state by analysing the eigenvalues of the iPT unit cell. Figures 5.5a and 5.5b shows the Γ_i coefficients of the iPT unit cell contracted with system propagators for different tunnelling strengths Δ. Furthermore, Fig. 5.5c shows the $\hat{\sigma}^x$, $\hat{\sigma}^y$, and $\hat{\sigma}^z$ expectation values of the steady state corresponding to the largest eigenvalue $\lambda_1 = 1$ for each tunnelling strength Δ.

We notice several properties in Fig. 5.5 that are consistent with our expectations. For the IBM limit ($\Delta = 0$) we notice that all four non-zero eigenvalues have unit norm, i.e. $\mathrm{Re}[\Gamma_1] = \mathrm{Re}[\Gamma_2] = \mathrm{Re}[\Gamma_3] = \mathrm{Re}[\Gamma_4] = 0$. Also, $\mathrm{Im}[\Gamma_1] = \mathrm{Im}[\Gamma_4] = 0$ and $\mathrm{Im}[\Gamma_2] = -\mathrm{Im}[\Gamma_3] = \epsilon = 1.0$. The four system operators corresponding to these eigenvalues are proportional to $\hat{X}_1 = |\uparrow\rangle\langle\uparrow|$, $\hat{X}_2 = |\downarrow\rangle\langle\uparrow|$, $\hat{X}_3 = |\uparrow\rangle\langle\downarrow|$, and $\hat{X}_4 = |\downarrow\rangle\langle\downarrow|$. Because the iPT unit cell contains no information on the initial state, the eigenvectors with respect to eigenvalues of unit norm must encode the entire subspace of possible

steady states. Therefore, for the IBM, *any* spin state rotating around the z axis with frequency ϵ is a possible steady state.

For the spin-boson model with non-zero tunnelling $\Delta > 0$ we notice that there is only one eigenvalue with unit norm and thus the steady state is unique. We find that $\mathrm{Re}\,[\Gamma_4] < \mathrm{Re}\,[\Gamma_3] = \mathrm{Re}\,[\Gamma_2] < \mathrm{Re}\,[\Gamma_1] = 0$, as well as $\mathrm{Im}\,[\Gamma_1] = \mathrm{Im}\,[\Gamma_4] = 0$ and $\mathrm{Im}\,[\Gamma_2] = -\mathrm{Im}\,[\Gamma_3] > \epsilon$. The system operator corresponding to the first eigenvalue is the steady state plotted in Fig. 5.5c, while the three other operators span the rest of the system's Liouville space and have zero trace as expected, i.e. $\mathrm{Tr}\,\hat{X}_n = 0$ for $n \in \{2, 3, 4\}$. Finally, we notice that the oscillatory part of the second and third eigenvalue increases with Δ, but stays below the level splitting $\sqrt{\epsilon^2 + \Delta^2}$ of the closed system. This is consistent with the expectation that the damped system oscillations have a lower effective frequency than the closed system oscillations.

5.3. Outlook

We have shown that infinite process tensors are a useful tool to study steady state properties of general open quantum systems, and that the iPT-TEMPO method can be used to construct such an infinite process tensor in an efficient MPO representation. The iPT-MPO approach can be used to study single and multi-time correlations of steady states even in non-equilibrium scenarios. This could be particularly useful for the study of out–of–equilibrium strong coupling quantum thermodynamics scenarios, such as the three level quantum chiller [160] with strongly coupled thermal baths.

We note that preliminary results indicate that the numerical efficiency of the iPT-TEMPO method heavily depends on the form of the long time tail of the correlation function $C(\tau)$. It thus seems desirable to gain a better understanding of the limitations of this method and to then optimise the contraction algorithm and MPO gauge accordingly. Finally, we note that an adaptation of the automatic compression of environments (ACE) method [55] to construct iPT-MPOs is also conceivable and could further significantly broaden the class of numerically accessible physical scenarios.

Chapter 6

Conclusion

In this thesis we have seen that the process tensor is a versatile approach to general open quantum systems, and that its tensor network representation as a PT-MPO makes a wide range of physical scenarios numerically accessible. The methods based on the PT-MPO not only allow the simulation of the reduced system dynamics, but also the computation of multi-time correlations, the optimisation of driving protocols, and the study of steady state properties. We have seen that the PT-MPO methods introduced in this thesis are applicable to single and many-body systems in equilibrium and non-equilibrium scenarios. Furthermore, the process tensor formalism is not restricted to a particular type of environment and several methods for the computation of PT-MPOs are available for a wide range of different environments, such as boson, fermion, and spin baths.

These numerical methods make a wide range of relevant applications numerically accessible. The method introduced in chapter 3 may, for example, be useful for various optimal control problems, in particular in solid state quantum devices where the coupling to vibrational modes is typically strong. The PT-TEBD approach presented in chapter 4 enables the exploration of how environments affect many-body phenomena, such as quantum transport and many-body localisation. Studies on these topics have so far been carried out in a Markovian approximation. Such an approximation models the environment as a source of white noise, which leads to the unphysical artefact that the many-body system is forced to lose coherence at all energy scales. Such unrealistic models are most likely to lead to equally unrealistic predictions that do not capture the true nature of these phenomena. Employing the PT-TEBD method allows a more realistic incorporation of thermal environments in such scenarios. Also, the infinite process tensor approach introduced in chapter 5 enables the study of periodically driven systems and quantum thermal machines with potentially strongly coupled and structured environments. Despite their relevance in quantum technological applications, such as the engineering of heat flow in nanostructures, these systems have so far been studied predominately assuming weakly coupled unstructured environments. The iPT-MPO method allows the simulation of these systems without any such assumption, which makes the results more applicable to real quantum technologies and also has the potential to lead to fundamental insights that are obscured by the canonical approximations.

Given the large number of interesting applications it seems desirable to provide the scientific community with a reliable access to efficient implementations of the numer-

ical methods introduced in this thesis. For that purpose *the TEMPO collaboration*[1] created an open source python package, called OQuPy (Open Quantum systems in Python) [104]. To date, this package provides easy-to-use numerical tools of nine recent publications [47, 49, 54, 67, 68, 161–164] to efficiently compute the dynamics of non-Markovian open quantum systems.

Besides the open source project and the possible applications, the concepts and methods introduced in this thesis also suggest further methodological developments. An alternative to the PT-MPO augmented TEBD approach presented in chapter 4 is to use PT-MPOs in combination with other many-body tensor network methods, such as projected entangled pair state methods [165] or tree tensor networks [166]. This would allow the study of more complex open many-body systems, which may help to better understand energy transport in complex chemical structures, such as organic and biological systems. Similarly, alternatives to the MPO representation of the process tensor might be more efficient for particular environments. For an environment with polynomially decaying correlations, a multi-scale entanglement renormalization ansatz (MERA) [167] could potentially reflect a resulting scale invariance of the process tensor. Finally, we note that measurement-induced phase transitions seen in quantum trajectory simulations [168, 169] may be conceptually related to the non-trivial multi-time correlations captured by the process tensor. Establishing such a connection may assist deeper insights into these phenomena.

[1] As of August 2022, main contributors to OQuPy are (alphabetically): Piper Fowler-Wright, Gerald E. Fux, Dominic Gribben, and Dainius Kilda. Lead development: Gerald E. Fux.

Bibliography

[1] J. Preskill. *Quantum Computing in the NISQ era and beyond.* Quantum, 2:79 (2018).

[2] I. Buluta, S. Ashhab, and F. Nori. *Natural and artificial atoms for quantum computation.* Rep. Prog. Phys., 74(10):104401 (2011).

[3] G. S. Engel, T. R. Calhoun, E. L. Read, T. K. Ahn, T. Mančal, Y. C. Cheng, R. E. Blankenship, and G. R. Fleming. *Evidence for wavelike energy transfer through quantum coherence in photosynthetic systems.* Nature, 446(7137):782 (2007).

[4] H. N. Motlagh, J. O. Wrabl, J. Li, and V. J. Hilser. *The ensemble nature of allostery.* Nature, 508(7496):331 (2014).

[5] J. Cao, R. J. Cogdell, D. F. Coker, H.-G. Duan, J. Hauer, U. Kleinekathöfer, T. L. C. Jansen, T. Mančal, R. J. D. Miller, J. P. Ogilvie, V. I. Prokhorenko, T. Renger, H.-S. Tan, R. Tempelaar, M. Thorwart, E. Thyrhaug, S. Westenhoff, and D. Zigmantas. *Quantum biology revisited.* Sci. Adv., 6(14):eaaz4888 (2020).

[6] L. Meng, Y. Zhang, X. Wan, C. Li, X. Zhang, Y. Wang, X. Ke, Z. Xiao, L. Ding, R. Xia, H.-L. Yip, Y. Cao, and Y. Chen. *Organic and solution-processed tandem solar cells with 17.3% efficiency.* Science, 361(6407):1094 (2018).

[7] C. Gardiner, P. Zoller, and P. Zoller. *Quantum noise: a handbook of Markovian and non-Markovian quantum stochastic methods with applications to quantum optics.* Springer Science & Business Media (2000).

[8] H.-P. Breuer and F. Petruccione. *The Theory of Open Quantum Systems.* Oxford University Press (2002).

[9] C. Gardiner and P. Zoller. *The Quantum World of Ultra-Cold Atoms and Light Book I: Foundations of Quantum Optics*, vol. 2. Imperial College Press (2014).

[10] C. Gardiner and P. Zoller. *The Quantum World of Ultra-Cold Atoms and Light Book II: The Physics of Quantum-Optical Devices*, vol. 4. Imperial College Press (2015).

[11] Á. Rivas, S. F. Huelga, and M. B. Plenio. *Quantum non-markovianity: characterization, quantification and detection.* Rep. Prog. Phys., 77(9):094001 (2014).

[12] H.-P. Breuer, E.-M. Laine, J. Piilo, and B. Vacchini. *Colloquium: Non-markovian dynamics in open quantum systems.* Rev. Mod. Phys., 88:021002 (2016).

[13] I. de Vega and D. Alonso. *Dynamics of non-markovian open quantum systems.* Rev. Mod. Phys., 89:015001 (2017).

[14] A. J. Leggett, S. Chakravarty, A. T. Dorsey, M. P. A. Fisher, A. Garg, and W. Zwerger. *Dynamics of the dissipative two-state system.* Rev. Mod. Phys., 59:1 (1987).

[15] L. Chirolli and G. Burkard. *Decoherence in solid-state qubits.* Adv. Phys., 57(3):225 (2008).

[16] I. Wilson-Rae and A. Imamoğlu. *Quantum dot cavity-QED in the presence of strong electron-phonon interactions.* Phys. Rev. B, 65(23):235311 (2002).

[17] C. Galland, A. Högele, H. E. Türeci, and A. Imamoğlu. *Non-Markovian Decoherence of Localized Nanotube Excitons by Acoustic Phonons.* Phys. Rev. Lett., 101(6):067402 (2008).

[18] A. J. Ramsay, T. M. Godden, S. J. Boyle, E. M. Gauger, A. Nazir, B. W. Lovett, A. M. Fox, and M. S. Skolnick. *Phonon-induced Rabi-frequency renormalization of optically driven single InGaAs/GaAs quantum dots.* Phys. Rev. Lett., 105(17):177402 (2010).

[19] C. Roy and S. Hughes. *Phonon-Dressed Mollow Triplet in the Regime of Cavity Quantum Electro-*

dynamics: Excitation-Induced Dephasing and Nonperturbative Cavity Feeding Effects. Phys. Rev. Lett., 106(24):247403 (2011).

[20] P. Rebentrost, M. Mohseni, I. Kassal, S. Lloyd, and A. Aspuru-Guzik. *Environment-assisted quantum transport.* New J. Phys., 11(3):033003 (2009).

[21] L. Nicolin and D. Segal. *Quantum fluctuation theorem for heat exchange in the strong coupling regime.* Phys. Rev. B, 84:161414(R) (2011).

[22] M. Horodecki and J. Oppenheim. *Fundamental limitations for quantum and nanoscale thermodynamics.* Nat. Commun., 4(1):2059 (2013).

[23] S. Vinjanampathy and J. Anders. *Quantum thermodynamics.* Contemp. Phys., 57(4):545 (2016).

[24] U. Seifert. *First and second law of thermodynamics at strong coupling.* Phys. Rev. Lett., 116:020601 (2016).

[25] M. T. Mitchison. *Quantum thermal absorption machines: refrigerators, engines and clocks.* Contemp. Phys., 60(2):164 (2019).

[26] F. Binder, L. A. Correa, C. Gogolin, J. Anders, and G. Adesso. *Thermodynamics in the quantum regime: fundamental aspects and new directions*, vol. 195. Springer (2019).

[27] P. Talkner and P. Hänggi. *Colloquium: Statistical mechanics and thermodynamics at strong coupling: Quantum and classical.* Rev. Mod. Phys., 92:041002 (2020).

[28] G. White, F. Pollock, L. Hollenberg, K. Modi, and C. Hill. *Non-markovian quantum process tomography.* PRX Quantum, 3:020344 (2022).

[29] S. Nakajima. *On quantum theory of transport phenomena: Steady diffusion.* Prog. Theor. Phys., 20(6):948 (1958).

[30] R. Zwanzig. *Ensemble method in the theory of irreversibility.* J. Chem. Phys., 33(5):1338 (1960).

[31] S. Chaturvedi and F. Shibata. *Time-convolutionless projection operator formalism for elimination of fast variables. Applications to Brownian motion.* Z. Phys. B, 35(3):297 (1979).

[32] A. Ivanov and H.-P. Breuer. *Extension of the nakajima-zwanzig approach to multitime correlation functions of open systems.* Phys. Rev. A, 92:032113 (2015).

[33] A. Nazir and D. P. S. McCutcheon. *Modelling exciton–phonon interactions in optically driven quantum dots.* J. Phys. Condens. Matter, 28(10):103002 (2016).

[34] M. Bundgaard-Nielsen, J. Mørk, and E. V. Denning. *Non-markovian perturbation theories for phonon effects in strong-coupling cavity quantum electrodynamics.* Phys. Rev. B, 103:235309 (2021).

[35] L. Diósi and W. T. Strunz. *The non-markovian stochastic schrödinger equation for open systems.* Phys. lett. A, 235(6):569 (1997).

[36] P. Gaspard and M. Nagaoka. *Non-markovian stochastic schrödinger equation.* J. Chem. Phys., 111(13):5676 (1999).

[37] E. Gull, A. J. Millis, A. I. Lichtenstein, A. N. Rubtsov, M. Troyer, and P. Werner. *Continuous-time monte carlo methods for quantum impurity models.* Rev. Mod. Phys., 83:349 (2011).

[38] R. Bulla, T. A. Costi, and T. Pruschke. *Numerical renormalization group method for quantum impurity systems.* Rev. Mod. Phys., 80:395 (2008).

[39] J. Prior, A. W. Chin, S. F. Huelga, and M. B. Plenio. *Efficient simulation of strong system-environment interactions.* Phys. Rev. Lett., 105(5):050404 (2010).

[40] A. W. Chin, Á. Rivas, S. F. Huelga, and M. B. Plenio. *Exact mapping between system-reservoir quantum models and semi-infinite discrete chains using orthogonal polynomials.* J. Math. Phys., 51(9):092109 (2010).

[41] J. Iles-Smith, N. Lambert, and A. Nazir. *Environmental dynamics, correlations, and the emergence of noncanonical equilibrium states in open quantum systems.* Phys. Rev. A, 90(3):032114 (2014).

[42] Y. Tanimura and R. Kubo. *Time Evolution of a Quantum System in Contact with a Nearly Gaussian-Markoffian Noise Bath.* J. Phys. Soc. Japan, 58(1):101 (1989).

[43] N. Makri and D. E. Makarov. *Tensor propagator for iterative quantum time evolution of reduced density matrices. I. Theory.* J. Chem. Phys., 102(11):4600 (1995).

[44] N. Makri and D. E. Makarov. *Tensor propagator for iterative quantum time evolution of reduced density matrices. II. Numerical methodology.* J. Chem. Phys., 102(11):4611 (1995).

[45] M. C. Bañuls, M. B. Hastings, F. Verstraete, and J. I. Cirac. *Matrix product states for dynamical simulation of infinite chains.* Phys. Rev. Lett., 102:240603 (2009).

[46] R. Hartmann and W. T. Strunz. *Exact open quantum system dynamics using the hierarchy of*

pure states (hops). J. Chem. Theory Comput., 13(12):5834 (2017).

[47] A. Strathearn, P. Kirton, D. Kilda, J. Keeling, and B. W. Lovett. *Efficient non-Markovian quantum dynamics using time-evolving matrix product operators.* Nat. Commun., 9(1):3322 (2018).

[48] N. Lambert, S. Ahmed, M. Cirio, and F. Nori. *Modelling the ultra-strongly coupled spin-boson model with unphysical modes.* Nat. Commun., 10(1):3721 (2019).

[49] M. R. Jørgensen and F. A. Pollock. *Exploiting the causal tensor network structure of quantum processes to efficiently simulate non-markovian path integrals.* Phys. Rev. Lett., 123:240602 (2019).

[50] U. Schollwöck. *The density-matrix renormalization group in the age of matrix product states.* Ann. Phys. (N. Y.), 326(1):96 (2011).

[51] R. Orús. *A practical introduction to tensor networks: Matrix product states and projected entangled pair states.* Ann. Phys. (N. Y.), 349:117 (2014).

[52] A. Strathearn. *Modelling Non-Markovian Quantum Systems Using Tensor Networks.* Springer Theses. Springer International Publishing, Cham (2020).

[53] A. Lerose, M. Sonner, and D. A. Abanin. *Influence matrix approach to many-body floquet dynamics.* Phys. Rev. X, 11:021040 (2021).

[54] G. E. Fux, E. P. Butler, P. R. Eastham, B. W. Lovett, and J. Keeling. *Efficient exploration of hamiltonian parameter space for optimal control of non-markovian open quantum systems.* Phys. Rev. Lett., 126:200401 (2021).

[55] M. Cygorek, M. Cosacchi, A. Vagov, V. M. Axt, B. W. Lovett, J. Keeling, and E. M. Gauger. *Simulation of open quantum systems by automated compression of arbitrary environments.* Nat. Phys., 18(6):662 (2022).

[56] M. Sonner, A. Lerose, and D. A. Abanin. *Influence functional of many-body systems: Temporal entanglement and matrix-product state representation.* Ann. Phys. (N. Y.), 435:168677 (2021). Special issue on Philip W. Anderson.

[57] E. Ye and G. K.-L. Chan. *Constructing tensor network influence functionals for general quantum dynamics.* J. Chem. Phys., 155(4):044104 (2021).

[58] J. Thoenniss, A. Lerose, and D. A. Abanin. *Non-equilibrium quantum impurity problems via matrix-product states in the temporal domain* (2022).

[59] S. J. Glaser, U. Boscain, T. Calarco, C. P. Koch, W. Köckenberger, R. Kosloff, I. Kuprov, B. Luy, S. Schirmer, T. Schulte-Herbrüggen, D. Sugny, and F. K. Wilhelm. *Training Schrödinger's cat: Quantum optimal control: Strategic report on current status, visions and goals for research in Europe.* Eur. Phys. J. D, 69(12):279 (2015).

[60] C. P. Koch. *Controlling open quantum systems: Tools, achievements, and limitations.* J. Phys. Condens. Matter, 28(21):213001 (2016).

[61] Y. Blanter and M. Büttiker. *Shot noise in mesoscopic conductors.* Phys. Rep., 336(1):1 (2000).

[62] N. Agraït, A. L. Yeyati, and J. M. van Ruitenbeek. *Quantum properties of atomic-sized conductors.* Phys. Rep., 377(2-3):81 (2003).

[63] F. Giazotto, T. T. Heikkilä, A. Luukanen, A. M. Savin, and J. P. Pekola. *Opportunities for mesoscopics in thermometry and refrigeration: Physics and applications.* Rev. Mod. Phys., 78:217 (2006).

[64] M. D. Losego, M. E. Grady, N. R. Sottos, D. G. Cahill, and P. V. Braun. *Effects of chemical bonding on heat transport across interfaces.* Nat. Mater., 11(6):502 (2012).

[65] J. R. Widawsky, W. Chen, H. Vázquez, T. Kim, R. Breslow, M. S. Hybertsen, and L. Venkataraman. *Length-Dependent Thermopower of Highly Conducting Au–C Bonded Single Molecule Junctions.* Nano Lett., 13(6):2889 (2013).

[66] L. Li, M. J. Hall, and H. M. Wiseman. *Concepts of quantum non-markovianity: A hierarchy.* Phys. Rep., 759:1 (2018). Concepts of quantum non-Markovianity: A hierarchy.

[67] F. A. Pollock, C. Rodríguez-Rosario, T. Frauenheim, M. Paternostro, and K. Modi. *Non-Markovian quantum processes: Complete framework and efficient characterization.* Phys. Rev. A, 97(1):012127 (2018).

[68] G. E. Fux, D. Kilda, B. W. Lovett, and J. Keeling. *Thermalization of a spin chain strongly coupled to its environment.* ArXiv:2201.05529 (2022).

[69] Á. Rivas and S. F. Huelga. *Time evolution in open quantum systems.* In *Open Quantum Systems*, pages 19–31. Springer (2012).

[70] G. D. Mahan. *Many-particle physics.* Springer Science & Business Media (2000).

[71] H. Abramczyk. *Introduction to laser spectroscopy.* Elsevier (2005).

[72] M. A. Nielsen and I. Chuang. *Quantum computation and quantum information*. American Association of Physics Teachers (2002).

[73] M. M. Wolf and J. I. Cirac. *Dividing Quantum Channels*. Commun. Math. Phys., 279(1):147 (2008).

[74] Á. Rivas, S. F. Huelga, and M. B. Plenio. *Entanglement and non-markovianity of quantum evolutions*. Phys. Rev. Lett., 105:050403 (2010).

[75] S. Milz, M. S. Kim, F. A. Pollock, and K. Modi. *Completely Positive Divisibility Does Not Mean Markovianity*. Phys. Rev. Lett., 123(4):040401 (2019).

[76] A. Kossakowski. *On quantum statistical mechanics of non-hamiltonian systems*. Rep. Math. Phys., 3(4):247 (1972).

[77] V. Gorini, A. Kossakowski, and E. C. G. Sudarshan. *Completely positive dynamical semigroups of n-level systems*. J. Math. Phys., 17(5):821 (1976).

[78] G. Lindblad. *On the generators of quantum dynamical semigroups*. Commun. Math. Phys., 48(2):119 (1976).

[79] D. Chruściński and A. Kossakowski. *Markovianity criteria for quantum evolution*. J. Phys. B, 45(15):154002 (2012).

[80] F. A. Pollock, C. Rodríguez-Rosario, T. Frauenheim, M. Paternostro, and K. Modi. *Operational Markov Condition for Quantum Processes*. Phys. Rev. Lett., 120(4):040405 (2018).

[81] M. Lax. *Formal theory of quantum fluctuations from a driven state*. Phys. Rev., 129:2342 (1963).

[82] G. W. Ford and R. F. O'Connell. *There is no quantum regression theorem*. Phys. Rev. Lett., 77:798 (1996).

[83] P. Talkner. *The failure of the quantum regression hypothesis*. Annals of Physics, 167(2):390 (1986).

[84] G. Ford and R. O'Connell. *Driven systems and the lax formula*. Opt. Commun., 179(1):451 (2000).

[85] G. Guarnieri, A. Smirne, and B. Vacchini. *Quantum regression theorem and non-markovianity of quantum dynamics*. Phys. Rev. A, 90:022110 (2014).

[86] M. Cosacchi, T. Seidelmann, M. Cygorek, A. Vagov, D. E. Reiter, and V. M. Axt. *Accuracy of the quantum regression theorem for photon emission from a quantum dot*. Phys. Rev. Lett., 127:100402 (2021).

[87] A. Jamiołkowski. *Linear transformations which preserve trace and positive semidefiniteness of operators*. Rep. Math. Phys., 3(4):275 (1972).

[88] R. P. Feynman and F. L. Vernon. *The theory of a general quantum system interacting with a linear dissipative system*. Ann. Phys. (N. Y.), 24(C):118 (1963).

[89] G. Chiribella, G. M. D'Ariano, and P. Perinotti. *Quantum circuit architecture*. Phys. Rev. Lett., 101:060401 (2008).

[90] O. Oreshkov, F. Costa, and Č. Brukner. *Quantum correlations with no causal order*. Nat. Commun., 3(1):1092 (2012).

[91] A. Klumper, A. Schadschneider, and J. Zittartz. *Equivalence and solution of anisotropic spin-1 models and generalized t-j fermion models in one dimension*. J. Phys. A, 24(16):L955 (1991).

[92] M. Fannes, B. Nachtergaele, and R. F. Werner. *Finitely correlated states on quantum spin chains*. Commun. Math. Phys., 144(3):443 (1992).

[93] G. Vidal. *Efficient classical simulation of slightly entangled quantum computations*. Phys. Rev. Lett., 91:147902 (2003).

[94] F. Verstraete, J. J. García-Ripoll, and J. I. Cirac. *Matrix product density operators: Simulation of finite-temperature and dissipative systems*. Phys. Rev. Lett., 93:207204 (2004).

[95] S. R. White. *Density matrix formulation for quantum renormalization groups*. Phys. Rev. Lett., 69:2863 (1992).

[96] S. R. White. *Density-matrix algorithms for quantum renormalization groups*. Phys. Rev. B, 48:10345 (1993).

[97] P. W. Langhoff, S. T. Epstein, and M. Karplus. *Aspects of time-dependent perturbation theory*. Rev. Mod. Phys., 44:602 (1972).

[98] J. Haegeman, J. I. Cirac, T. J. Osborne, I. Pižorn, H. Verschelde, and F. Verstraete. *Time-dependent variational principle for quantum lattices*. Phys. Rev. Lett., 107:070601 (2011).

[99] G. Vidal. *Efficient simulation of one-dimensional quantum many-body systems*. Phys. Rev. Lett., 93:040502 (2004).

[100] M. Zwolak and G. Vidal. *Mixed-state dynamics in one-dimensional quantum lattice systems: A time-dependent superoperator renormalization algorithm.* Phys. Rev. Lett., 93:207205 (2004).

[101] G. Vidal. *Classical simulation of infinite-size quantum lattice systems in one spatial dimension.* Phys. Rev. Lett., 98:070201 (2007).

[102] H. F. Trotter. *On the product of semi-groups of operators.* Proc. Am. Math. Soc., 10(4):545 (1959).

[103] M. P. Zaletel, R. S. K. Mong, C. Karrasch, J. E. Moore, and F. Pollmann. *Time-evolving a matrix product state with long-ranged interactions.* Phys. Rev. B, 91:165112 (2015).

[104] The TEMPO collaboration. *OQuPy: A Python 3 package to efficiently compute non-Markovian open quantum systems.* (2022).

[105] E. M. Stoudenmire and S. R. White. *Minimally entangled typical thermal state algorithms.* New J. Phys., 12(5):055026 (2010).

[106] H. Häffner, C. Roos, and R. Blatt. *Quantum computing with trapped ions.* Phys. Rep., 469(4):155 (2008).

[107] G. Wendin. *Quantum information processing with superconducting circuits: a review.* Rep. Prog. Phys., 80(10):106001 (2017).

[108] H. L. Huang, D. Wu, D. Fan, and X. Zhu. *Superconducting quantum computing: a review.* Sci. China Inf. Sci., 63(8):1 (2020).

[109] Z. Wang. *Topological quantum computation.* 112. American Mathematical Soc. (2010).

[110] R. L. Amoroso. *Universal Quantum Computing.* World Scientific (2017).

[111] D. Lidar and T. Brun, editors. *Quantum Error Correction.* Cambridge University Press (2013).

[112] S. Gröblacher, A. Trubarov, N. Prigge, G. D. Cole, M. Aspelmeyer, and J. Eisert. *Observation of non-Markovian micromechanical Brownian motion.* Nat. Commun., 6(1):7606 (2015).

[113] F. F. Floether, P. De Fouquieres, and S. G. Schirmer. *Robust quantum gates for open systems via optimal control: Markovian versus non-Markovian dynamics.* New J. Phys., 14(7):073023 (2012).

[114] C. Addis, E.-M. Laine, C. Gneiting, and S. Maniscalco. *Problem of coherent control in non-markovian open quantum systems.* Phys. Rev. A, 94:052117 (2016).

[115] N. Mirkin, P. Poggi, and D. Wisniacki. *Entangling protocols due to non-Markovian dynamics.* Phys. Rev. A, 99(2):020301 (2019).

[116] P. Rebentrost, I. Serban, T. Schulte-Herbrüggen, and F. K. Wilhelm. *Optimal control of a qubit coupled to a non-Markovian environment.* Phys. Rev. Lett., 102(9):090401 (2009).

[117] R. Schmidt, A. Negretti, J. Ankerhold, T. Calarco, and J. T. Stockburger. *Optimal control of open quantum systems: Cooperative effects of driving and dissipation.* Phys. Rev. Lett., 107(13):130404 (2011).

[118] B. Hwang and H. S. Goan. *Optimal control for non-Markovian open quantum systems.* Phys. Rev. A, 85(3):032321 (2012).

[119] J. Cerrillo and J. Cao. *Non-Markovian dynamical maps: Numerical processing of open quantum trajectories.* Phys. Rev. Lett., 112(11):110401 (2014).

[120] D. M. Reich, N. Katz, and C. P. Koch. *Exploiting Non-Markovianity for Quantum Control.* Sci. Rep., 5(1):12430 (2015).

[121] D. Tamascelli, A. Smirne, S. F. Huelga, and M. B. Plenio. *Nonperturbative Treatment of non-Markovian Dynamics of Open Quantum Systems.* Phys. Rev. Lett., 120(3):30402 (2018).

[122] R. Puthumpally-Joseph, E. Mangaud, V. Chevet, M. Desouter-Lecomte, D. Sugny, and O. Atabek. *Basic mechanisms in the laser control of non-Markovian dynamics.* Phys. Rev. A, 97(3):033411 (2018).

[123] E. Mangaud, R. Puthumpally-Joseph, D. Sugny, C. Meier, O. Atabek, and M. Desouter-Lecomte. *Non-markovianity in the optimal control of an open quantum system described by hierarchical equations of motion.* New J. Phys., 20(4):043050 (2018).

[124] M. H. Goerz and K. Jacobs. *Efficient optimization of state preparation in quantum networks using quantum trajectories.* Quantum Sci. Technol., 3(4):045005 (2018).

[125] D. Tamascelli, A. Smirne, J. Lim, S. F. Huelga, and M. B. Plenio. *Efficient Simulation of Finite-Temperature Open Quantum Systems.* Phys. Rev. Lett., 123(9):90402 (2019).

[126] J. Fischer, D. Basilewitsch, C. P. Koch, and D. Sugny. *Time-optimal control of the purification of a qubit in contact with a structured environment.* Phys. Rev. A, 99(3):033410 (2019).

[127] A. D. Somoza, O. Marty, J. Lim, S. F. Huelga, and M. B. Plenio. *Dissipation-Assisted Matrix*

Product Factorization. Phys. Rev. Lett., 123(10):100502 (2019).

[128] F. Mascherpa, A. Smirne, A. D. Somoza, P. Fernández-Acebal, S. Donadi, D. Tamascelli, S. F. Huelga, and M. B. Plenio. *Optimized auxiliary oscillators for the simulation of general open quantum systems.* Phys. Rev. A, 101(5):052108 (2020).

[129] M. Brenes, J. J. Mendoza-Arenas, A. Purkayastha, M. T. Mitchison, S. R. Clark, and J. Goold. *Tensor-Network Method to Simulate Strongly Interacting Quantum Thermal Machines.* Phys. Rev. X, 10(3):031040 (2020).

[130] Y. Tanimura. *Numerically "exact" approach to open quantum dynamics: The hierarchical equations of motion (HEOM).* J. Chem. Phys., 153(2):020901 (2020).

[131] S. Boyd, S. P. Boyd, and L. Vandenberghe. *Convex optimization.* Cambridge university press (2004).

[132] D. J. Wales and J. P. K. Doye. *Global optimization by basin-hopping and the lowest energy structures of lennard-jones clusters containing up to 110 atoms.* The Journal of Physical Chemistry A, 101(28):5111 (1997).

[133] R. Storn and K. Price. *Differential Evolution - A Simple and Efficient Heuristic for Global Optimization over Continuous Spaces.* J. Glob. Optim., 11(4):341 (1997).

[134] P. R. Eastham, A. O. Spracklen, and J. Keeling. *Lindblad theory of dynamical decoherence of quantum-dot excitons.* Phys. Rev. B, 87(19):195306 (2013).

[135] A. M. Weiner, D. E. Leaird, J. S. Patel, and J. R. Wullert. *Programmable Shaping of Femtosecond Optical Pulses by Use of 128-Element Liquid Crystal Phase Modulator.* IEEE J. Quantum Electron., 28(4):908 (1992).

[136] A. M. Weiner. *Femtosecond pulse shaping using spatial light modulators.* Rev. Sci. Instrum., 71(5):1929 (2000).

[137] E. P. Butler, G. E. Fux, B. W. Lovett, J. Keeling, and P. R. Eastham. *Work in preparateion* (2022).

[138] S. Bose. *Quantum communication through an unmodulated spin chain.* Phys. Rev. Lett., 91:207901 (2003).

[139] A. Wójcik, T. Łuczak, P. Kurzyński, A. Grudka, T. Gdala, and M. Bednarska. *Unmodulated spin chains as universal quantum wires.* Phys. Rev. A, 72:034303 (2005).

[140] N. Lambert, Y. N. Chen, Y. C. Cheng, C. M. Li, G. Y. Chen, and F. Nori. *Quantum biology.* Nat. Phys., 9(1):10 (2013).

[141] N. Makri. *Communication: Modular path integral: Quantum dynamics via sequential necklace linking.* J. Chem. Phys., 148(10):101101 (2018).

[142] N. Makri. *Modular path integral methodology for real-time quantum dynamics.* J. Chem. Phys., 149(21):214108 (2018).

[143] S. Suzuki, H. Oshiyama, and N. Shibata. *Quantum annealing of pure and random ising chains coupled to a bosonic environment.* J. Phys. Soc. Japan, 88(6):061003 (2019).

[144] A. Purkayastha, G. Guarnieri, S. Campbell, J. Prior, and J. Goold. *Periodically refreshed baths to simulate open quantum many-body dynamics.* Phys. Rev. B, 104:045417 (2021).

[145] N. Makri. *Small matrix modular path integral: iterative quantum dynamics in space and time.* Phys. Chem. Chem. Phys., 23(22):12537 (2021).

[146] S. Kundu and N. Makri. *Efficient matrix factorisation of the modular path integral for extended systems.* Mol. Phys., 119(13):e1797200 (2021).

[147] S. Kundu and N. Makri. *Exciton-Vibration Dynamics in J-Aggregates of a Perylene Bisimide from Real-Time Path Integral Calculations.* J. Phys. Chem. C, 125(1):201 (2021).

[148] S. Flannigan, F. Damanet, and A. J. Daley. *Many-body quantum state diffusion for non-markovian dynamics in strongly interacting systems.* Phys. Rev. Lett., 128:063601 (2022).

[149] A. Bose and P. L. Walters. *A multisite decomposition of the tensor network path integrals.* J. Chem. Phys., 156(2):024101 (2022).

[150] A. J. Daley, C. Kollath, U. Schollwöck, and G. Vidal. *Time-dependent density-matrix renormalization-group using adaptive effective hilbert spaces.* J. Stat. Mech.: Theory Exp., 2004(04):P04005 (2004).

[151] M. Suzuki. *General theory of higher-order decomposition of exponential operators and symplectic integrators.* Phys. Lett. A, 165(5):387 (1992).

[152] A. S. Trushechkin, M. Merkli, J. D. Cresser, and J. Anders. *Open quantum system dynamics and the mean force Gibbs state.* ArXiv:2110.01671 (2021).

[153] R. Kubo. *The fluctuation-dissipation theorem.* Rep. Prog. Phys., 29(1):255 (1966).

[154] R. Kubo, M. Toda, and N. Hashitsume. *Statistical physics II: nonequilibrium statistical mechanics*, vol. 31. Springer Science & Business Media (2012).

[155] A. A. Clerk, M. H. Devoret, S. M. Girvin, F. Marquardt, and R. J. Schoelkopf. *Introduction to quantum noise, measurement, and amplification.* Rev. Mod. Phys., 82:1155 (2010).

[156] T. Prosen. *Matrix product simulations of non-equilibrium steady states of quantum spin chains.* J. Stat. Mech.: Theory Exp., 2009(02):P02035 (2009).

[157] M. Žnidarič, T. Prosen, G. Benenti, G. Casati, and D. Rossini. *Thermalization and ergodicity in one-dimensional many-body open quantum systems.* Phys. Rev. E, 81:051135 (2010).

[158] T. Prosen. *Exact nonequilibrium steady state of a strongly driven open xxz chain.* Phys. Rev. Lett., 107:137201 (2011).

[159] Y.-F. Chiu, A. Strathearn, and J. Keeling. *Numerical evaluation and robustness of the quantum mean-force gibbs state.* Phys. Rev. A, 106:012204 (2022).

[160] R. Kosloff, E. Geva, and J. M. Gordon. *Quantum refrigerators in quest of the absolute zero.* J. Appl. Phys., 87(11):8093 (2000).

[161] A. Strathearn, B. W. Lovett, and P. Kirton. *Efficient real-time path integrals for non-markovian spin-boson models.* New J. Phys., 19(9):093009 (2017).

[162] D. Gribben, A. Strathearn, G. E. Fux, P. Kirton, and B. W. Lovett. *Using the environment to understand non-markovian open quantum systems.* Quantum, 6:847 (2022).

[163] D. Gribben, D. M. Rouse, J. Iles-Smith, A. Strathearn, H. Maguire, P. Kirton, A. Nazir, E. M. Gauger, and B. W. Lovett. *Exact dynamics of nonadditive environments in non-markovian open quantum systems.* PRX Quantum, 3:010321 (2022).

[164] P. Fowler-Wright, B. W. Lovett, and J. Keeling. *Efficient many-body non-markovian dynamics of organic polaritons.* Phys. Rev. Lett., 129:173001 (2022).

[165] F. Verstraete and J. I. Cirac. *Renormalization algorithms for Quantum-Many Body Systems in two and higher dimensions.* ArXiv:cond-mat/0407066 (2004).

[166] Y.-Y. Shi, L.-M. Duan, and G. Vidal. *Classical simulation of quantum many-body systems with a tree tensor network.* Phys. Rev. A, 74:022320 (2006).

[167] G. Vidal. *Entanglement renormalization.* Phys. Rev. Lett., 99:220405 (2007).

[168] S. Dhar and S. Dasgupta. *Measurement-induced phase transition in a quantum spin system.* Phys. Rev. A, 93:050103 (2016).

[169] B. Skinner, J. Ruhman, and A. Nahum. *Measurement-induced phase transitions in the dynamics of entanglement.* Phys. Rev. X, 9:031009 (2019).